Organic Self-Assembled Thin Films for Second Order Nonlinear Optics

Kylie J. Gaskins

Thesis submitted to the Faculty of Virginia Polytechnic Institute
and State University in partial fulfillment of
the requirements for the degree of

MASTER OF SCIENCE
In
Chemical Engineering

Richey M. Davis, Chairman
James R. Heflin
Eva Marand

July 29, 2004
Blacksburg, VA

Keywords: nonlinear optics, second harmonic generation, organic thin films, hybrid covalent electrostatic deposition, self-assembly, electro-optic coefficient

Organic Self-Assembled Thin Films for Second Order Nonlinear Optics

Kylie J. Gaskins

ABSTRACT

With a growing demand in industry for cost effective, increased data handling capabilities great attention has been paid to the study of various polymer systems for use in optical telecommunications. Inorganic crystals, currently used in such systems, have high performance, but are more expensive and less obtainable than organic materials. Recent advances in techniques for developing highly efficient and inexpensive organic polymeric electro-optic (EO) devices compatible with current state-of-the-art electronics have created an interest in the commercialization of such electro-optic devices. In light of the many advantages of utilizing organic materials for electro-optic applications, numerous methods have been developed to produce nonlinear optically (NLO)-active polymeric films for such purposes. Ionic self-assembled multilayer (ISAM) films are a recently developed class of materials that allows detailed structural and thickness control at the molecular level, combined with ease of manufacturing and low cost. However, the layer-by-layer deposition technique utilized for this method currently requires lengthy processing times that challenge the feasibility of fabricating a thick film suitable for EO modulator device fabrication. This study focuses on addressing the influence of several pertinent processing variables affecting these challenges for application to electro-optic device fabrication. This study investigated (1) the effect of forced convection, varying deposition time and varying dye concentration on the properties of PAH/Procion Brown films fabricated via the hybrid reactive deposition scheme, (2) the automation and optimization of the fabrication of thick NLO active films and (3) the use of the hybrid covalent-electrostatic deposition scheme to fabricate a polymeric waveguide device with an electro-optic coefficient comparable to that of lithium niobate ($LiNbO_3$).

At fixed deposition time and concentration conditions, the presence of convection had little demonstrated effect on films with deposition times shorter than 2 minutes. For the 5 minute case, the presence of convection correlated with a ~45% increase in $\chi^{(2)}_{zzz}$ values and a 25% increase in absorbance per bilayer. At a constant dye concentration of 5 mg/ml, the deposition time had little effect on SHG for deposition times less than two minutes. In the presence of convection, the increase in deposition time from 2 minutes to 5 minutes showed a 57% increase

in $\chi^{(2)}_{zzz}$ and a 30% increase in absorbance per bilayer. For a deposition time of 2 minutes in the presence of convection, the dye solution concentration was successfully reduced 5-fold (from 5 mg/ml to 1 mg/ml) with less than a 5% difference in $\chi^{(2)}_{zzz}$, less than a 15% decrease in absorbance per bilayer and no detriment to film quality. These results strongly indicate that the deposition conditions remain well outside of the transport-limited regime at a dye concentration of 1 mg/ml. Rather, the surface reaction rate apparently is controlling. Depositing slides at an elevated temperature (~35°C), had an undetermined effect on $\chi^{(2)}_{zzz}$, but showed a 15% increase in absorbance per bilayer.

An automatic dipper was programmed to replicate the current manual deposition method to fabricate a film suitable for EO modulator devices. Utilizing the optimal conditions for the processing variables, an optically-homogeneous, 100 nm-thick film was fabricated utilizing the automated process, yielding a $\chi^{(2)}_{zzz} \sim 23 \times 10^{-9}$ esu.

A three-layer coplanar electro-optic device was fabricated utilizing the hybrid reactive deposition method. For this device, the presence of added salt was found to increase the electro-optic coefficient r_{33} by a factor of 3 compared to its value when made with no added salt. The electro-optic coefficient of the added salt case was found to be about 1/2 that of lithium niobate ($LiNbO_3$).

To my family and those before me that made this opportunity possible

Acknowledgements

There are so many people to thank for getting me to where I am today. To my parents for their never-ending support. Words cannot even express all that you've done. Mom thanks for helping me reign over all adversity. Dad thanks for instilling your work ethic in me and sparking my interest in engineering. To Tony, my Technical Specialist, thanks for all of the advice and free computers. To my Head Cheerleader Sonya, thanks for the words of encouragement. This is the first technical graduate degree in our family of many more to come. April, Christy, Tasha and Mike, thanks for all the laughs when I especially needed them. Dr. Bemley, I am not sure that I will fulfill all of your hopes for me, but this should do just fine. (Thanks so much for the help with my publications and the exposure. Big things are still to come.) Ivy, thanks so much for your business savvy advice. You are always right on time.

I would finally like to thank my committee and co-workers at Virginia Tech for helping me achieve my goals. Cemil, thanks for all the late hours spent measuring my samples. Akhilesh, thanks for all of your help with the dreaded dipper experiment. I would also like to thank all of my classmates in the Williams and Marand labs for the entertainment and laughs.

TABLE OF CONTENTS

FIGURES AND TABLES

Tables

Chapter 2

Chapter 3

Chapter 4

Chapter 5

Figures

Chapter 2

Chapter 3

Chapter 4

Chapter 5

Chapter 1

Introduction

Background

Electro-Optic (EO) Applications of Organic Thin Films

Recent advances in techniques for developing highly efficient and inexpensive organic polymeric electro-optic devices compatible with current state-of-the-art electronics have created an interest in the commercialization of such electro-optic devices.[1] The potential applications of organic polymeric nonlinear optical (NLO) materials include cable television, analog-to-digital (A/D) converters and fiber optic telecommunications. Optical transmission of data involves the conversion of an optical signal to an electrical signal which requires encoding at variable frequency rates. For such a purpose, a key device utilized is an electro-optic (EO) modulator. One such modulator is based on a Mach-Zender (MZ) interferometer. In this device, the application of an electric field to one arm of the MZ results in a phase shift of incoming light relative to the signal propagating through the second arm and destructive interference at the device output.[2] This device configuration can be used to fabricate more sophisticated devices such an ultra-fast analog to digital converters.[3,4]

Polymeric EO/NLO Materials

Since the late sixties organic molecules have attracted an increasing amount of interest due to their potential application in nonlinear optical (NLO) devices. This interest is motivated not only by the large NLO response, but also by the versatility, ease of processing and ready availability of such materials. Organic molecules can also be tailored to possess high hyperpolarizabilities and may be processed into good optical quality thin films and NLO active crystals.[5] Inorganic crystals, such as lithium niobate ($LiNbO_3$)[6] and potassium niobate ($KNbO_3$),[7] currently used for fiber optic systems yield high performance in the critical areas of data transmission speed and minimal optical loss, but these materials are inferior to organic materials in the areas of cost, availability and lengthy processing times for crystal growth.[8,9]

Some advantages of EO modulators based on organic devices are low material cost, low optical signal loss, mass production capability and the ability to engineer desired properties. For optical devices, transparency is needed in the near-IR region, rather than in the visible region because wavelengths between 1.3 μm and 1.5 μm are used in optical telecommunications. Organic materials can have high losses in the near-infrared region (0.8-1.6 μm) due to C-H bond vibrational absorption. However, these losses can be reduced by the incorporation of heavier atoms into the chemistry.[10] A strong point for the use of polymeric electro-optic materials is the adaptability of these materials to sophisticated processing techniques and the fabrication of integrated devices. The large bandwidths, low-drive voltages and ease of integration of polymeric electro-optic materials provide a strong argument for increased utilization in integrated devices.

The requirements of organic polymeric electro-optic materials for utilization in integrated devices include high electro-optic coefficient (r_{33}>30 pm/V), minimal optical loss, no scattering or absorption of light and good thermal stability. These materials must have no orientational relaxation during operation (25-80˚C) during the lifetime of the device (5-10 years), and also minimal physical, chemical and optical activity degradation at short (10-30 minute) excursions to temperatures of 250-300°C (temperatures encountered in device fabrication processes). These requirements hold generally for most EO device applications.

NLO Film Fabrication Methods

Several experimental techniques have been developed for creating nonlinear optically (NLO) active thin films suitable for optical communication and photonic devices.[11,12,13] Electric field poled polymer films,[14,15] Langmuir-Blodgett films[10,16] and self-assembled organosilane[17] films have all produced NLO-active films with high nonlinear responses. However, poled polymer films face challenges for practical device application due to the instability of the acentric alignment of the NLO chromophores, which degrades the electro-optic activity over time. Langmuir-Blodgett films are desirable due to their cheap fabrication and fine control on film thickness and refractive index. However, problems typically arise in the form of poor mechanical stability and high propagation losses due to scattering and insufficient thickness.

Ionic Self-Assembled Monolayer (ISAM) Techniques

Polymer-Polymer Deposition

Ionic self-assembled multilayer (ISAM) films are a recently developed class of materials that allows detailed structural and thickness control at the molecular level, combined with ease of manufacturing and low cost. While ISAM films have been shown to have excellent temporal, thermal and structural stability, their NLO performance is currently too low for practical devices, typically exhibiting $\chi^{(2)} \sim 1 \times 10^{-9}$ esu. This is mainly due to orientational limitations imparted by (1) the necessity of dipole orientation towards layers both above and below the polymeric layer, resulting partial cancellation of orientation, (2) the random orientation of dipoles within thicker monolayers, and (3) steric constraints on orientation induced by bulky chromophores on the polymer backbone.

Polymer-Polymer ISAM Deposition

The ISAM technique for the deposition of polyelectrolytes has been reviewed in a number of recent papers.[18,19,20] The method involves the alternate dipping of a charged substrate into an aqueous solution of a polyanion and polycation at room temperature. The advantages of this technique include simple, rapid, inexpensive production and long-term stability of the acentric $\chi^{(2)}$ without the need for additional processing such as electric-field poling or chemical reactions. Polymer-polymer ISAM films fabricated by Heflin et al.[21] exhibited linear scaling of $I_{2\omega}^{1/2}$ vs film thickness (up to 120 nm), demonstrating the uniform maintenance of orientation with layer-by-layer growth. This effort has produced the only successful attempt of any group working with films of this type thicker than a few tens of bilayers. In addition, the films exhibited exceptional thermal stability with no measurable decay of $\chi^{(2)}$ at 150°C for more than 15 hours, in sharp contrast to electric-field poled polymers.

Reactive ISAM Deposition

ISAM deposition schemes that involve a reactive deposition step alternated with an electrostatic deposition step are evolving into a prevalent class of NLO film fabrication techniques.[22] A novel layer-by-layer methodology for fabricating NLO thin films has been developed[23,24] with the aim of increasing the stability of chromophore-dipole orientation, reducing steric constraints from polymer-backbone attachment (often encountered in traditional

ISAM films) and producing a large nonlinear optical response. This method builds films layer-by-layer by alternately immersing a substrate into aqueous solutions of an NLO-inactive polyelectrolyte "glue" and a reactive chromophoric dye. The adsorption of the layers alternates between electrostatic interaction and covalent reaction. The chromophore is attached covalently which yields anisotropic ordering and high second-order NLO activity in these films. The hybrid method has been tested with a number of commercially-available monomeric dyes, including Procion Red, Procion Orange and most recently, Procion Brown. Laschewsky et al. recently attempted reactive films growth with Procion Red dye and a synthetically-produced amine. The films experienced no regular layer-by-layer growth and exhibited no significant nonlinear optical activity.

Prior Studies

Prior studies of the fabrication of NLO active films utilizing the hybrid reactive method with Procion Brown yielded exceptional results in nonlinear optical response ($\chi^{(2)}_{zzz}$= 56 x 10^{-9} esu) and thermal stability in comparison to other organic films for similar studies.[25] However, the layer-by-layer deposition technique utilized for this method currently requires lengthy processing times that challenge the feasibility of fabricating a thick film for EO modulator device fabrication. The effect of several pertinent processing variables affecting these challenges had not been examined to date. In view of these outstanding issues, this study focuses on addressing the influence of these processing variables for application to electro-optic device fabrication.

Research Objectives

This study aims to achieve the following objectives:

- **Examine the effect of forced convection, varying deposition time and varying dye concentration on the properties of PAH/Procion Brown films fabricated via the hybrid reactive deposition scheme.** This study aims to determine the deposition conditions that result in the most rapid film deposition utilizing the minimal amount of dye. The films fabricated using these optimal deposition conditions are expected to produce NLO results comparable to previous studies. The reduction of deposition time and dye required is key for practical fabrication of thick (~ 1 μm) films for polymeric electro-optic modulator devices.

- **Automate and optimize the fabrication of thick NLO active films.** The objectives of this work are: **(1)** Program an automatic dipper to replicate the current manual deposition method to fabricate a 1 micron-thick film suitable for EO modulator devices. **(2)** Optimize the operating parameters of automated dipper operation (i.e. rinse time, etc.) to produce optically homogeneous films utilizing a minimal cycle time with minimal consumption of materials.

- **Investigate the use of the hybrid covalent-electrostatic deposition scheme to fabricate a polymeric waveguide device with an electro-optic coefficient comparable to that of lithium niobate ($LiNbO_3$).** Polymeric electro-optic devices have been successfully fabricated utilizing the poled polymer approach. This work will demonstrate the feasibility of fabricating polymeric electro-optic devices using the hybrid deposition scheme developed in prior work within this group. Furthermore, this work aims to demonstrate the performance of such devices in terms of the electro-optic coefficient r_{33}.

Thesis Outline

Chapter 2: Literature Review

This chapter gives an overview of the science and technology of organic thin films and their applications in electronic device fabrication. The following topics are reviewed in detail:

- Second order nonlinear optics
- Electro-optic applications of organic thin films
- Polymer/azo dye surface adsorption
- Thin film deposition methods

Chapter 3: Effect of Forced Convection, Deposition Time and Dye Concentration on Organic NLO-Active Films

Chapter 3 discusses the study conducted to address Objective #1. The reactive NLO chromophore Procion Brown (Burnt Orange MX-GRN) was used with the optically inactive polymer, poly(allylamine hydrochloride) {PAH} to fabricate ionically self-assembled films using a manual dipping procedure. This work is a continuation of prior studies that determined the following optimal parameters for film deposition: **(1)** commercially-available

chromophore/polymer combination, **(2)** pH of deposition solutions and **(3)** ionic strength for chromophore deposition. The absorbance, film thickness, tilt angle and second harmonic intensity were all measured to determine the minimal deposition time and dye concentration required to produce films with suitable quality and optical response for NLO electro-optic applications as well as the effect of convection on film formation.

Chapter 4: Automation and Optimization of Thick NLO-Active Film Fabrication

Chapter 4 discusses the study conducted to address Objective #2 and is a continuation of the work described in Chapter 3. The fabrication of ionically self-assembled Procion Brown/PAH films was automated to produce device-applicable films utilizing the optimal conditions determined in Chapter 3 using a manual deposition procedure. The automated operation parameters were closely monitored to optimize deposition conditions. The active flow-through bath was modeled as a continuously-stirred tank reactor to determine the effectiveness of the rinse step, the most critical step to proper film formation. Automatically fabricated films were characterized by absorbance, film thickness, tilt angle and second harmonic susceptibility $\chi^{(2)}$. The finalized automated procedure was utilized to deposit a 500 nm-thick (total on both sides) film onto a glass substrate.

Chapter 5: Organic Polymeric Device Fabrication for Electro-Optic Coefficient Measurement

Chapter 5 discusses the study conducted to address Objective #3. Procion Brown/PAH films were deposited onto ITO-coated substrates to fabricate a three-layer coplanar electro-optic device. The films were characterized by absorbance, tilt angle and electro-optic coefficient. This study probed three major areas: **(1)** the suitability of ISAM deposited Procion Brown/PAH films for waveguide device fabrication, **(2)** measurement of the electro-optic coefficient of such films utilizing a classical reflection modulation technique and **(3)** the effect of added salt on waveguide device performance in terms of electro-optic coefficient. The presence of added salt was found to increase the electro-optic coefficient r_{33} by a factor of 3 compared to its value when made with no added salt. The electro-optic coefficient of the added salt case was found to be about 1/2 that of lithium niobate ($LiNbO_3$).

References

[1] Lee, K. –S. "*Polymers for photonics applications I"* Springer, Berlin, Germany (2002) pp. 1-7, 12, 65-73.

[2] Lindsay, G. A. 'Second-order nonlinear optical polymers: an overview' In: Lindsay, G. A. *Polymers for second-order nonlinear optics* American Chemical Society, Washington, DC (1995) Chapter 1.

[3] Dalton, L. R. 'Polymers for electro-optic modulator waveguides' In: Wise, D. L., Wnek, G.; Trantolo, D. J.; Cooper, T. M.; Gresser, J. D. *Electrical and optical polymer systems* Marcel Dekker, New York, (1998) Chapter 18.

[4] Kaino, T. 'Waveguide fabrication using organic nonlinear optical materials' *J. Opt. A.: Pure Appl. Opt.* **2** (2000). R1-R7.

[5] Lee, K. –S. "*Polymers for Photonics Applications II"*, Heidelberg, Germany: Springer-Verlag, 2003.

[6] Ni, P.; Ma, B.; Wang, X.; Cheng, B.; Zhang, D. 'Second-Harmonic Generation in Two-Dimensional Periodically Poled Lithium Niobate Using Second-Order Quasiphase Matching' *Appl. Phys. Lett.* **82** (2003) 4230-4232.

[7] Fluck, D.; Pliska, T.; Günter, P.; Beckers, L.; Buchal,C. 'Blue-light second-harmonic generation in ion-implanted KNbO[sub 3] channel waveguides of new design' *Appl. Phys. Lett.* **69** (1996) 4133-4135.

[8] Kitamura, K.; Yamamoto, J. K.; Iyi, N.; Kimura, S. 'Stoichiometric $LiNbO_3$ single crystal growth by double crucible Czochralski method using automatic powder supply system' *J. Crystal Growth* **116** (1992) 327-332.

[9] Takagi, T.; Fujii, T.; Sakabe, Y. 'Growth and characterization of $KNbO_3$ by vertical Bridgman method' *Journal of Crystal Growth* **259 (**2003) 296-301.

[10] Sottini, S.; Grando, D.; Palchetti, L.; Giorgetti, E.; Ricceri, R.; Gabrielli, G. 'Organic films for guided nonlinear optics' *Materials Science and Engineering* **C5** (1998) 167-172.

[11] Thakur, M.; Titus, J.; Mishra, A. 'Single-crystal thin films of organic molecular salt may lead to a new generation of electro-optic devices' *Opt. Eng.* **42** (2003) 456-458.

[12] Koeste, M.; Laschewsky, A.; Jonas, A. M.; Verbiest, T. 'Orientation of functional groups in polyelectrolyte multilayers studied by second-harmonic generation (SHG)' *Colloids and Surface A* **198-200** (2002) 275-280.

[13] Kaino, T. 'Waveguide fabrication using organic nonlinear optical materials' *J. Opt. A: Pure Appl. Opt.* **2** (2002) R1-R7.

[14] Yu, H.H.; Hwang, S.-J. 'E-O functional waveguide using the electric-field-poled polymeric material for integrated-optic devices' *Optics Communications* **219** (2003) 183-192.

[15] Ma, H.; Liu, S.; Luo, J.; Suresh, S.; Liu, L.; Kang, S. H.; Haller, M.; Sassa, T.; Jen, A. K. Y.; Dalton, L. R. 'Highly efficient and thermally stable electro-optical dendrimers for photonics' - *Adv. Funct. Mater* **12** (2002) 565-574.

[16] Ashwell, G. J.; Jackson, P. D.; Crossland, W. A. 'Noncentrosymmetry and second harmonic generation in Z-type Langmuir-Blodgett Films' *Nature* **368** (1994) 438-440.

[17] Wang, W.; Zhu, P.; Marks, T. J.; Ketterson, J. B. 'Ultrafast frequency-selective optical switching based on thin self-assembled organic chromophoric films with a large second-order nonlinear response' *Appl. Phys. Lett.* **81** (2002) 2169-2171.

[18] Decher, G.; Hong, J. D.; Schmitt, J. 'Buildup of ultrathin multilayer films by a self-assembly process: consecutively alternating adsorption of anionic and cationic polyelectrolytes on charged surfaces' *Thin Solid Films* **210/211** (1992) 831-835.

[19] Hammond, P. T. 'Recent explorations in electrostatic multilayer thin film assembly' *Current Opinion in Colloid & Interface Science* **4** *(1999)* 430-442.

[20] Kotz, J.; Kosmella, S.; Beitz, T. 'Self-assembled polyelectrolyte systems' *Prog. Poly. Sci.* **26** (2001) 1199-1232.

[21] Heflin, J. R. 'Thickness dependence of second harmonic generation in thin films fabricated from ionically self-assembled monolayers' *Appl. Phys. Lett.* **74** (1999) 495-497.

[22] Koeste, M.; Laschewsky, A.; Verbiest, T. 'Films grown from polyamines and reactive dyes by alternating adsorption/surface activation' *Mater. Sci. Eng. C* **10** (1999) 107-113.

[23] Van Cott, K. E.; Guzy, M.; Neyman, P.; Brands, C.; Heflin, J. R.; Gibson, H. W.; Davis, R. M. 'Layer-by-layer deposition and ordering of low-molecular weight dye molecules for second-order nonlinear optics' *Angew. Chem. Int. Ed.* **41** (2002) 3236-3328.

[24] Heflin, J. R.; Neyman, P. J.; Guzy, M.; Shah, S. M.; Davis, R. M.; Van Cott, K. E.; Wang, H.; Gibson, H. W.; Brands, C. 'Hybrid covalent/ionic self-assembly of organic second order nonlinear optical films, in Organic Thin Films for Photonic Applications, *OSA Trends in Optics and Photonics Series* **64** (2002) 3-8.

[25] Guzy, M. Organic Self-Assembled Layer-by-Layer Thin Films for Second-Order Nonlinear Optics, Ph.D. Thesis, Virginia Tech, 2003.

Chapter 2
Literature Review

Nonlinear Optics

The field of nonlinear optics had its birth in 1875 with Kerr's publication of his findings of a quadratic electric field induced change in the refractive index, known as the Kerr effect. The observation of this phenomena was followed shortly by other materials, including quartz.[1] The theory of nonlinear optics builds on the well-understood theory of linear optics, particularly that part known as the interaction of light and matter. The fundamental parameter in this light-matter interaction theory is the electronic polarization of the material induced by light. When the intensity of the light is sufficiently high (i.e. from a laser), a small additional polarization will arise, so that the total polarization P can be written as

$$P = P_L + P_{NL} \tag{2.1}$$

where P_L is the linear portion of the polarization and P_{NL} is a nonlinear function of the applied field. In linear optics, the nonlinear part of the polarization may be neglected, as given by

$$P = P_0 + \chi_{ij}^{(1)} E_j \tag{2.2}$$

where P_0 is the static dipole moment and $\chi^{(1)}$ is the first order susceptibility and E is the electric field strength.

In the nonlinear optical regime, the nonlinear part of the polarization can no longer be ignored. The polarization of a material P_i under an applied electric field can be expressed as follows

$$P_i = \chi_{ij}^{(1)} E_j + \chi_{ijk}^{(2)} E_j E_k + \chi_{ijk}^{(3)} E_j E_k E_l + \mathrm{K} \tag{2.3}$$

The second-order term $\chi^{(2)}$ in Equation 2.3, expressly for a noncentrosymmetric and anisotropic material, is the primary focus of this study.

Second Order Nonlinear Optics

Second harmonic generation (SHG) involves the conversion of radiation at a frequency ω into radiation at a frequency 2ω exiting the nonlinear material. The demonstration of second harmonic generation, also known as frequency doubling, in a quartz crystal sparked the study of the field of nonlinear optics.[2] Another important development in nonlinear optical materials occurred in 1970, when Davydov et al.[3] reported strong second harmonic generation (SHG) in organic molecules having electron donor and acceptor groups connected with a benzene ring. Conjugated organic molecules with electron donor and acceptor groups were found to exhibit extremely large optical nonlinear responses, lending to promising applications in second harmonic generation. This breakthrough led to the emergence of second order nonlinear optics, the subject of most advanced device technology development in this field. Second order nonlinear optics is chiefly characterized by the second order susceptibility $\chi^{(2)}$ which, for an organic film can be described by

$$\chi^{(2)} = NF\beta\left\langle \cos^3\theta \right\rangle \tag{2.4}$$

where β is the hyperpolarizability of the chromophore, N is the chromophore number density, θ is the dipole tilt angle relative to the film normal vector and F is a local field effect factor.

The three basic requirements for materials exhibiting NLO activity are polarizability, asymmetric charge distribution (incorporation of donor and acceptor molecules) and most importantly noncentrosymmetry at the macroscopic level (no inversion center). Such requirements are best met by dipolar, highly polarizable donor-π bond-acceptor systems showing charge transfer between electron donating and electron drawing groups. The development of NLO chromophores aims to design, synthesize and characterize highly active chromophore molecules which have a high hyperpolarizability β. Factors such as increased π conjugation length, increased planarity and the strength of donors and acceptors all play significant roles in the NLO activity of the species.

The design of nonlinear optical chromophores has progressed markedly in recent years.[4,5,6,7] High quality noncentrosymmetric materials have been fabricated from inorganic crystals and organic molecules. Inorganic crystals, such as lithium niobate ($LiNbO_3$)[8,9,10] and

potassium niobate ($KNbO_3$),[11,12,13] currently used for fiber optic systems yield high performance in the critical areas of data transmission speed and minimal optical loss, but these materials are inferior in the areas of cost, availability and lengthy processing times for crystal growth.[14-15] Since the late sixties, organic molecules have attracted an increasing amount of interest due to their potential application in nonlinear optical (NLO) devices. This interest is motivated not only by the large NLO response, but also by the low dielectric constant, ease of processing, physical robustness and ready availability of such materials. Organic molecules can also be tailored to possess high hyperpolarizabilities and may be processed into good optical quality thin films and NLO active crystals.[16] Organic materials are now being designed into organized films for a variety of functions and applications. In the past, organic films were considered to be too fragile and of insufficient purity to yield consistent properties and render useful. However, with newly developed materials, many new compounds and polymers are being synthesized and made into thin films by a variety of techniques.[17] Significant progress had been made in the design and preparation of chromophores with large hyperpolarizabilities for use in electro-optic applications. There has been an increase in the use of organic thin films in many electronic, optical and mechanical devices. For example, organic photoconductors are being used in copiers and printers. Liquid crystal displays are now common in watches and laptops. Some new applications of organic thin films are light emitting diodes (LEDs), nonlinear optical (NLO) materials, photorefractives and organic transistors.[18]

Electro-Optic Effect

The electro-optic (EO) effect is described as the modification of optical parameters produced by the application of low-frequency electric fields. Specifically, the EO effect refers to changes in the optical dielectric tensor of a medium when a low frequency field is applied to the medium.[19] This effect is achieved by placing the medium between two electrodes and applying a voltage to the electrodes. The EO effect can alter the absorption as well as refraction properties of the medium. A change in the refractive properties with an applied electric field is an effect called electro-refraction. This phenomenon is most commonly referred to as the linear electro-optic effect. For a nonlinear optical medium in the presence of both an optical field (oscillating at optical frequency ω) and an applied electric field, the second-order nonlinear polarization of the medium can be written as

$$P_i^{\omega} = 2\varepsilon_0 \chi_{ijk}^{(2)} \left(E_j^{\omega}\right)\left(E_k^{\omega}\right) \tag{2.5}$$

where ε_0 is the dielectric constant, $\chi^{(2)}$ is the second order susceptibility, E_j and E_k are the electric fields and the subscripts refer to the directions of polarization of the fields. Using symmetry relations and the refractive index tensor n_{ijk}, the electro-optic (or Pockels) tensor r_{ijk} is derived

$$r_{ijk} = -\frac{2\chi_{ijk}^{(2)}}{n_i^2 n_j^2} \tag{2.6}$$

The symmetry of the electro-optic tensor and tensor algebra is used to reduce the first two subscripts and write $r_{ijk} = r_{jik} \rightarrow r_{lk}$. The subscripts are then transformed to numbers, which gives the familiar convention of the linear electro-optic coefficient r_{33}.

The electro-optic effect is significant in the area of device development because the electric-field induced variation of refractive index allows the fabrication of various types of modulators and switches for use in fiber optic networks and communications devices. A commonly-studied type of modulator is a Mach-Zender (MZ) interferometer. In this device, the application of an electric field to one arm of the MZ results in a phase shift of incoming light relative to the signal propagating through the second arm and destructive interference at the device output.[20]

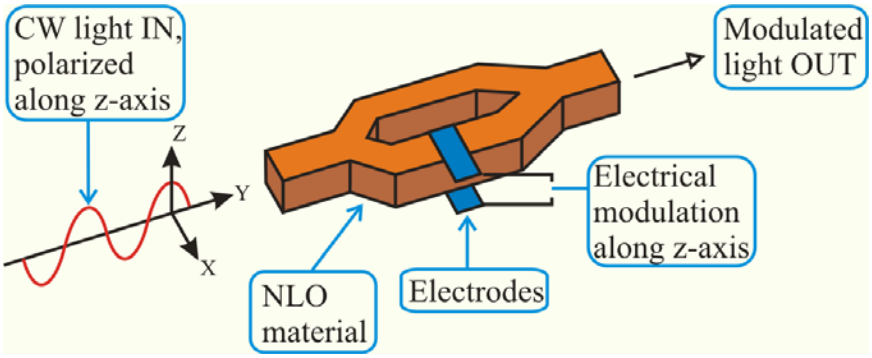

Figure 1. Schematic of MZ interferometer.

EO modulators are designed to operate with a minimal halfwave voltage V_π (preferably, less than 1 V). The voltage required to obtain a phase shift of π is described as

$$V_\pi = \frac{\lambda h n}{2L\chi^{(2)}} \tag{2.7}$$

where h is the height of the device, L is the arm length and n is the refractive index.

The linear electro-optic coefficient r_{33} of polymeric electro-optic materials is often measured using optical interferometry. The most commonly used methods for measuring the EO effect include the waveguide method,[21] the Michelson[22,23] interferometer, the Fabry–Perot interferometer,[24,25,26] Mach–Zehnder interferometer [27,28,29,30] and the reflection method.[31,32] An EO measurement can be performed using a number of configurations including two-beam wavefront interferometry and single-beam polarization interferometry. The single-beam reflection interferometry method was introduced by Teng and Man and later modified by others[33] This method is based on the polarization rotation of a laser beam due to the electro-optic effect. The EO effect is measured while a polymeric film undergoes low-voltage electrical poling. For this technique, the electro-optic coefficient is defined as

$$r_{33} = \frac{3\lambda I_m}{4\pi V_m I_c} \frac{\left(n^2 - \sin^2\theta\right)^{1/2}}{n^2 \sin^2\theta} \tag{2.8}$$

where λ is the wavelength of light, I_m is the modulation amplitude, I_c is the half-max laser intensity, V_m is the applied modulation voltage, θ is the incident angle of the laser beam and n is the refractive index of the film without an applied electric field, also known as n_0. This method is relatively complicated, but has proven to be (1) more time efficient and (2) more tolerant of light absorption, often encountered in polymer systems, than the more conventional waveguiding method. With all of these factors considered, the reflection method has proven to lend an accurate and widely-used technique to measure the electro-optic coefficient for polymeric electro-optic devices.

Refractive index is one of the most important parameters in determining the nonlinear optical susceptibility as well as designing optical waveguides, because the propagation of waves is dominated by the refractive index *n* of a substrate, waveguide layer and overlying layers. The refractive index is modified by the electro-optic coefficient r_{33} by

$$n = n_0\left(1 - \frac{1}{2} n_0^2 r_{33} E\right) \tag{2.9}$$

where *n* is the refractive index, and *E* is the applied electric field.

NLO Film Fabrication Methods

Ordered thin organic films ranging in thickness from a few to several hundred nanometers currently hold considerable technological promise. Electronic and optical devices incorporate structures in this thickness range and organic thin films have been proposed as fabrication components. Several experimental techniques have been developed for creating nonlinear optically (NLO) active thin films suitable for optical communication and photonic devices.[34,35,36,37,38,39] Organic materials that have been studied for second-order nonlinear fall into several categories Langmuir-Blodgett (LB) films, poled polymers and self-assembled paradigms.

Poled Polymer Films

By the method of poled polymer films,[40,41,42] spin-cast chromophores are aligned above glass transition temperature T_g by an electric poling field for a specified time on the order of minutes to hours.

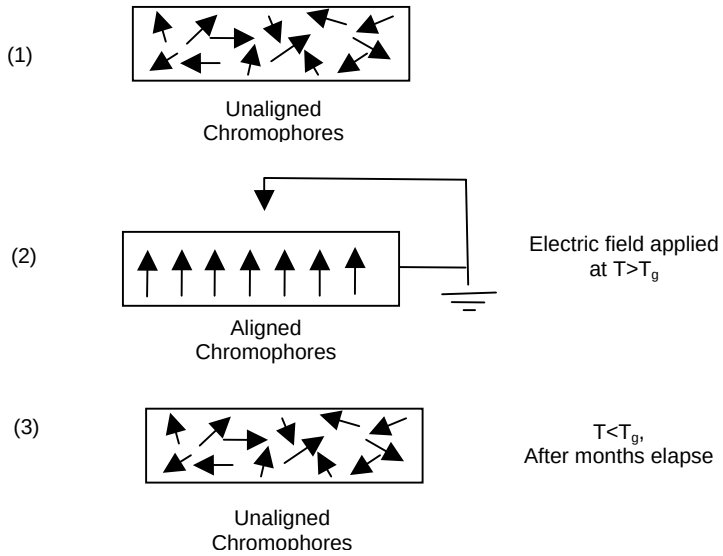

Figure 2. Schematic representation of poled polymer films generated by corona poling.

After poling, the polymer film sample, is cooled by a rapid quench below glass transition temperature of the composite, resulting in an oriented film. Shi et al. have demonstrated poled polymer devices with full optical modulation at V_{π}<1 V and a frequency >100 GHz.[43] Singer and Dalton and coworkers have produced poled polymer films with $\chi^{(2)}$ values in the range of 10^{-8} to 10^{-9} esu. Poled polymer films face challenges for practical device application due to the instability of the acentric alignment of the chromophores, which degrades over the course of weeks or months at ambient conditions. This degradation of the chromophore orientation is problematic for EO devices due to the decay of the EO coefficient as a result of corresponding loss of chromophore alignment. Improved films can be fabricated through the use of cross-linking agents and specially-designed chromophores.[44,45] The state of the art in poled polymers has been claimed by Dalton et al.[46] In this work a poled polymer dendrimer with high poling efficiency was developed. The film was found to have an electro-optic coefficient (r_{33}= 60 pm/V) twice that of lithium niobate. Furthermore, the films were found to exhibit unmatched thermal stability at 85°C for 1000 hours. Development of poled polymer films with a high poling efficiency, large NLO response and good thermal stability are still in development.

Alternating Layer Methods

The study of alternating film structures has attracted wide attention,[47,48,49] as it has been seen as the road to the formation of practical devices which might compete favorably with devices formed using alternate methods.

Langmuir-Blodgett Films

Langmuir-Blodgett films[50,51,52] (LB) are formed by a deposition process composed of alternating dipping steps. These films are formed with molecules intrinsically aligned by the self-assembly process itself. LB films have been seen as a potential prevention of the orientational relaxation seen in poled polymer films. On the upward stroke, hydrophilic interaction is responsible for adhesion. The deposition ratio is defined as the ratio of the area of film deposited to the change in area at the air/water interface corresponding to this deposition. If this deposition ratio is near one for both upward and downward strokes, the material is said to be deposited in the Y mode (Figure 3).

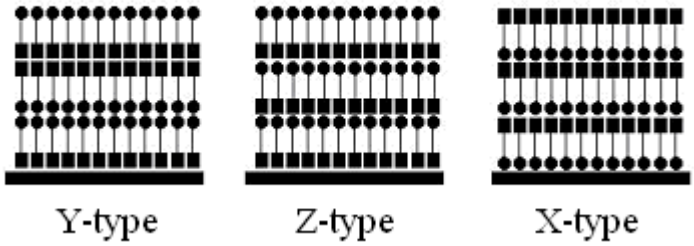

Figure 3. Schematic of the various Langmuir-Blodgett film types.

If this ratio is near one on the up stroke and near zero on the down stroke, the deposition is said to be in the Z mode and the opposite situation leads to deposition in the X mode. Z and X deposition would lead to a noncentrosymmetric structure in some cases. But in many cases, there is some degree of rearrangement after deposition so that apparent X or Z deposition leads to a structure similar to that which one would achieve Y deposition and a structure of regular bilayers is produced. Langmuir-Blodgett films are desirable due to their cost-effective fabrication and fine control on film thickness and refractive index. However, due to requirements of high surface planarity, suitable substrates for LB film deposition are limited in number. Frequently, problems typically arise with LB films in the form of poor mechanical stability and high propagation losses due to scattering and insufficient thickness.[53]

Organosilane Films

Self-assembled organosilane[54,55,56,57] films have also produced NLO-active films with high nonlinear responses $\chi^{(2)}$. The process involves a layer-by-layer assembly process for the formation of intrinsically polar thin films using functionalized, protected deprotecting agents (Figure 4).

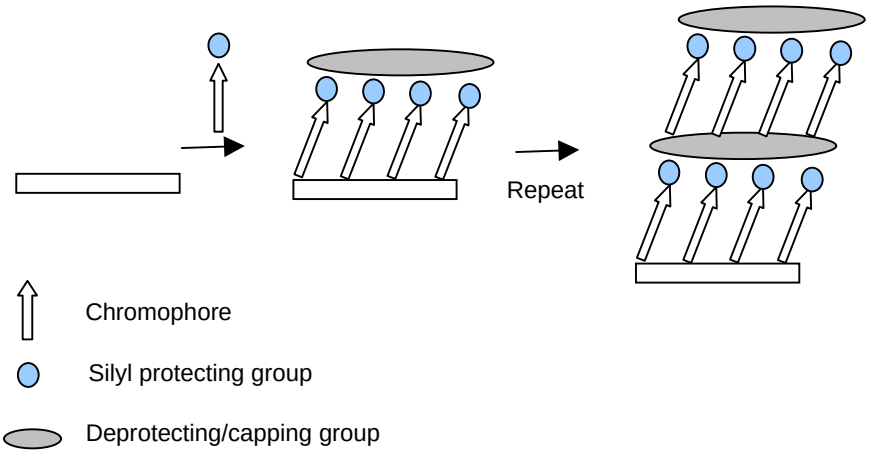

Figure 4. Schematic representation of the two-step organosilane self-assembly method.

The chromophore is covalently attached to the system, yielding closely packed films which promote chromophore alignment. Furthermore, chromophore orientation is fixed by covalent cross-links promoting notable temporal stability within the films. Wang et al. have produced siloxane-based films with high $\chi^{(2)}$ values (>100 x 10^{-9} esu), quadratic growth of second harmonic intensity with film thickness and good thermal stability. However, the process requires complex, prolonged synthesis of interlayer precursors. Also, with deposition times nearing 40 minutes per bilayer (3.2 nm/40 minutes), this method has limitations for practical film fabrication due to lengthy processing times.

Polymer-Polymer ISAM Deposition

The ionically self-assembled monolayer (ISAM) technique for the deposition of polyelectrolytes has been reviewed in a number of recent papers.[58,59,60] The method involves the

alternate dipping of a charged substrate into an aqueous solution of a polyanion and polycation at room temperature. The advantages of this technique include simple, rapid, inexpensive production and long-term stability of the acentric $\chi^{(2)}$ without the need for additional processing such as electric-field poling or chemical reactions. Polymer-polymer ISAM films fabricated by Heflin et al.[61] exhibited linear scaling of $I_{2\omega}^{½}$ vs film thickness (up to 120 nm), demonstrating the uniform maintenance of orientation with layer-by-layer growth. This effort has produced the only successful attempt of any group working with films of this type thicker than a few tens of bilayers. In addition, the films exhibited exceptional thermal stability with no measurable decay of $\chi^{(2)}$ at 150°C for more than 15 hours, in sharp contrast to electric-field poled polymers. However, the films exhibited modest $\chi^{(2)}$ values, typically ~ 1x 10^{-9} esu, in comparison to other organic films, likely due to (1) the necessity of dipole orientation towards layers both above and below the polymeric layer, resulting partial cancellation of orientation, (2) the random orientation of dipoles within thicker monolayers, and (3) steric constraints on orientation induced by bulky chromophores on the polymer backbone.

Hybrid Covalent Method

A novel layer-by-layer methodology for fabricating NLO thin films has been developed[62,63] with the aim of increasing the stability of chromophore-dipole orientation, reducing steric constraints from polymer-backbone attachment (often encountered in traditional ISAM films) and producing a large nonlinear optical response. This method builds films layer-by-layer by alternately immersing a substrate into aqueous solutions of an NLO-active polyelectrolyte “glue” and a reactive chromophoric dye. The adsorption of the layers alternates between electrostatic interaction and covalent reaction.

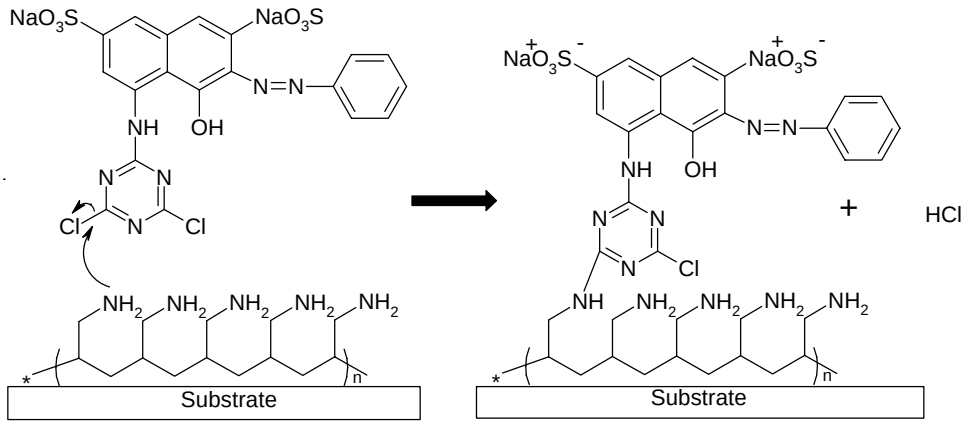

Figure 5. Schematic of hybrid deposition process with Procion Red MX-5B and PAH.

The chromophore is attached covalently which yields anisotropic ordering and high second-order NLO activity in these films. The hybrid deposition method has proven capable of producing films with regular layer-by-layer growth with sustained chromophore orientation. Films with quadratic scaling of square root of second harmonic intensity with film thickness have been fabricated for films up to 100 nm as described in Chapter 4. This lends a promising prospect for fabrication of a thick film (>500 nm). Prior analysis of hybrid covalent/electrostatic self-assembled systems for EO device applications has pointed to processing time and thermal stability as primary areas of weakness. However, recent studies have made two key advancements in these areas: (1) Findings show that a 60% reduction in deposition time (5 minutes to 2 minutes) can be achieved with negligible effect to nonlinear optical activity. (2) Films fabricated from this novel class of films exhibit excellent thermal stability at 150°C with only a 9% decrease in $\chi^{(2)}$. Films have been found to exhibit no permanent loss in SHG activity with hours 24 hours of heating at 150°C and 36 hours at 85°C. However, the films yield modest $\chi^{(2)}$ values (typically ~10 x 10^{-9} esu) that will be addressed with novel, synthesized chromophores.

It has been found that pH and ionic strength have significant effects on the properties of ISAM films including absorbance, nonlinear optical activity and layer thickness. The ionic strength I_{eff} for a charged species in solution is given as

$$I_{eff} = \frac{1}{2}\sum_i c_i\left(z_i^2\right) \tag{2.10}$$

where c is the polymer concentration and z is the counterion valency. Assuming counterion condensation occurs, the relationship for solution containing polyelectrolyte and salt is[64]

$$I_{eff} = \frac{1}{6}c_{poly} + c_{NaCl} + 10^{-pH} + 10^{-pH} \tag{2.11}$$

The conformation of a polyelectrolyte in solution is determined in part by the Debye length κ^{-1}. The Debye length is the characteristic length scale for electrostatic interactions in solution and (for water at 25°C and in units of nm^{-1}) is given by[65]

$$\kappa^{-1} = \frac{0.32}{I_{eff}^{1/2}} \tag{2.12}$$

As the Debye length is reduced, the repulsion of neighboring ions on the polymer is reduced to electrostatic screening by the counterions. This, in turn allows more curvature in the polymer backbone or a reduction in chain stiffness. At low ionic strengths, where the screening is low, the polyelectrolyte adopts an extended conformation and adsorbs onto an oppositely charged surface in a flat, train-like conformation. With an increase in ionic strength, fixed charges on the polymer chain and between the surfaces are increasingly screened and the polymer gains conformational entropy by extending into the solution.[66] The amount of polymer absorbed on an oppositely charged surface increases with more segments adsorbed as loops and tails, resulting in a thicker adsorbed layer. The ability to control the bilayer thickness by adjusting the parameters of the immersion solutions illustrates the power and versatility of the ISAM process.

Kinetics of Adsorption

Polymer Adsorption

The kinetics of adsorption of charged molecules onto a charged surface has been probed in several studies.[67,68] The rate of adsorption of polymers is mainly determined by two processes: (1) transport of the polymer by convection and/or diffusion from the solution to the surface, and (2) attachment to the interface. The second step may consist of the rearrangement of the polymer chain toward an adsorbed state with increased entropy.[69] The adsorbed amount Γ (mg/m^2) of a

charged polymer species onto an oppositely charged substrate is found to occur in the following kinetic steps. Initially, Γ increases linearly with time (Figure 6), implying diffusion-controlled adsorption. This stage is followed by a region where the rate of adsorption dΓ/dt dramatically slows. Finally, the surface adsorption reaches a plateau value Γ_p where Γ remains constant with time.

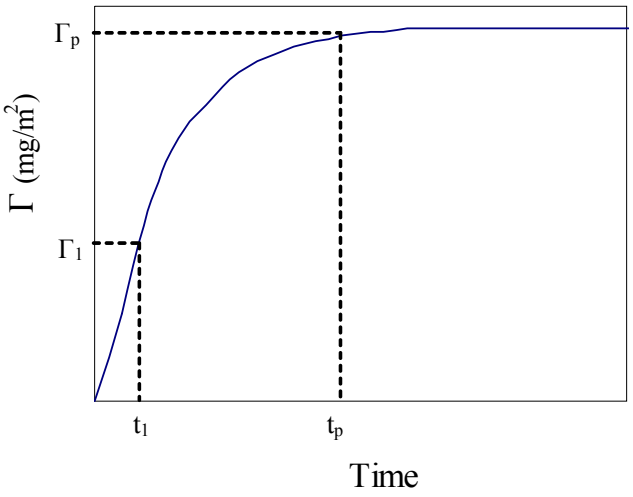

Figure 6. Surface coverage Γ of charged polymer onto an oppositely charged surface as a function of time.

In the process of reaching a stable equilibrium state, polymer adsorption is thought to undergo a stage of adsorption reversibility.[70,68] Studies have shown that the adsorption process approaches a non-equilibrium, reversible stage dominated by a resistant barrier, mainly kinetic in nature.[70,71,72] These studies have focused on the relevant parameters driving the adsorption process, leading to a relationship that describes the height of the electrostatic barrier that builds up as a charged polyelectrolyte adsorbs onto a charged substrate. As the surface coverage Γ increases, a number of driving and resistance effects factor into surface adsorption. Electrostatics drive the adsorption process, but coincidentally limit it due to the repulsion arising from the accumulation of charges at the surface. The incoming molecules experience an electrostatic repulsion with the charged polymers already adsorbed to the surface, hindering further adsorption. The height of the electrostatic barrier has been analyzed from a kinetically-focused approach. The adsorption flux is the ratio of the polymer adsorption driving force to the resistance hindering adsorption. The adsorbing flux is defined by Geffroy et al. as

$$\frac{d\Gamma}{dt} = \frac{C_{bulk} - C_{eq}(\Gamma)}{R^{tr} + R^{e}} \tag{2.13}$$

where C_{bulk} is the bulk concentration at the surface of the adsorbing layer, C_{eq} is the equilibrium concentration, R^{tr} is the transport-limiting resistance and R^{e} is the electrostatic resistance.

The kinetics of adsorption directly depends upon the height of the electrostatic barrier encountered after the polymer approaches the charged surface. High electrostatic barriers lead to a previously described non-equilibrium state which can be reduced by electrostatic screening. Such increases are characteristically introduced by an increase in ionic strength (equation 2.10).

Studies of the kinetics of polyelectrolyte adsorption onto a charged substrate by Geffroy et al. show that most of the deposition of a charged self-assembled polymer film could take place in less than a minute given appropriate deposition conditions that would minimize the electrostatic barrier (i.e. concentration, ionic strength, flow conditions and pH).[73]

Azo Dye Adsorption

Surface-Reaction Dominated Kinetics

The deposition kinetics of the NLO chromophore Procion Red onto poly(alyllamine hydrochloride) {PAH} films were measured by C. Brands using *in-situ* second harmonic generation (SHG) measurements[74,75] and modeled using a Langmuir-type growth model.[76] In this model the adsorbed molecules are assumed to be non-interacting, but inhibiting to other molecules landing on the adsorption site. The amount of material deposited per unit time is given by

$$\frac{dq}{dt} = K_f\, C\left(q_m - q\right) - K_r q \tag{2.14}$$

where q is the amount of material deposited, q_m is one full monolayer coverage, C is the concentration, K_f is the adsorption rate and K_r is the desorption rate. The density of coverage is defined as $Q = q/q_m$. The coverage density Q can be calculated from the coverage density flux dQ/dt

$$q_m \frac{dQ}{dt} = K_f C(q_m - q_m Q) - K_r q_m Q \tag{2.15}$$

$$Q = \frac{1 - \exp[-(1+L)K_f Ct]}{1+L} \tag{2.16}$$

where L is defined as K_r/K_fC. For in-situ experiments, $K_fC >> K_r$ and $L<<1$. The square root of the SHG signal of the film is proportional to the amount of deposited material Q. This relation is expressed as:

$$\sqrt{SHG_{film}} \propto Q = 1 - \exp(-K_f Ct) \tag{2.17}$$

where K_f is the attachment rate constant, C is the concentration of dye in solution and t is the deposition time. Cited values for K_f at Procion Red concentrations studied are given as

Table 1. Attachment rate constant as a function of Procion Red concentration for in-situ SHG kinetic studies. Values corrected from original values cited in Brands' thesis.

Procion Red Conc. (mM)	K_f (mg/ml-s)
1	0.068
0.1	0.2
0.01	0.18

The *in-situ* data for Procion Red film formation show a rapid increase in film adsorption followed by stabilization of film deposition rate after ~1 minute (Procion Red concentration= 1 mM, 0 M added NaCl, pH 10.0).

Diffusive-Transport Dominated Kinetics

A diffusion model was developed to model the adsorption of an incoming dye molecule in the absence of convective transport limitations (Figure 6). Under these conditions, the time for the molecule to diffuse to the adsorption surface is assumed far greater than the time for the molecule to attach to the surface. Therefore, the reaction rate is negligible compared to the rate of diffusion. A perfect sink condition, where the adsorption is limited by transport toward the surface, was assumed at the adsorption surface. The governing equation for diffusion-limited adsorption is described in relation to the concentration flux at the surface

$$\frac{\partial c}{\partial t} = D\frac{\partial^2 c}{\partial x^2} \tag{2.18}$$

where D is the diffusion coefficient.

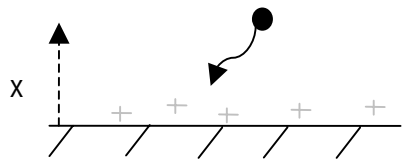

Figure 7. Orientation of adsorbing dye molecule to charged surface.

Scaling of Equation 2.18 into dimensionless parameters for concentration Θ, diffusion coefficient and time 2η, followed by the application of scaled boundary conditions describes the concentration of dye at the surface as

$$\Theta(\eta) = \frac{2}{\sqrt{\pi}}\int_0^{\eta} e^{-\eta^2}\, d\eta \tag{2.19}$$

where $\eta = x/2(Dt)^{1/2}$. Following a series of integrations, the deposited amount of dye Γ (mass or moles/area) at time t is related to the dye concentration and diffusion coefficient by

$$\Gamma(t) = 2c_0\left(\frac{Dt}{\pi}\right)^{1/2} \tag{2.20}$$

More generally for Procion Brown or Procion Red ($D \sim 2.4 \times 10^{-6}$ cm^2/sec)

$$\Gamma(t) = 17.5\, c_0 (t)^{1/2} \tag{2.21}$$

where Γ [=] mg/m^2, c_0 [=] mg/ml, t [=] sec. For example, after 1 second, $\Gamma(t)$= 87.4 mg/m^2, which is two orders of magnitude larger than coverage of one monolayer. Based on this model and assuming that the kinetics for Procion Brown are similar to those of Procion Red, film deposition at the following conditions: (1) high dye concentration (~7 times that of *in-situ* experiments), (2) high pH (>9) and (3) in the presence of added salt, this adsorption kinetics model finds that the deposition time for complete monolayer coverage q_m (Γ_{mono}=0.26 mg/m^2) of azo dyes (Procion Brown or Procion Red) via a hybrid electrostatic-covalent deposition scheme could take place within 30-120 seconds, increasing the practicality of utilizing azo dye chemistries for thick EO device films.

References

[1] Baldwin, G. C. 'An introduction to nonlinear optics' New York: Plenum Press; 1969.

[2] Franken, P. A.; Hill, L. E.; Peters, C. W.; Weinreich, G. 'Generation of optical harmonics' *Phys. Rev. Lett.* **7** (1961) 118-119.

[3] Davydov, B.E.; Derkacheva, L.D.; Dunina, V.V.; Zhabotinskii, M.E.; Zolin, V.K.; Kreneva, L.G.; Samokhina, M.A. 'Connection between charge transfer and laser second harmonic generation', *JEPT Lett.*, **12** (1970) 16-21.

[4] Clays, K.; Coe, B. 'Design strategies versus limiting theory for engineering large second-order nonlinear optical polarizabilities in charged organic molecules' *Chem. Mater.* **15** (2003) 642-648.

[5] Staub, K.; Levina, G. A.; Barlow, S.; Kowalczyk, T. C.; Lacritz, H. S.; Barzoukas, M.; Fort, A.; Marder, S. R. 'Synthesis and stability studies of conformationially locked 4-(diarylamino)aryl- and 4-(dialkylamino)phenyl-substituted second-order nonlinear optical polyene chromophores' *J. Mater. Chem.* **13** (2003) 825-833.

[6] Ki Hong Park, K. H.; Kwak, M. G.; Jahng, W. S.; Lee, C. J.; Kim, N. 'Nonlinear optical polymers with novel benzoxazole chromophores: III. Synthesis and characterization of self-crosslinkable glycidyl methacrylate copolymers' *Reactive and Functional Polymers* **40** (1999) 41-49.

[7] Park, K. H.; Yeon, K. M.; Lee, M. Y., Lee, S. -D., Shin, D. -H., Lee, C. J.; Kim, N. 'Synthesis and nonlinear optical properties of PMMA copolymers having novel benzoxazole chromophores attached with various electron-withdrawing groups' *Polymer* **39** (1998) 7061-7066.

[8] L.-H. Peng, L.-H.; Hsu, C.,-C, Shih, Y.-C 'Second-Harmonic Green Generation from Two-Dimensional Chi[sup (2)] Nonlinear Photonic Crystal with Orthorhombic Lattice Structure' *Appl. Phys. Lett.* **83** (2003) 3447-3455.

[9] Ni, P.; Ma, B.; Wang, X.; Cheng, B.; Zhang, D. 'Second-Harmonic Generation in Two-Dimensional Periodically Poled Lithium Niobate Using Second-Order Quasiphase Matching' *Appl. Phys. Lett.* **82** (2003) 4230-4238.

[10] Zeng, X.; Chen, X.; Chen, Y.; Xia, Y.; Chen, Y. 'Observation of all-optical wavelength conversion based on cascaded effect in periodically poled lithium niobate waveguide' *Optics & Laser Technology* ***35*** (2003) 187-190.

[11] Kim, J. H.; Yoon, C.S. 'Domain switching characteristics and fabrication of periodically poled potassium niobate for second-harmonic generation' *Appl. Phys. Lett.* **81** (2002) 3332-3338.

[12] Beckers, L.; Buchal, C.; Fluck, D.; Pliska, T.; Günter, P. 'Potassium niobate waveguides: He^+ implantation in bulk single crystals and pulsed laser deposition of thin films' *Materials Science*

and Engineering A **253** (1998) 292-295.

[13] Fluck, D.; Pliska, T.; Günter, P.; Beckers, L.; Buchal,C. 'Blue-light second-harmonic generation in ion-implanted KNbO[sub 3] channel waveguides of new design' *Appl. Phys. Lett.* **69** (1996) 4133-4139.

[14] Kitamura, K.; Yamamoto, J. K.; Iyi, N.; Kimura, S. 'Stoichiometric $LiNbO_3$ single crystal growth by double crucible Czochralski method using automatic powder supply system' *J. Crystal Growth* **116** (1992) 327-343.

[15] Takagi, T.; Fujii, T.; Sakabe, Y. 'Growth and characterization of $KNbO_3$ by vertical Bridgman method' *Journal of Crystal Growth* **259 (**2003) 296-301.

[16] Lee, K. –S. *Polymers for Photonics Applications II*, Heidelberg, Germany: Springer-Verlag, 2003.

[17] He, M.; Zhu, J.; Harper, A. W.; Sun, S.; Dalton, L. R.; Garner, S. M.; Chen, A.; Steier, W. H.Chapter 19 in " Progress toward the translation of large microscopic nonlinearities to large macroscopic nonlinearities in high-μβ materials" (2001) 586.

[18] Yesodha, S. K. 'Stable polymeric materials for nonlinear optics: a review based on azobenzene systems' *Prog. Polym. Sci.* **29** (2004) 45-74.

[19] Sutherland, R. L. *Handbook of Nonlinear Optics*, Marcel Dekker, (2003).

[20] Lindsay, G. A. 'Second-order nonlinear optical polymers: an overview' In: Lindsay, G. A. *Polymers for second-order nonlinear optics* American Chemical Society, Washington, DC (1995) Chapter 1.

[21] Horsthius, W. H. G.; Krijnen, G. J. M. 'Simple measuring method for electro-optic coefficients in poled polymer waveguides' *Appl. Phys. Lett.* **55** (1989) 616-618.

[22] Maertens, C.; Detrembleur, C.; Dubois, P.; Jérôme, R.; Blanche, P.-A.; Lemaire, Ph. C. 'Synthesis and electrooptic properties of a new chromophore dispersed or grafted in a carbazolyl methacrylate matrix' *Chem. Mater.* **10** (1998) 1010 -1016.

[23] Ding, Y. J.; Mu, X.; Yin, X. 'Electro-optic and electromechanical properties of poled polymer thin films' *Appl. Phys. Lett.* **79** (2001) 3749-3751.

[24] Meyrueix, R.; Dickens, M. J.; Lemonnier, O.; Lecomte, J. P.; Tapolsky, G. 'Fabry-Pérot interferometry applied to the study of piezoelectric and electro-optical properties of a poled NLO polyurethane' *Opt. Comm.* **110** (1994) 445-455.

[25] Zhang, D. M.; Yi, M. B.; Tian, X. J.; Sun, W.; Hou, A. L.; Sun, J. Z.; Ma, Y. G.; Tian, W. J.; Shen, J. C. 'External electro-optic measurement utilizing poled polymer-based asymmetric Fabry-Perot reflection film' *J. Appl. Phys.* **86** (1999) 6184-6188.

[26] Chen, K. X.; Yang, H.; Zhang, H. B.; Zhao, Y.; Yi, M.B. 'Sampling high-frequency signals using a poled-polymer asymmetric Fabry-Perot microcavity as an electro-optic probe tip' *Appl. Phys. B* **74** (2002) 363-366.

[27] Cho, H. R.; Shin, M. J.; Han, S. H.; Wu, J. W. 'Mach–Zehnder interferometer measurement of the Pockels effect in a poled polymer film with a coplanar electrode structure' *Appl. Phys. Lett*. **69** (1996) 3788-3790.

[28] Song, H. –C.; Oh, M. –C.; Ahn, S. –W.; Steier, W. H.; Fetterman, H. R.; Zhang, C. 'Flexible low-voltage electro-optic polymer modulators' *Appl. Phys. Lett.* **82** (2003) 4432-4434.

[29] Ribeiro, P. A.; Balogh, D. T.; Fonseca, J. L. C.; Giacometti, J. A.; 'Chromophore Relaxation in a Side-Chain Methacrylate Copolymer Functionalized with 4-[*N*-Ethyl-*N*-(2-hydroxyethyl)]amino-2'-chloro-4'-nitroazobenzene' *Macromolecules* **37** (2004) 2618-262.

[30] Geis, W.; Sinta, R.; Mowers, W.; Deneault, S. J.; Marchant, M. F.; Krohn, K. E.; Spector, S. J.; Calawa, D. R.; Lyszczarz T. M. 'Fabrication of crystalline organic waveguides with an exceptionally large electro-optic coefficient' *Appl. Phys. Lett.* **84** (2004) 3729-3731.

[31] Teng, C. C.; Man, H. T. 'Simple reflection technique for measuring the electro-optic coefficient of poled polymers' *Appl. Phys. Lett*. **56** (1990) 1734-1736.

[32] Shuto, Y.; Amano, M. 'Reflection measurement technique of electro-optic coefficients in lithium niobate crystals and poled polymer films' *J. Appl. Phys.* **77** (1995) 4632-4638.

[33] Mortazavi, M. A.; Knoesen, A.; Kowel, S. T.; Henry, R. A.; Hoover, J. M.; Lindsay, G. A. 'Second-order nonlinear optical properties of poled coumaromethacrylate coplymers' *Appl. Phys. B* **53** (1991) 287-294.

[34] Thakur, M.; Titus, J.; Mishra, A. 'Single-crystal thin films of organic molecular salt may lead to a new generation of electro-optic devices' *Opt. Eng.* **42** (2003) 456-458.

[35] Koeste, M.; Laschewsky, A.; Jonas, A. M.; Verbiest, T. 'Orientation of functional groups in polyelectrolyte multilayers studied by second-harmonic generation (SHG)' *Colloids and Surface A* **198-200** (2002) 275-280.

[36] Koeste, M.; Laschewsky, A.; Verbiest, T. 'Films grown from polyamines and reactive dyes by alternating polyelectrolyte adsorption/surface activation (CoMPAS)' *Materials Science and Engineering* **10** (1999) 107-133.

[37] Guo, L. J.; Cheng, X.; Chao, C. Y. 'Fabrication of photonic nanostructures in nonlinear optical polymers' *J. Mod. Opt.* **49** (2002) 663-673.

[38] Kaino, T. 'Waveguide fabrication using organic nonlinear optical marerials' *J. Opt. A: Pure Appl. Opt.* **2** (2002) R1-R7.

[39] Bertrand, P.; Jonas, A.; Laschewsky, A.; Legras, R. 'Ultrathin polymer coatings by complexation of polyelectrolytes at interfaces: suitable materials, structures and properties' *Macromol. Rapid Commun.* **21** (2000) 319-348.

[40] Yu, H.H.; Hwang, S.-J. 'E-O functional waveguide using the electric-field-poled polymeric material for integrated-optic devices' *Optics Communications* **219** (2003) 183-192.

[41] Shi, Y,; Zhang, H.; Bechtel, J. H.; Dalton, L. R.; Robinson, B.H.; Steier, W. H.; 'Low (Sub-1-Volt) halfwave voltage polymeric electro-optic modulators achieved by controlling chromophore shape' *Science* **288** (2000) 119-122.

[42] Dalton, L. R. 'Polymeric electro-optic materials: optimization of electro-optic activity, minimizatiojn of optical loss, and fine-tuning of device performance' *Opt. Eng.* **39** (2000) 589-595.

[43] Shi, Y.; Zhang, C.; Bechtel, J. H.; Dalton, L. R.; Robinson, B. H.; Steier, W. H. 'Low halfwave voltage polymeric electro-optic modulators achieved by controlling chromophore shape' *Science* **288** (2000) 119-122.

[44] Jungbauer, D.; Reck, B.; Twieg, R.; Yoon, D. Y.; Wilson, C. G.; Swalen, J. D. 'Highly efficient and stable nonlinear optical polymers via chemical crosslinking under electric field' *Appl. Phys. Lett.* **56** (1990) 2610-2612.

[45] Ma, H.; Liu, S.; Luo, J.; Suresh, S.; Liu, L.; Kang, S.; Haller, M.; Sassa, T.; Dalton, L. R.; Jen, A. K. –Y. 'Highly efficient and thermally stable electro-optical dendrimers for photonics' *Adv. Funct. Mater.* **12** (2002) 565-574.

[46] Ma, H.; Liu, S.; Luo, J.; Suresh, S.; Liu, L.; Kang, S. H.; Haller, M.; Sassa, T.; Jen, A. K. Y.; Dalton, L. R. 'Highly efficient and thermally stable electro-optical dendrimers for photonics' - *Adv. Funct. Mater* **12** (2002) 565-574.

[47] Bertrand, P.; Jonas, A.; Laschewsky, A.; Legras, R. 'Ultrathin polymer coatings by complexation of polyelectrolytes at interfaces: suitable materials, structure and properties' *Macromol. Rapid Commun.* **21** (2000) 319-348.

[48] Lvov, Y.; Ariga, K.; Onda, M.; Ichinose, I.; Kunitake, T. 'A careful examination of the adsorption step in the alternate layer-by-layer assembly of linear polyanion and polycation' *Coll. And Surf. A: Phys. And Eng. Asp* **146** (1999) 337-346.

[49] Ariga, K.; Lvov, Y.; Kunitake, T. 'Assembling alternate dye-polyion molecular films by electrostatic layer-by-layer adsorption' *J. A. Chem. Soc.* **119** (1997) 2224-2231.

[50] Sottini, S.; Grando, D.; Palchetti, L.; Giorgetti, E.; Ricceri, R.; Gabrielli, G. 'Organic films for guided nonlinear optics' *Materials Science and Engineering* **C5** (1998) 167-172.

[51] Ashwell, G. J.; Jackson, P. D.; Crossland, W. A. 'Noncentrosymmetry and second harmonic generation in Z-type Langmuir-Blodgett Films' *Nature* **368** (1994) 438-440.

[52] Decher, M. 'Molecular multilayer films: the quest for order, orientation and optical properties' in Photonic and Optoelectronic Polymers, Jenekhe, S. A.; Wynne, K. J., Ed. American Chemical Society (1995) 445-450.

[53] Sottini, S.; Grando, D.; Palchetti, L.; Giorgetti, E.; Ricceri, R.; Gabrielli, G. 'Organic films for guided nonlinear optics' *Materials Science and Engineering* **C5** (1998) 167-172.

[54] Zhu, P.; van der Boom, M. E.; Kang, H.; Evmeneko, G.; Dutta, P.; Marks, T. J. 'Realization of expeditious layer;by-layer siloxane-based self-assembly as an efficient route to structurally regular acentric superlattices with large electro-optic responses' *Chem. Mater.* **14** (2002) 4982-4989.

[55] Fachetti, A.; Abbotto, A.; Beverina, L.; van der Boom, M. E.; Dutta, P.; Evmeneko, G.; Pagano, G. A.; Marks, T. J. 'Layer-by-layer self-assembled pyrrole-based donor-acceptor chromophores as electro-optic materials' *Chem. Mater.* **15** (2003) 1064-1072.

[56] Zhao, Y. –G.; Chang, S.; Wu, A.; Lu, H. –L.; Ho, S. T.; van der Boom, M. E.; Marks, T. J. 'Second-generation approach to all-organic modulators based on intrinsically polar self-assembled molecular superlattices' *Opt. Eng.* **42** (2003) 298-299.

[57] Wang, W.; Zhu, P.; Marks, T. J.; Ketterson, J. B. 'Ultrafast frequency-selective optical switching based on thin self-assembled organic chromophoric films with a large second-order nonlinear response' *Appl. Phys. Lett.* **81** (2002) 2169-2171.

[58] Decher, G.; Hong, J. D.; Schmitt, J. 'Buildup of ultrathin multilayer films by a self-assembly process: consecutively alternating adsorption of anionic and cationic polyelectrolytes on charged surfaces' *Thin Solid Films* **210/211** (1992) 831-835.

[59] Hammond, P. T. 'Recent explorations in electrostatic multilayer thin film assembly' *Current Opinion in Colloid & Interface Science* **4** *(1999)* 430-442.

[60] Kotz, J.; Kosmella, S.; Beitz, T. 'Self-assembled polyelectrolyte systems' *Prog. Poly. Sci.* **26** (2001) 1199-1232.

[61] Heflin, J. R. 'Thickness dependence of second harmonic generation in thin films fabricated from ionically self-assembled monolayers' *Appl. Phys. Lett.* **74** (1999) 495-497.

[62] Van Cott, K. E.; Guzy, M.; Neyman, P.; Brands, C.; Heflin, J. R.; Gibson, H. W.; Davis, R. M. 'Layer-by-layer deposition and ordering of low-molecular weight dye molecules for second-order nonlinear optics' *Angew. Chem. Int. Ed.* **41** (2002) 3236-3328.

[63] Heflin, J. R.; Neyman, P. J.; Guzy, M.; Shah, S. M.; Davis, R. M.; Van Cott, K. E.; Wang, H.; Gibson, H. W.; Brands, C. 'Hybrid covalent/ionic self-assembly of organic second order nonlinear optical films, in Organic Thin Films for Photonic Applications, OSA Trends in Optics and Photonics Series **64** (2002) 3-8.

[64] Manning, G. 'Limiting laws and counterion condensation in polyelectrolyte solutions. IV. The approach to the limit and the extraordinary stability of the charge fraction' *Biophysical Chemistry* **7** (1977) 95-102.

[65] Shaw, D. "Introduction to Colloid and Surface Chemistry" Butterworth Heinemann, Boston 1996.

[66] Evans, D. F.; Wennerström, H., Ed. "The colloidal domain:where physics, chemistry, biology and technology meet" Wiley, New York (1999) 392.

[67] Koopal, L. K.; Avena, M. J. 'A simple model for adsorption kinetics at charged solid-liquid interfaces' *Colloids and Surfaces A* **192** (2001) 93-107.

[68] Cohen Stuart, M. A.; Hoogendam, C. W.; de Keizer, A. 'Kinetics of polyelectrolyte adsorption' *J. Phys.: Condens. Matter* **9** (1997) 7767-7783.

[69] Dijt, J. C.; Cohen Stuart, M. A.; Fleer, G. J. 'Reflectometry as a tool for adsorption studies' *Adv. Colloid Interf. Sci.* **50** (1994) 79 -104.

[70] Göbel, J. G.; Besseling, N. A. M.; Cohen Stuart, M. A.; Poncet, C.; 'Adsorption of hydrophobically modified polyacrylic acid on a hydrophobic surface: hysteresis caused by an electrostatic adsorption barrier' *Journal of Colloid Interface Science* **209** (1999) 129 - 135.

[71] De Laat, A. W. M.; Van den Heuvel, G. L. T.; Böhmer, M. R. 'Kinetic aspects in the adsorption of polyacrylic acid salts onto BaTiO3' *Colloids Surf. A: Physiochem. Eng. Aspects* **98** (1995) 61 - 71.

[72] Geffroy, C.; Persello, J.; Foissy, A.; Cabane, B. 'Molar mass selectivity in the adsorption of polyacrylates on calcite' *Colloids Surf. A: Physiochem. Eng. Aspects* **162** (2000) 107-121.

[73] Geffroy, C.; Labeau, M. P.; Wong, K.; Cabane, B.; Stuart, M. A. 'Kinetics of adsorption of polyvinylamine onto cellulose' *Colloids and Surfaces A* **172** (2000) 47-56.

[74] Brands, C.; Neyman, P. J.; Guzy, M. T.; Shah, S.; Davis, R. M.; Van Cott, K. E.; Wang, H.; Gibson, H. W.; Heflin, J. R. 'In situ measurements of the formation of ionically self-assembled monolayers by second harmonic generation' *MRS Symp. Proc.* **707** (2002) DD12.5.1-6.

[75] Brands, C. 'Interface effects and deposition process of ionally self-assembled monolayer films: in situ and ex situ second harmonic generation measurements' Ph.D. Thesis, Virginia Tech 2003.

[76] Langmuir, I. 'The adsoprtion of gases on plane surfaces of glass, mica and platinum' *Am. Chem. Soc.* **40** (1918) 1361-1403.

Chapter 3

The Effect of Forced Convection and Varying Deposition Times on the Properties of Nonlinear Optical (NLO) Films

Introduction

Industrial and consumer demands for faster and cheaper optical communication devices are increasing in the digital age. Inorganic crystals, such as lithium niobate ($LiNbO_3$)[1,2,3] and potassium niobate ($KNbO_3$),[4,5,6] currently used for fiber optic systems yield high performance in the critical areas of data transmission speed and minimal optical loss, but these materials are inferior in the areas of cost, availability and lengthy processing times for crystal growth.[7-8] Since the late sixties organic molecules have attracted an increasing amount of interest due to their potential application in nonlinear optical (NLO) devices. This interest is motivated not only by the potentially large NLO response, but also by the versatility, ease of processing and ready availability of such materials. Organic molecules can also be tailored to possess high hyperpolarizabilities and may be processed into good optical quality thin films and NLO active crystals.[9] Consequently, research relating to such devices has been driven towards developing alternative methods and materials for fabricating such devices.

NLO Film Fabrication Methods

Several experimental techniques have been developed for creating nonlinear optically (NLO) active thin films suitable for optical communication and photonic devices.[10,11,12,13,14,15] Electric field poled polymer films,[16,17,18,19] Langmuir-Blodgett films[20,21] and self-assembled organosilane[22,23,24,25] films have all produced NLO-active films with high nonlinear responses. However, poled polymer films face challenges for practical device application due to the instability of the acentric alignment of the NLO chromophores, which degrades the electro-optic activity over time. Langmuir-Blodgett films are desirable due to their cheap fabrication and fine control on film thickness and refractive index. However, problems typically arise in the form of poor mechanical stability and high propagation losses due to scattering and insufficient thickness.[26] Ionic self-assembled multilayer (ISAM) films are a recently developed class of materials that allows detailed structural and thickness control at the molecular level, combined

with ease of manufacturing and low cost. Polymer-polymer ISAM films studied by Heflin et al.[27] demonstrated the unprecedented maintenance of uniform orientation with layer-by-layer growth for films thicker than a few tens of bilayers. More recently, a novel layer-by-layer methodology for fabricating NLO thin films has been developed[28,29] with the aim of increasing the stability of chromophore-dipole orientation, reducing steric constraints from polymer-backbone attachment (often encountered in traditional ISAM films) and producing a large nonlinear optical response. This method builds films layer-by-layer by alternately immersing a substrate into aqueous solutions of an NLO-active polyelectrolyte "glue" and a reactive chromophoric dye. The adsorption of the layers alternates between electrostatic interaction and covalent reaction. The chromophore is attached covalently which yields anisotropic ordering and high second-order NLO activity in these films.

Effect of Salt on Hybrid Covalent Films

It has been found that pH and ionic strength have significant effects on the properties of ISAM films including absorbance, nonlinear optical activity and layer thickness. The ionic strength I_{eff} for a charged species in solution is given as

$$I_{eff} = \frac{1}{2}\sum_i c_i\left(z_i^2\right) \tag{3.1}$$

where c is the polymer concentration and z is the counterion valency. Assuming counterion condensation occurs, the relationship for solution containing polyelectrolyte and salt is[30]

$$I_{eff} = \frac{1}{6}c_{poly} + c_{NaCl} + 10^{-pH} + 10^{-pH} \tag{3.2}$$

The conformation of a polyelectrolyte in solution is determined in part by the Debye length κ^{-1}. The Debye length is the characteristic length scale for electrostatic interactions in solution and (for water at 25°C in units if nm^{-1}) is given by[31]

$$\kappa^{-1} = \frac{0.32}{I_{eff}^{1/2}} \tag{3.3}$$

As the Debye length is reduced, the repulsion of neighboring ions on the polymer is reduced to electrostatic screening by the counterions. This, in turn allows more curvature in the polymer backbone or a reduction in chain stiffness. At low ionic strengths, where the screening

is low, the polyelectrolyte adopts an extended conformation and adsorbs onto an oppositely charged surface in a flat, train-like conformation. With an increase in ionic strength and hence electrostatic screening, the polymer gains conformational entropy by extending into the solution and the ions act as counterions for incoming charged molecules.[32] In addition, increasing the ionic screening between Procion Brown molecules allows them to pack more densely, increasing the chromophore number density *N*. The amount of polymer absorbed onto an oppositely charged surface increases with more segments adsorbed as loops and tails, resulting in a thicker adsorbed layer. The ability to control the bilayer thickness by adjusting the parameters of the immersion solutions illustrates the power and versatility of the ISAM process.

Second-order nonlinear optical properties of organic molecules are evaluated in terms of the second-order nonlinear susceptibility $\chi^{(2)}$ and hyperpolarizability β. Second-order NLO device performance is best characterized in terms of $\chi^{(2)}$ and r_{33}, the electro-optic coefficient. $\chi^{(2)}$ is related to the β of the chromophore, chromophore number density *N*, dipole tilt angle θ relative to the film normal vector and a local field effect factor *F* by:

$$\chi^{(2)} = NF\beta\left\langle \cos^3\theta \right\rangle \tag{3.4}$$

Adsorption Kinetics

The kinetics of adsorption of charged molecules onto a charged surface has been probed by several research efforts.[33,34,35] Prior studies of the kinetics of polyelectrolyte adsorption onto an oppositely charged substrate show that most of the deposition of a self-assembled polymer film could take place in less than a minute given appropriate deposition conditions (i.e. concentration, ionic strength, flow conditions and pH).[36,37] These studies have focused on the relevant parameters driving the adsorption process, leading to a relationship that describes the height of the electrostatic barrier that builds up as a charged polyelectrolyte adsorbs onto a charged substrate. In general, the adsorption rate expression for a polyelectrolyte adsorbing onto a charged surface is

$$\frac{d\Gamma}{dt} = \frac{C_{bulk} - C_{eq}(\Gamma)}{R^{tr} + R^{e}} \tag{3.5}$$

where Γ is the adsorbed amount, C_s is the bulk concentration at the surface of the adsorbing layer, C_{eq} is the equilibrium concentration, R^{tr} is the transport-limiting resistance and R^e is the electrostatic resistance. It has been shown theoretically that the resistance R^e decreasing with I_{eff}, i.e. the adsorption rate $d\Gamma/dt$ increases as the electrostatic screening increases between a charged polyelectrolyte and the layer of already adsorbed polyelectrolyte on a surface.

The deposition kinetics of the NLO chromophore Procion Red and poly(alyllamine hydrochloride) {PAH} films were measured using *in-situ* second harmonic generation (SHG) measurements[38,39] and modeled using a Langmuir-type growth model.[40] In this model the adsorbed molecules are assumed to be non-interacting, but inhibiting to other molecules landing on the adsorption site. The square root of the SHG signal of the film is proportional to the amount of deposited material Q. This relation is expressed as:

$$\sqrt{SHG_{film}} \propto Q = 1 - \exp\left(-K_f C t\right) \tag{3.6}$$

where K_f is the attachment rate constant, C is the concentration of dye in solution and t is the deposition time. The *in-situ* data for Procion Red film formation show a rapid reaction rate-controlled increase in dye deposition followed by stabilization of film deposition rate after ~2 minutes (Procion Red concentration= 1mM, 0 M added NaCl, pH 10.0). Cited values for K_f at Procion Red concentrations studied are listed in
Table 1.

Table 1. Attachment rate constant as a function of Procion Red concentration for in-situ SHG kinetic studies. Values corrected from original values cited in Brands' thesis.

Procion Red Conc. (mM)	K_f (mg/ml-s)
1	0.068
0.1	0.2
0.01	0.18

Rearranging equation 3.6,

$$t = \frac{-\ln\left(1-Q\right)}{K_f C} \tag{3.7}$$

For 99% surface coverage, i.e. Q=0.99,

$$t_{0.99} \approx \frac{4.605}{K_f C} \tag{3.8}$$

where C is the dye concentration in mg/ml. Assuming that the kinetics for Procion Brown are similar to those of Procion Red and using K_f =0.068 mg/m-s, the time required for Procion Brown to reach 99% coverage is

$$t_{0.99} \approx \frac{67.7}{C} \tag{3.9}$$

For C=5 mg dye/ml, $t_{0.99}$= 14 seconds. These estimates suggest that deposition of Procion Brown dye needed for monolayer coverage could potentially take place within 30-120 seconds assuming the following deposition conditions: (1) high dye concentration (~7 times that of *in-situ* experiments, 5 mg/ml) and (2) high pH (>9). Based on these estimates, it was hypothesized that the deposition time could be significantly reduced with complete monolayer coverage.

Prior Studies

Prior studies of the fabrication of NLO active films with the polycation poly(alyllyamine hydrochloride) and the NLO active chromophore Procion Brown yielded exceptional results in nonlinear optical response.[41] The studies showed that the optimal deposition conditions for PAH occurred at a neutral pH where the amine groups are highly protonated, which promotes electrostatic film deposition. Optimal deposition of the chromophore occurred at a pH >9 where the amine groups were largely unprotonated so that covalent reaction of the dichlorotriazine and amine groups occur. The studies found that an increase in ionic strength reduced the electrostatic repulsion between incoming adsorbing species and those already absorbed onto the surface for the dye species. The optimal deposition condition was found to take place in the presence of added salt (NaCl) and at pH=10.5 for Procion Brown with no added salt and at pH=7 for PAH. For Procion Brown films made without added NaCl, the films yielded a $\chi^{(2)}_{zzz} = 30 \times 10^{-9}$ esu. As the ionic strength of the deposition solution increased to 0.5M NaCl, the $\chi^{(2)}_{zzz}$ increased approximately 50% to 56 x 10^{-9} esu. This final value is 28% of the $\chi^{(2)}$ value of the organic crystal lithium niobate ($LiNbO_3$), the leading material currently being used for nonlinear optical applications.

This study addresses the aim of fabricating organic nonlinear optical (NLO) thin films via rapid film formation. Forced convection in both deposition steps and in the water rinsing step was employed to increase the mass transfer rate to the film surface from bulk solutions. Convective forces are expected to eliminate diffusion as the rate-limiting deposition step, increase the mass transfer coefficient and also lead to films with fewer defects due to contaminant particles being rinsed off. A significant increase in the mass transfer coefficient is expected to produce a transport rate to the surface of the substrate which is faster than the reaction rate at the surface of the substrate. This could reduce the film deposition time and dye concentration required for suitable film formation. Reduction of dye concentration and deposition time is crucial for practical processing of these films for fabrication of optical waveguides, typically ~1 micron in thickness. The current layer-by-layer method of fabricating optical waveguides would require approximately 8 days of non-stop operation and approximately 80 grams of dye (purified by a desalting step) to fabricate a 1 micron-thick film. Based on prior studies and theoretical modeling, it was hypothesized that the deposition time may be reduced by a factor of two with NLO results comparable to prior studies, thus reducing the amount of dye required to ~20 grams and the processing time for a 1 micron-thick film to approximately 4 days.

The experiments conducted in this study probe the effects of varying deposition time, presence of forced convection and dye concentration on the properties of PAH/Procion Brown NLO films.

Experimental

Materials. All aqueous solutions were made with deionized water (Barnstead, resistivity > 17 MΩ/cm). The polycation poly{allylamine hydrochloride}, (Aldrich, lot 06305DI, MW ~ 70,000) was used as received to prepare a solution with a concentration of 0.01M repeat unit basis (r.u.). The dichlorotriazine chromophore used for this study was Procion Brown MX-GRN (Pro Burnt Orange 515, Pro Chemical and Dye, Somorset, MA, CAS 68892-31-9). The films were deposited onto glass microscope slides (Fisher Scientific) prepared using the RCA cleaning procedure[42] in which the substrates were immersed in a 6:2:1 solution of H_2O, H_2O_2 (Hydrogen Peroxide 30%, Fluka, lot 1018886) and NH_4OH (Aldrich, lot 016816) at 70 ± 5 °C for 20 minutes. The slides

were then rinsed and placed in a 6:2:1 acid bath consisting of H_2O, H_2O_2 and HCl (EM Science, lot 42326) for 20 minutes and were then rinsed and baked at 130°C for one hour.

Dye Purification. While the manufacture of optical materials traditionally requires highly pure reagents, commercially available azo dyes originally manufactured for textile industry use are usually impure. The purity of the commercially available chromophore used in this study, Procion Brown, was determined by HPLC to be highly variable.[43] Reactive impurities can interfere with the molecular ordering of the primary chromophore and further decrease NLO performance. Procion Brown was purified to remove ionic salts and buffers that are in the as-received powder. Solid phase extraction (SPE) with octadecyl functionalized silica was used to desalt the dye (Alltech High Capacity 75 ml C18 column, lot 173801). The dye was dissolved in 50 mM ammonium acetate (Baker, lot 016816) at ~10 mg/ml. This solution was vacuum filtered with a Buchner funnel to remove any particulate impurities. The column was first washed with ~50 ml of methanol (Budrick & Jackson, lot 42326; EMD, lot 43308345) followed by at least 100 ml (~5 bed volumes) of 50 mM ammonium acetate solution and then the dye solution. The column was again flushed with >100 ml of the ammonium acetate solution, allowing the column to run dry. The dye molecules were eluted from the C_{18} packing by passing ~20 ml of methanol through the column. This solution was collected and the methanol was removed by a centrifuge vacuum. Inductively coupled plasma (ICP) emission spectroscopy analysis (Virginia Tech Soil Analysis Lab, SpectroFlame Modula ICP) showed a ~90% reduction in the Na^+ concentration of purified Procion Brown dye.

Table 2. Results of ICP analysis for purified and unpurified Procion Brown dye. Procion Brown was purified using the manual purification method. Data reported as part per million.

Dye/Concentration	Na	Fe	K	Ca	Si	S
Procion Brown/ 5 mg/ml (Unpurified)	1180	0.21	159.5	0.87	0.45	231
Procion Brown/ 5 mg/ml (Purified)	135.2	0.04	35.7	1.64	0.45	596

Due to lengthy processing times, the manual procedure was converted to an automated flash chromatography-based procedure. This procedure was utilized to purify dye for all experiments conducted with a reduced dye concentration (1 mg/ml) with 0.5M added NaCl. A

flash chromatography system (CombiFlash Retrieve) equipped with a solid phase extraction column (RediSep Reverse Phase C_{18}, 43 g, 35-60 μm particle size) was used to desalt the as-received dye. The chromatography system was operated at the optimal flowrate of the column (45 ml/min). The dye was dissolved in 50 mM ammonium acetate (Baker, lot 016816) at ~20 mg/ml. This solution was then vacuum filtered with a Buchner funnel to remove any particulate impurities. The column was first washed with ~525 ml (~ 7 bed volumes) of methanol followed by ~225ml of 50 mM ammonium acetate solution and then 50 ml of dye solution. The column was again flushed with ~150 ml of the ammonium acetate solution. With the column remaining wet, the dye molecules were eluted from the C_{18} packing by passing ~50 ml of methanol through the column. This solution was collected and the methanol was first reduced by rotary evaporation (Büchi Rotovapor RE-111, T< 40°C) and finally removed by a centrifuge vacuum. Inductively coupled plasma (ICP) emission spectroscopy analysis (Virginia Tech Soil Analysis Lab, SpectroFlame Modula ICP) showed a ~99% reduction in the Na^+ concentration of chromatography-purified Procion Brown dye.

Table 3. Results of ICP analysis for purified and unpurified Procion Brown dye. Procion Brown was purified using the flash chromatography method. Data reported as part per million.

Dye/Concentration	Na	Fe	K	Ca	Si	S
Procion Brown/ 5 mg/ml (Unpurified)	1180	0.17	152.0	1.03	0.45	199.0
Procion Brown/ 5 mg/ml (Purified)	3.26	0.01	0.53	1.65	0.28	628.0

Film Preparation and Characterization

Film Fabrication/Deposition. All aqueous PAH solutions (0.01M repeat unit basis) were stirred overnight and adjusted to a pH of 7.0 for film deposition. The aqueous solutions of Procion Brown (5 mg dye/ml, 0.5M added NaCl) were stirred for <5 minutes and adjusted to a pH of 10.5 for film deposition. All Procion Brown solutions were discarded after approximately 5 hours of use. The pH of all aqueous solutions was adjusted using NaOH (0.1N NaOH, Fisher Scientific, lot 024521-24) or HCl (diluted 1N HCl, Fisher Scientific, lot 024735-24). All pH measurements were made with an Orion Model 407 specific ion meter. All films were deposited at room temperature with the exception of two cases where the deposition was performed at an

elevated temperature (35 °C). Films were prepared using varying deposition times (Table 4) in the presence or absence of forced convection.

Table 4 . Summary of experimental conditions. This study focused on the effect of varying deposition time and the presence of forced convection. The effect of elevated deposition temperature (35 °C) was studied for two cases (4114*, 4112*).

Deposition Time (sec)	Convection	Dye Conc. (mg/ml)	Number Bilayers	Date	Series ID
300	N	5	40	Jan-04	4001
300	Y	5	40	Jan-04	4007
120	Y	5	60	April-04	4114*
120	Y	5	60	April-04	4023-2
120	Y	5	60	May-04	4034
120	Y	5	60	May-04	4204
120	Y	2.5	60	May-04	4224
120	Y	1	60	May-04	4244
60	N	5	60	Mar-04	4013
60	Y	5	60	Mar-04	4023
45	N	5	60	Mar-04	4015
45	Y	5	60	Mar-04	4025
30	N	5	40	Jan-04	4003
30	Y	5	40	Jan-04	4005
30	N	5	60	Mar-04	4011
30	Y	5	60	Mar-04	4021
30	Y	5	60	April-04	4112*

Films were prepared by the sequential immersion of an RCA-cleaned glass slide into the polycation solution (PAH) for 10 minutes for the initial layer and 5 minutes for each subsequent layer for each 5 minute deposition time experiment. For series 4003 and 4005, the glass substrate was immersed into the PAH solution for 1 minute for the initial layer and 0.5 minutes for each subsequent layer. For series 4001 and 4007, the glass substrate was immersed into the PAH solution for 10 minutes for the initial layer and 5 minutes for each subsequent layer. For series 4011-4025, the glass substrate was immersed into the PAH solution for 10 minutes for the initial layer. For series 4112, 4114 and 4023-2, the glass substrate was immersed into the PAH solution for 5 minutes for the initial layer. After the polycation deposition, all slides were then rinsed in a bench-scale flow through tank utilizing a water displacement pump to aid in slide rinsing and active tank circulation. Preliminary studies on the flow-through rinse tank set-up determined that the dye concentration was reduced to 20% of the original concentration and 80% of the deposition concentration after 2 minutes. The slides were immersed in the flow-through rinse

tank for 2 minutes and then submerged into the Procion Brown solution for the designated deposition time, following the same rinsing procedure. Sodium chloride (NaCl) (Fisher Scientific, lot 028794) was used as the salt for adjusting the ionic strength of the dye solutions. The polycation and dye solutions were stirred at approximately 240 revolutions per minute (rpm) during film deposition to generate forced convection. Modeling the deposition baths with forced convection as continuously stirred tanks, the Reynolds number for the flow in the dye and polycation baths is defined as

$$\mathrm{Re} = \frac{N d_i^2 \rho_L}{\mu_L} \tag{3.10}$$

where N is the rotational speed of the impeller (stir rod), d_i is the diameter of the impeller, ρ_L is the density of the fluid and μ_L is the viscosity of the fluid.[44] Assuming that the fluid properties of both the dye and polycation solutions are similar to those of water, the Reynolds number for the flow in the deposition baths is ~2500, placing the flow well into the turbulent flow regime (d_i=2.5 in, N=240 rpm). The ends of the slides (4 slides, 1.75" immersed in fluid) rest ~0.5" above the stirring bar (Figure 1).

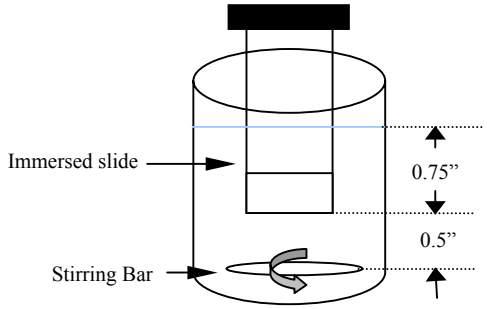

Figure 1. Schematic of forced convection set-up for bench-scale experiments.

The diameter of the stirring bar is approximately equal to the diameter of the deposition bath (fluid height = 2.5"). The turbulent boundary layer at the surface of the glass slides has enhanced mass transport, in comparison to stagnant solutions, due to motion of eddies.

For each set of conditions, two sets of slides were made with 10, 20, 30 and 40 bilayers (total on both sides) for series 4001-4007 or 10, 20, 40 and 60 bilayers (total on both sides) for all other slide series.

UV-Vis Spectroscopy. The films were deposited at room temperature and characterized using UV-Vis spectroscopy (Milton Roy Spectronic 1201). Slides were dried with N_2 gas every 10 bilayers and the UV absorbance measurements were taken at the absorbance maximum of 407 nm. Linear regression was used to determine the slope in absorbance vs. bilayer number graphs.

Ellipsometry. Film thickness measurements were made using a variable angle spectroscopic ellipsometer (J.A. Woolam Ellipsometer VB-200, with WVASE32 software, Ver. 3.361). Initially a rough scan of each film was taken for wavelengths 250 to 1000 nm at 10 nm intervals. This wavelength range was repeated over angles ranging from 50˚ to 70˚ in 4˚ intervals. The Brewster angle was determined to ±5º from a graph of the phase factor Δ vs. scan angle. Following the determination of the Brewster angle, spectroscopic scan measurements were taken for wavelengths 250 to 800 nm at 40 nm intervals. The wavelength range was repeated over angles within a 5˚ range of the Brewster angle, specifically from 55˚ to 60˚ in 1˚ intervals. The accuracy of each fit was determined by the fit of the experimental amplitude factor ψ and phase factor Δ to the Lorentz oscillator model. Ellipsometric measurements were taken at three points on each slide and averaged. The error in thickness measurements was calculated using propagation of error (Appendix A).

Second Harmonic Generation. SHG measurements were made by Professor Heflin's group (C. Durak) using a standard setup using a 10-nanosecond pulse width, Q-switched Nd:YAG laser with a fundamental wavelength of 1064 nm.[45] The SHG data were averaged over 100 shots per data point. Typical spot radius and pulse energy values were 30 μm and 70 mJ/pulse, respectively. The sample was rotated with respect to the incident beam, accounting for the film deposited on both sides of the substrate, leading to interference fringes of the SHG intensity. The sample was rotated from 30° to 60° away from a normal incidence using a stepper motor controlled rotation stage. The $I^{2\omega}$ value is determined from the peak of the interference fringe in the vicinity of 45°. By comparison to Maker fringes in a 68-bilayer PS-119/PAH ionically self-assembled monolayer (ISAM) film, $\chi^{(2)}_{eff}$ of a film is obtained from:

$$\chi^{(2)}_{s,eff} = \chi^{(2)}_{ref}\left(\frac{l_{ref}}{l_s}\right)\left(\sqrt{\frac{I^{2\omega}_s}{I^{2\omega}_{ref}}}\right) = \chi^{(2)}_{ref}\left(\frac{l_{ref}}{l_s}\right)\left(\frac{m\, n_b}{\sqrt{I^{2\omega}_{ref}}}\right) = \chi^{(2)}_{ref}\left(\frac{l_{ref}}{l_{s,bilayer}}\right)\left(\frac{m}{\sqrt{I^{2\omega}_{ref}}}\right) \quad (3.11)$$

where l_{ref} is the total path length (film thickness) through the 68-bilayer standard (measured with the films for which $\chi^{(2)}_s$ is being calculated), l_s is the path length through the sample film (film thickness), n_b is the number of bilayers of the sample film, $I^{2\omega}_{ref}$ is the second harmonic intensity for the 68-bilayer standard, $I^{2\omega}_s$ is the intensity of the second harmonic for the sample film, m is the slope of the plot of the square root of the second harmonic intensity vs. number of bilayers deposited and $l_{s,bilayer}$ is the sample film thickness per bilayer. For the PS-119/PAH standard film l_{ref} = 217.6 nm and $\chi^{(2)}$ = 1.5 x 10^{-9} esu. An optical parametric oscillator (OPO) was incorporated into the SHG set-up (April 2004), altering the prior method for determining the second harmonic intensity. All calculations from measurements performed with the OPO incorporated into the setup, must adjust the second harmonic intensity to reflect the upward shift of the Maker fringe minima from zero. The $I^{2\omega}_s$ in this case is calculated by

$$I^{2\varpi}_s = I^{2\varpi}_{s\ peak} + I^{2\varpi}_{s\ \min imum} \quad (3.12)$$

Tilt Angle. The tilt angle of the films was determined by SHG measurements (performed by Prof. Heflin's group, C. Durak) at varying polarizations (s- or p-) of incident light. The measurements were taken using a standard setup of 10-nanosecond pulse width, Q-switched Nd:YAG laser with a fundamental wavelength of 1064 nm.46 The SHG data were averaged over 100 shots per data point. Typical spot radius and pulse energy values were 30 μm and 70 mJ/pulse, respectively. The SHG data was taken at both s- and p- polarizations of light. The maximum of the second harmonic intensity generated from the p-polarized light is represented as $I^{p\to p}_{2\omega}$, whereas, $I^{s\to p}_{2\omega}$ represents the *s*-polarization maximum second harmonic intensity.

The average tilt angle $\overline{\psi}$ from the film normal is calculated by:[47]

$$\overline{\psi} = arc\cot\sqrt{\frac{1}{2}\left[\sqrt{\frac{I^{p\to p}_{2\omega}}{I^{s\to p}_{2\omega}}}\csc^2\theta - 3\cot^2\theta\right]} \quad (3.13)$$

where θ is the incident angle (50˚). From the tilt angle calculation, the ratio of s-polarization to p-polarization is determined. The $\chi^{(2)}_{zzz}$ is then calculated using equation 3.14

$$\chi^{(2)}_{zzz} = \frac{\chi^{(2)}_{eff}}{\left(\frac{3}{2\cot^2\overline{\Psi}}\right)\sin\theta\cos^2\theta + \sin^3\theta} \tag{3.14}$$

where

$$\frac{\chi^{(2)}_{zzz}}{\chi^{(2)}_{zxx}} = \sqrt{\frac{I^{p\to p}_{2\omega}}{I^{s\to p}_{2\omega}}}\csc^2\theta\, 3\cot^2\theta \tag{3.15}$$

Results

Absorbance per bilayer. For all films in this study the absorbance of the films increased linearly with the number of bilayers deposited (Figure 2) which is characteristic of uniform layer-by-layer deposition for ISAM films. The slope of this linear relationship between the absorbance and number of bilayers is proportional to the amount of dye deposited per layer.

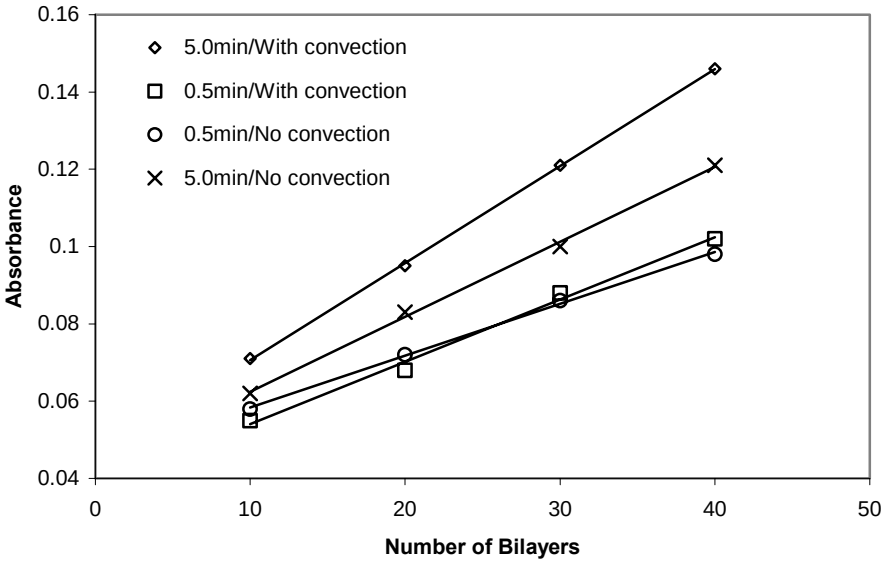

Figure 2. Plot of UV-Vis Absorbance (λ=407 nm) as a function of bilayer number for Procion Brown (PB) films with varying deposition times in the presence or absence of convection. PAH 10mM RU (pH 7.0); PB 5mg/ml, 0.5M NaCl (pH 10.5).

Homogeneity. The films exhibited excellent homogeneity upon visual inspection. The graphs of second harmonic generation intensity as a function of incidence angle measured at three different positions in the films superimpose for all 5 minute deposition experiments, further demonstrating that the films were relatively homogeneous with respect to chromophore concentration and distribution. Films fabricated under conditions of convection demonstrated even superior homogeneity according to SHG results (a-d) for both 5 minute and 0.5 minute deposition experiments. SHG measurements taken for 0.5 minute deposition experiments with no convection (Figure 3c) showed significantly varying results, suggesting some degree of film inhomogeneity.

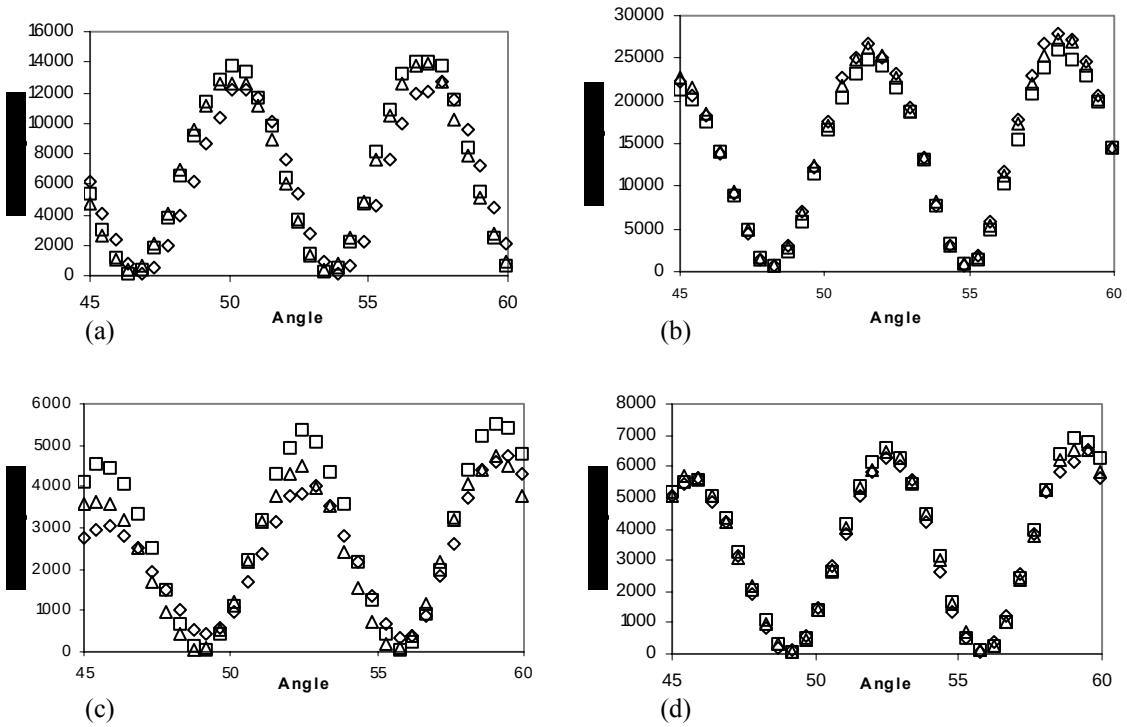

Figure 3a-d. Plot of second harmonic intensity vs. incidence angle at three different positions. □=Position 0; Δ=Position 10; ◊=Position 20; Figure a. 5 min. deposition with no convection; Figure b. 5 min. deposition with convection; Figure c. 0.5 min. deposition with no convection; Figure d. 0.5 min. deposition with convection. Graphical alignment of the three measurements signifies film homogeneity.

Film Thickness/Ellipsometry. Film thickness results were obtained from a fit of ellipsometric measurements to a two-layer model. The two layers of the model consisted of one for the glass substrate and a second layer that represented the film. The layer representing the film was constructed using a Lorentz oscillator model. The film thickness data and optical constants (*n* and *k*) obtained from the two-layer model(a-b) correlate well with prior measurements.

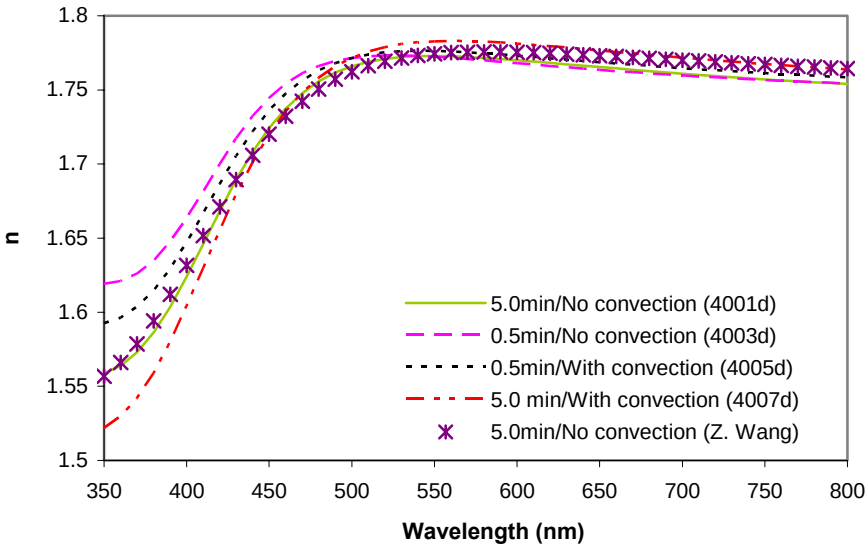

Figure 4a. Plot of refractive index *n* vs. wavelength of PAH/PB films with varying deposition times in the presence or absence of convection.

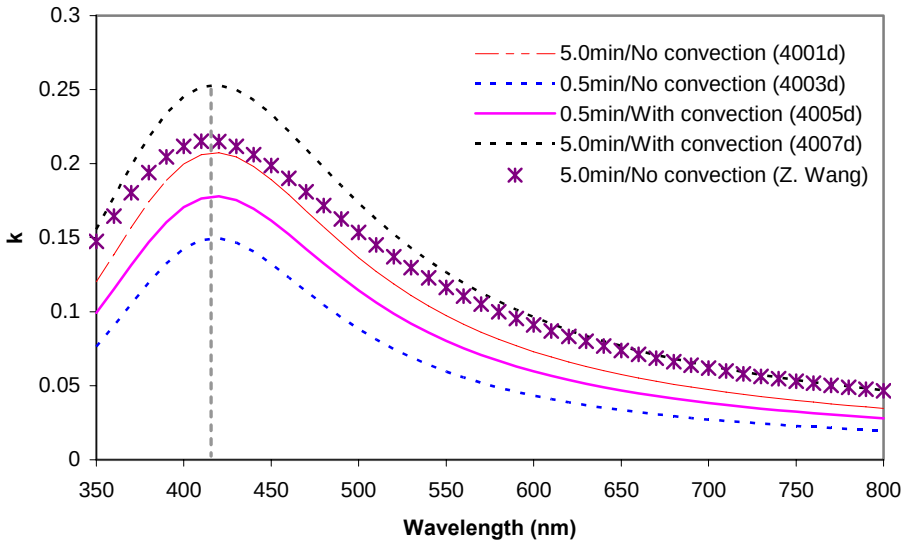

Figure 4b. Plot of extinction coefficient *k* vs. wavelength of PAH/PB films with varying deposition times in the presence or absence of convection. The maximum of the extinction coefficient corresponds with the Procion Brown absorbance maximum of λ=407nm.

film thickness data for similar deposition conditions (Z. Wang Aug. 2003), indicating a reliable fit to the two-layer model developed for this study. Bilayer thickness and refractive index results were averaged over all three measurements for each slide with the highest number of bilayers.

Second Harmonic Generation. Results of the second harmonic generation measurements are shown in Figure 5, which shows the square root of the second harmonic intensity ($I_{2\omega}^{1/2}$) as a function of the number of bilayers deposited.

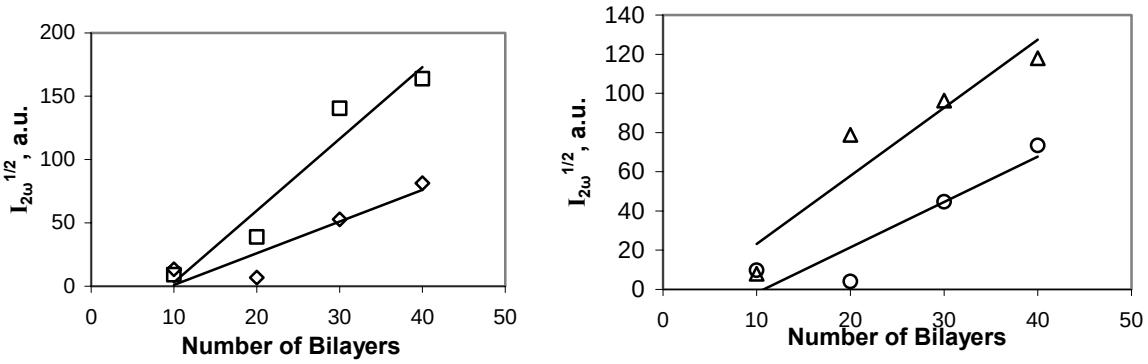

Figure 5. Plot of square root of the second harmonic intensity as a function of the number of bilayers deposited. ◊= 0.5 min./No convection (Series 4003); □= 5 min./No convection (Series 4001); ○= 0.5 min./With convection (Series 4005); Δ= 5 min./With convection (Series 4007). A linear relationship signifies long-range polar layer-by-layer orientation.

Linear scaling of the square root of the second harmonic intensity with the number of bilayers indicates preferential polar orientation and sustained orientation as additional layers are added. For all experimental conditions shown above, slides showed an initial lack of orientation for the first 20 bilayers with an increase in SHG intensity as subsequent layers are deposited. Assuming this increase represents some degree of bulk orientation, the $\chi^{(2)}_{eff}$ and $\chi^{(2)}_{zzz}$ of the varying deposition conditions are reported in Table 5.

Table 5. Summary of Procion Brown deposition with varying deposition time in the presence and absence of convection. (*Data modeled by Z. Wang/Experimentally obtained by M. Guzy). Errors on absorbance per bilayer and bilayer thickness are standard deviations. Errors on $\chi^{(2)}$ values are standard deviations calculated by propagation of error. All slides made at room temperature (except 4112, 4114, deposited at 35°C). PAH 10 mM RU, pH 7.0, PB 5mg dye/ml, 0.5M NaCl, pH 10.5.

Convection	Deposition Time (sec)	Dye Concentration (mg/ml)	$\chi^{(2)}_{zzz}$ (10^{-9} esu)	$\chi^{(2)}_{eff}$ (10^{-9} esu)	Absorbance/ Bilayer	Bilayer Thickness (nm)	Tilt Angle (°)	Series ID	# Bilayers
N	300	5	**48.1**	21.9 ± 4.6	0.00203	0.88 ± 0.11	39.3, 38.8	4001	40
Y	300	5	**69.4**	32.2 ± 5.7	0.00255	1.04 ± 0.14	40.3, 38.7	4007	40
Y	120	5	**41.9**	20.7 ± 2.9	0.00181	0.91 ± 0.10	40.0, 39.4	4114*	60
Y	120	5	**28.1**	14.1 ± 1.8	0.00182	1.02 ± 0.13	40.1, 39.8	4023-2	60
Y	120	5	**28.5**	13.7 ± 2.1	0.00200	0.93 ± 0.13	39.1, 39.7	4034	60
Y	120	5	**25.9**	13.2 ± 1.5	0.00200	0.97 ± 0.11	39.8, 40.8	4204	60
Y	120	2.5	**31.3**	15.9 ± 1.8	0.00173	0.90 ± 0.10	39.9, 41.1	4224	60
Y	120	1	**31.9**	16.4 ± 2.1	0.00173	0.79 ± 0.10	40.8, 41.2	4244	60
N	60	5	**22.6**	11.3 ± 9.0	0.00134	0.75 ± 0.11	39.4, 40.1	4013	60
Y	60	5	**13.7**	7.6 ± 1.3	0.00133	1.09 ± 0.28	41.5	4023	60
N	45	5	**17.9**	9.6 ± 1.6	0.00105	0.79 ± 0.11	41.1, 41.2	4015	60
Y	45	5	**6.9**	4.6 ± 0.7	0.00095	0.81 ± 0.08	44.8	4025	60
N	30	5	**39.0**	18.4 ± 6.5	0.00130	0.73 ± 0.11	40.2, 38.6	4003	40
Y	30	5	**26.5**	18.1 ± 6.6	0.00159	0.83 ± 0.12	45.5, 45.9	4005	40
N	30	5	**10.7**	5.4 ± 1.3	0.00084	0.82 ± 0.10	39.8, 39.9	4011	60
Y	30	5	**16.8**	8.9 ± 2.2	0.00121	0.90 ± 0.09	41.4, 39.8	4021	60
Y	30	5	**34.3**	15.7 ± 1.1	0.00209	0.98 ± 0.05	38.1, 37.9	4112*	60

Discussion

This study investigated the effects of the presence of convection, deposition time and dye concentration on the optical properties of hybrid covalent/electrostatic self-assembled films.

Effect of Convection

At fixed deposition time and concentration conditions, the presence of convection had little demonstrated effect on films with deposition times shorter than 2 minutes (Figure 6). For the 5 minute case, the presence of convection correlated with a ~45% increase in $\chi^{(2)}_{zzz}$ values and 25% increase in absorbance per bilayer. The tilt angle and film thicknesses both seemed relatively unaffected by the presence of convection.

Effect of Deposition Time

At a constant dye concentration of 5 mg/ml, the deposition time had little effect on SHG for deposition times less than two minutes. Deposition times ranging from 30 - 60 seconds, showed no significant difference in SHG for most cases. In the presence of convection, the increase in deposition time from 2 minutes to 5 minutes showed a 2.4 fold increase in $\chi^{(2)}_{zzz}$ and a 30% increase in absorbance per bilayer.

Effect of Dye Concentration

For a deposition time of 2 minutes in the presence of convection, the dye solution concentration was successfully reduced 5-fold (from 5 mg/ml to 1 mg/ml) with less than a 5% difference in $\chi^{(2)}_{zzz}$, less than a 15% decrease in absorbance per bilayer and no detriment to film (Figure 7). Error bars reported estimated ±10%. These results strongly indicate that the deposition conditions remain well outside of the transport-limited regime at a dye concentration of 1 mg/ml. Rather, the surface reaction rate apparently is controlling.

Effect of Temperature

Depositing slides at an elevated temperature (~35°C), had an undetermined effect on $\chi^{(2)}_{zzz}$ (Figure 6), but showed a 15% increase in absorbance per bilayer. There was less than a standard deviation in difference between some $\chi^{(2)}_{zzz}$ values for films with a 30 second deposition time deposited at room temperature and the film deposited at 35°C (30 second deposition time).

Overall, the optical quality of the films made in this study was excellent and consistently exhibited linear layer-by-layer growth. For all conditions studied, the slides consistently showed bilayer thickness values ~0.95 ±0.1 nm/bilayer deposited, corresponding well to previous studies. Most slides exhibited quadratic scaling of the second harmonic intensity with film thickness. In some cases, this relationship deviated from linearity for the first 20 bilayers deposited, suggesting that the films undergo an initial phase where the chromophores gradually gain preferential orientation. Further analysis should be given in the small-bilayer range (2-20 bilayers, both sides) to identify any potential phenomena regarding chromophore orientation in this range.

As previously mentioned, many data points for shorter deposition times (30 sec – 2 minutes) have appreciable scatter of $\chi^{(2)}_{zzz}$ values due to difficulty in precisely controlling

conditions during short deposition times. This suggests that the realm of the experiments conducted in this study may be insufficient to determine specific deposition kinetics of the PAH/dye deposition steps on the order of seconds. Future work should entail more detailed kinetic adsorption analysis of the polymer and dye species utilizing a quartz crystal microbalance (QCM), in-situ SHG measurements and biological amine assays. In-situ SHG studies and QCM measurements will give valuable data relating to the mass transfer coefficient and reaction rate of Procion Brown deposition. Studies of polyelectrolyte adsorption to a charged surface show that a small increase in ionic strength can significantly increase the polymer adsorption rate. Sodium chloride was used in this study as an electrostatic charge barrier in the dye deposition solution (0.5M NaCl). The effect of various halogen salts (i.e. NaBr, NaI) on the adsorption kinetics and NLO activity should be investigated in future work. A recent study[48] found that solutions containing halogen counterions (50 mM added salt) with a larger ionic radius exhibit a faster adsorption of a species onto an oppositely-charged layer. Larger exchange ions are found to be more loosely bound to the surface and would exchange more rapidly than smaller, more tightly bound ions. Ions with smaller ionic radii (F^-, r=1.33Å; Cl^-, r=1.81 Å) were found to have adsorption rates 53% and 73% (respectively) that of the larger ion I^- (r=2.16 Å).

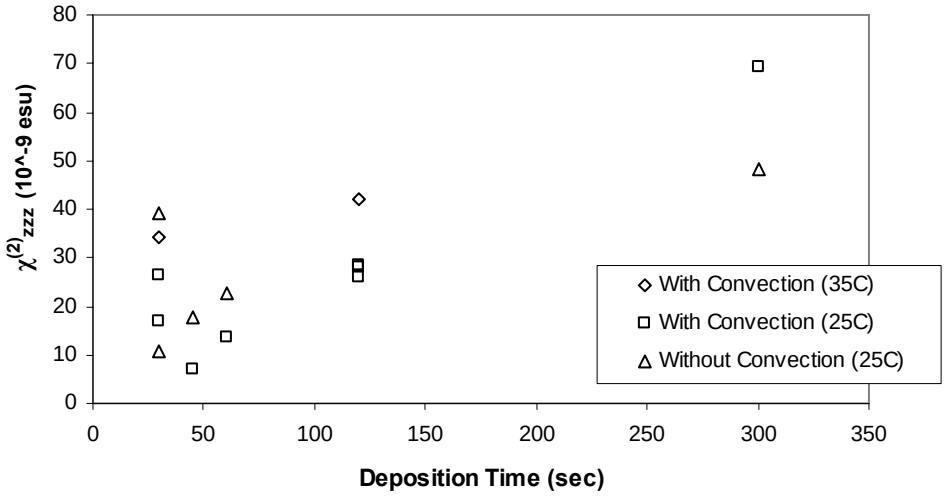

Figure 6. Plot of $\chi^{(2)}_{zzz}$ vs. deposition time in the presence and absence of convection at dye concentration=5 mg/ml.

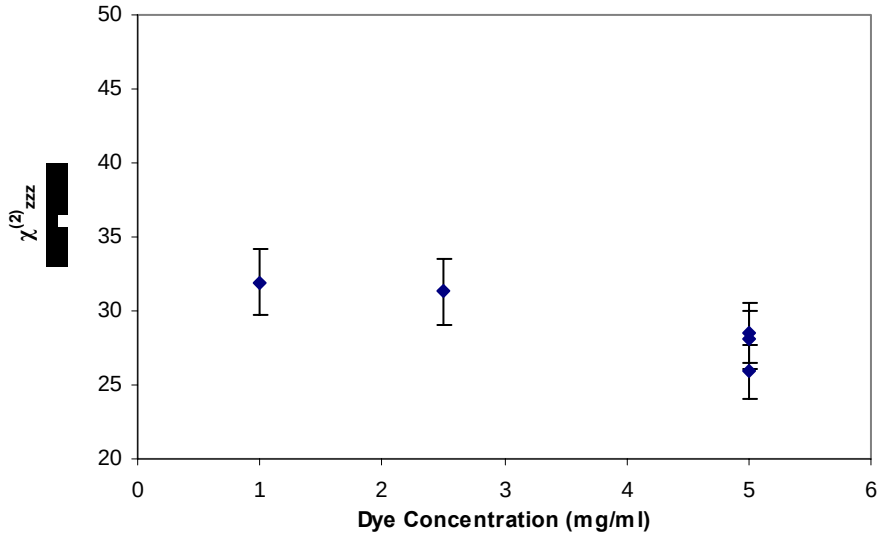

Figure 7. Plot of $\chi^{(2)}_{zzz}$ vs. dye concentration at deposition time = 120 seconds and at 25°C.

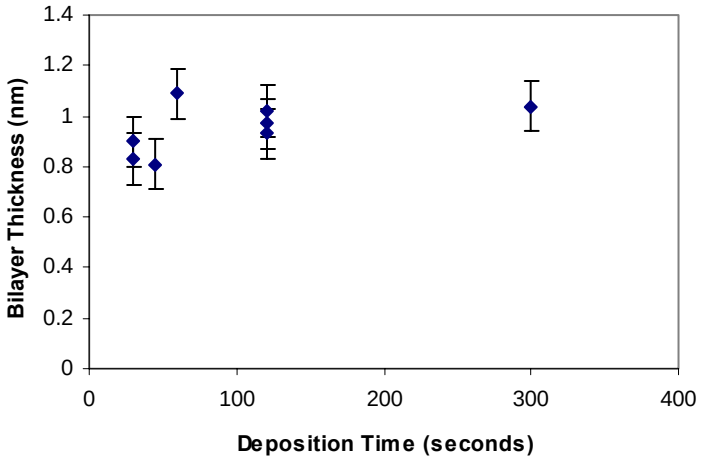

Figure 8. Summary plot of bilayer thickness as a function of deposition time for dye concentration = 5 mg/ml and at 25°C.

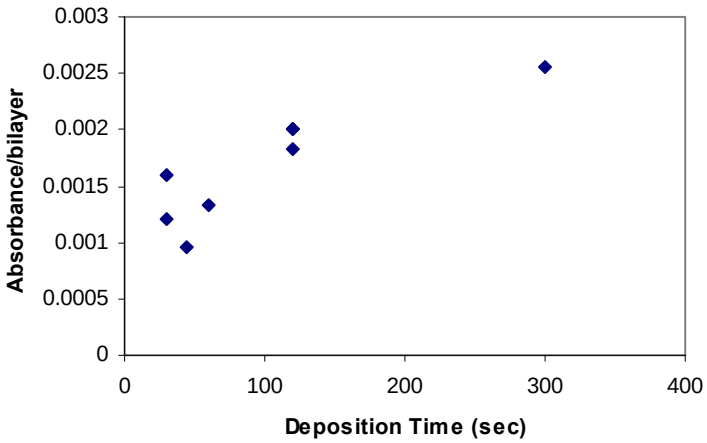

Figure 9. Summary plot of absorbance per bilayer as a function of deposition time for dye concentration= 5 mg/ml and at 25°C.

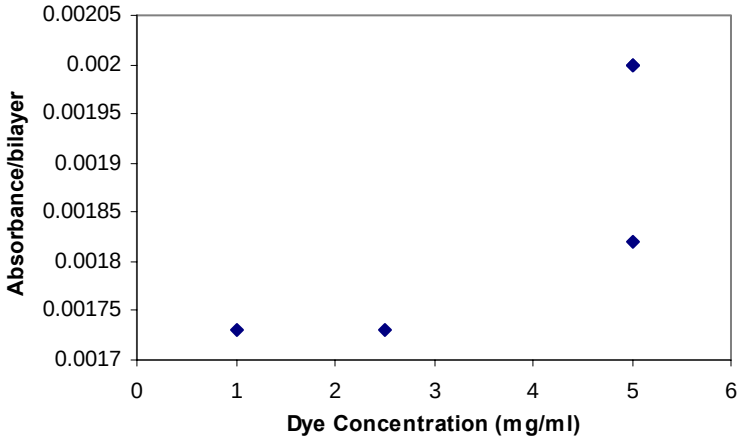

Figure 10. Summary plot of absorbance per bilayer as a function of dye concentration at a deposition time= 120 seconds and at 25°C.

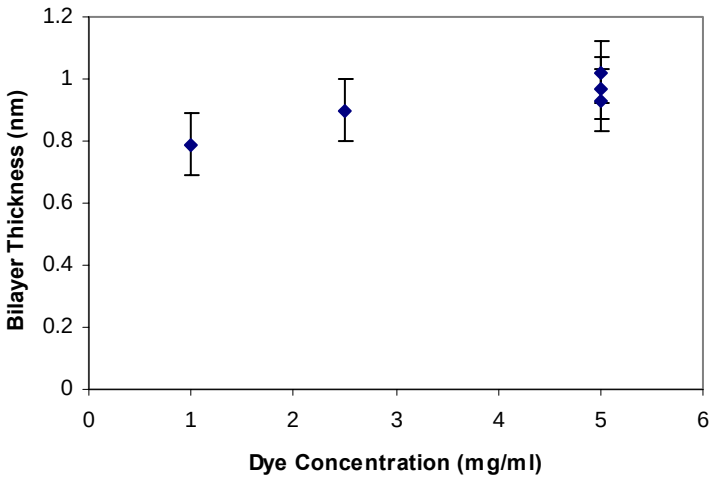

Figure 11. Summary plot of bilayer thickness as a function of dye concentration at a deposition time=120 seconds and at 25°C.

Conclusions

This study investigates the effect of various processing variables encountered in the hybrid covalent deposition method. The results were characterized in terms of $\chi^{(2)}$, film thickness, tilt angle and absorbance per bilayer. Convection was found to have a negligible effect on the characterized properties for deposition times less than 5 minutes. The dye concentration was successfully reduced 5 fold with no detriment to film quality or second harmonic generation. Deposition time had negligible effect on SHG for deposition times less than 2 minutes. However, a 2 fold increase in $\chi^{(2)}_{zzz}$ was found for a 2 fold increase in deposition time from 2 minutes to 5 minutes.

References

[1] L.-H. Peng, L.-H.; Hsu, C.,-C, Shih, Y.-C 'Second-Harmonic Green Generation from Two-Dimensional Chi[sup (2)] Nonlinear Photonic Crystal with Orthorhombic Lattice Structure' *Appl. Phys. Lett.* **83** (2003) 3447-3455.

[2] Ni, P.; Ma, B.; Wang, X.; Cheng, B.; Zhang, D. 'Second-Harmonic Generation in Two-Dimensional Periodically Poled Lithium Niobate Using Second-Order Quasiphase Matching' *Appl. Phys. Lett.* **82** (2003) 4230-4238.

[3] Zeng, X.; Chen, X.; Chen, Y.; Xia, Y.; Chen, Y. 'Observation of all-optical wavelength conversion based on cascaded effect in periodically poled lithium niobate waveguide' *Optics & Laser Technology* ***35*** (2003) 187-190.

[4] Kim, J. H.; Yoon, C.S. 'Domain switching characteristics and fabrication of periodically poled potassium niobate for second-harmonic generation' *Appl. Phys. Lett.* **81** (2002) 3332-3338.

[5] Beckers, L.; Buchal, C.; Fluck, D.; Pliska, T.; Günter, P. 'Potassium niobate waveguides: He^+ implantation in bulk single crystals and pulsed laser deposition of thin films' *Materials Science and Engineering A* **253** (1998) 292-295.

[6] Fluck, D.; Pliska, T.; Günter, P.; Beckers, L.; Buchal,C. 'Blue-light second-harmonic generation in ion-implanted KNbO[sub 3] channel waveguides of new design' *Appl. Phys. Lett.* **69** (1996) 4133-4139.

[7] Kitamura, K.; Yamamoto, J. K.; Iyi, N.; Kimura, S. 'Stoichiometric $LiNbO_3$ single crystal growth by double crucible Czochralski method using automatic powder supply system' *J. Crystal Growth* **116** (1992) 327-343.

[8] Takagi, T.; Fujii, T.; Sakabe, Y. 'Growth and characterization of $KNbO_3$ by vertical Bridgman method' *Journal of Crystal Growth* **259 (**2003) 296-301.

[9] Lee, K. –S. *Polymers for Photonics Applications II*, Heidelberg, Germany: Springer-Verlag, 2003.

[10] Thakur, M.; Titus, J.; Mishra, A. 'Single-crystal thin films of organic molecular salt may lead to a new generation of electro-optic devices' *Opt. Eng.* **42** (2003) 456-458.

[11] Koeste, M.; Laschewsky, A.; Jonas, A. M.; Verbiest, T. 'Orientation of functional groups in polyelectrolyte multilayers studied by second-harmonic generation (SHG)' *Colloids and Surface A* **198-200** (2002) 275-280.

[12] Koeste, M.; Laschewsky, A.; Verbiest, T. 'Films grown from polyamines and reactive dyes by alternating polyelectrolyte adsorption/surface activation (CoMPAS)' *Materials Science and Engineering* **10** (1999) 107-133.

[13] Guo, L. J.; Cheng, X.; Chao, C. Y. 'Fabrication of photonic nanostructures in nonlinear optical polymers' *J. Mod. Opt.* **49** (2002) 663-673.

[14] Kaino, T. 'Waveguide fabrication using organic nonlinear optical marerials' *J. Opt. A: Pure Appl. Opt.* **2** (2002) R1-R7.

[15] Bertrand, P.; Jonas, A.; Laschewsky, A.; Legras, R. 'Ultrathin polymer coatings by complexation of polyelectrolytes at interfaces: suitable materials, structures and properties' *Macromol. Rapid Commun.* **21** (2000) 319-348.

[16] Yu, H.H.; Hwang, S.-J. 'E-O functional waveguide using the electric-field-poled polymeric material for integrated-optic devices' *Optics Communications* **219** (2003) 183-192.

[17] Shi, Y,; Zhang, H.; Bechtel, J. H.; Dalton, L. R.; Robinson, B.H.; Steier, W. H.; 'Low (Sub-1-Volt) halfwave voltage polymeric electro-optic modulators achieved by controlling chromophore shape' *Science* **288** (2000) 119-122.

[18] Dalton, L. R. 'Polymeric electro-optic materials: optimization of electro-optic activity, minimizatiojn of optical loss, and fine-tuning of device performance' *Opt. Eng.* **39** (2000) 589-595.

[19] Ma, H.; Liu, S.; Luo, J.; Suresh, S.; Liu, L.; Kang, S. H.; Haller, M.; Sassa, T.; Jen, A. K. Y.; Dalton, L. R. 'Highly efficient and thermally stable electro-optical dendrimers for photonics' - *Adv. Funct. Mater* **12** (2002) 565-574.

[20] Sottini, S.; Grando, D.; Palchetti, L.; Giorgetti, E.; Ricceri, R.; Gabrielli, G. 'Organic films for guided nonlinear optics' *Materials Science and Engineering* **C5** (1998) 167-172.

[21] Ashwell, G. J.; Jackson, P. D.; Crossland, W. A. 'Noncentrosymmetry and second harmonic generation in Z-type Langmuir-Blodgett Films' *Nature* **368** (1994) 438-440.

[22] Zhu, P.; van der Boom, M. E.; Kang, H.; Evmeneko, G.; Dutta, P.; Marks, T. J. 'Realization of expeditious layer;by-layer siloxane-based self-assembly as an efficient route to structurally regular acentric superlattices with large electro-optic responses' *Chem. Mater.* **14** (2002) 4982-4989.

[23] Fachetti, A.; Abbotto, A.; Beverina, L.; van der Boom, M. E.; Dutta, P.; Evmeneko, G.; Pagano, G. A.; Marks, T. J. 'Layer-by-layer self-assembled pyrrole-based donor-acceptor chromophores as electro-optic materials' *Chem. Mater.* **15** (2003) 1064-1072.

[24] Zhao, Y. –G.; Chang, S.; Wu, A.; Lu, H. –L.; Ho, S. T.; van der Boom, M. E.; Marks, T. J. 'Second-generation approach to all-organic modulators based on intrinsically polar self-assembled molecular superlattices' *Opt. Eng.* **42** (2003) 298-299.

[25] Wang, W.; Zhu, P.; Marks, T. J.; Ketterson, J. B. 'Ultrafast frequency-selective optical switching based on thin self-assembled organic chromophoric films with a large second-order nonlinear response' *Appl. Phys. Lett.* **81** (2002) 2169-2171.

[26] Sottini, S.; Grando, D.; Palchetti, L.; Giorgetti, E.; Ricceri, R.; Gabrielli, G. 'Organic films for guided nonlinear optics' *Materials Science and Engineering* **C5** (1998) 167-172.

[27] Heflin, J. R.; Figura, C.; Marciu, D.; Liu, Y.; Claus, R. O. 'Thickness dependence of second harmonic generation in thin films fabricated from ionically self-assembled monolayers' *Appl. Phys. Lett.* **74** (1999) 495-497.

[28] Van Cott, K. E.; Guzy, M.; Neyman, P.; Brands, C.; Heflin, J. R.; Gibson, H. W.; Davis, R. M. 'Layer-by-layer deposition and ordering of low-molecular weight dye molecules for second-order nonlinear optics' *Angew. Chem. Int. Ed.* **41** (2002) 3236-3328.

[29] Heflin, J. R.; Neyman, P. J.; Guzy, M.; Shah, S. M.; Davis, R. M.; Van Cott, K. E.; Wang, H.; Gibson, H. W.; Brands, C. 'Hybrid covalent/ionic self-assembly of organic second order nonlinear optical films, in Organic Thin Films for Photonic Applications, OSA Trends in Optics and Photonics Series **64** (2002) 3-8.

[30] Manning, G. 'Limiting laws and counterion condensation in polyelectrolyte solutions. IV. The approach to the limit and the extraordinary stability of the charge fraction' *Biophysical Chemistry* **7** (1977) 95-102.

[31] Shaw, D. "Introduction to Colloid and Surface Chemistry" Butterworth Heinemann, Boston 1996.

[32] Evans, D. F.; Wennerström, H., Ed. "The colloidal domain:where physics, chemistry, biology and technology meet" Wiley, New York (1999) 392.

[33] Koopal, L. K.; Avena, M. J. 'A simple model for adsorption kinetics at charged solid-liquid interfaces' *Colloids and Surfaces A* **192** (2001) 93-107.

[34] Cohen Stuart, M. A.; Hoogendam, C. W.; de Keizer, A. 'Kinetics of polyelectrolyte adsorption' *J. Phys.: Condens. Matter* **9** (1997) 7767-7783.

[35] Dijt, J. C.; Cohen Stuart, M. A.; Hofman, J. E.; Fleer, G. J. 'Kinetics of polymer adsorption in stagnation point flow' *Colloids and Surfaces* **51** (1990) 141-158.

[36] Geffroy, C.; Labeau, M. P.; Wong, K.; Cabane, B.; Stuart, M. A. 'Kinetics of adsorption of polyvinylamine onto cellulose' *Colloids and Surfaces A* **172** (2000) 47-56.

[37] Dijt, J. C.; Stuart, M. A.; Fleer, G. J. 'Kinetics of polymer adsoprtion and desorption in capillary flow' *Macromolecules* **25** (1992) 5416-5423.

[38] Brands, C.; Neyman, P. J.; Guzy, M. T.; Shah, S.; Davis, R. M.; Van Cott, K. E.; Wang, H.; Gibson, H. W.; Heflin, J. R. 'In situ measurements of the formation of ionically self-assembled monolayers by second harmonic generation' *MRS Symp. Proc.* **707** (2002) DD12.5.1-6.

[39] Brands, C. 'Interface effects and deposition process of ionally self-assembled monolayer films: in situ and ex situ second harmonic generation measurements' Ph.D. Thesis, Virginia Tech 2003.

[40] Langmuir, I. 'The adsoprtion of gases on plane surfaces of glass, mica and platinum' *Am. Chem. Soc.* **40** (1918) 1361-1403.

[41] Guzy, M. Organic Self-Assembled Layer-by-Layer Thin Films for Second-Order Nonlinear Optics, Ph.D. Thesis, Virginia Tech, 2003.

[42] Itano, M.; Kern, F.; Miyashita, M.; Ohmi, T. 'Particle removal from silicon wafer surface in wet cleaning processes' *IEEE Trans. on Semicond. Manu.* **6** (1993) 258-267.

[43] Van Cott, K.; Amos, T.; Gibson, H.; Davis, R.; Heflin, J. 'Characterization of the Purity and Stability of Commercially Available Dichlorotriazine Chromophores Used in Nonlinear Optical Materials' *Dyes and Pigments* **58** (2003) 144-145.

[44] Middleman, S. *An Introduction to Mass and Heat Transfer*, New York: Wiley and Sons, 1997.

[45] Neyman, P.; Guzy, M.; Shah, S; Davis, R.; Van Cott, K.; Wang, H.; Gibson, H.; Brands, C.; Heflin, J. 'Second-Order Nonlinear Optical Responses of Ionically Self-Assembled Films: Polycation Variations and Dianionic Chromophores', *SPIE Proceedings* **4461** (2001) 214-226.

[47] Neyman, P. Nonlinear Optical Properties and Structural Characteristics of Ionically Self-Assembled Nanoscale Polymer Films Influenced by Ionic Concentration and Incorporation of Monomer Chromophores, MS Thesis, Virginia Tech 2004 Chapter 3.

[48] Mermut, O.; Barrett, C. J. 'Effects of charge density and counterions on the assembly of polyelectrolyte multilayers' *J. Phys. Chem. B* **107** (2003) 2525-2530.

Chapter 4

Automated ISAM Film Fabrication: Development & Optimization

Introduction

There is a growing demand in industry for increased data handling capabilities, which include processing, transmission and storage.[1] Over the last decade great attention has been paid to the study of various polymer systems for use in optical telecommunications. This technology can be applied to several devices, such as frequency modulators, tunable filters, broadband optical modulators and waveguides. Inorganic crystals, such as lithium niobate ($LiNbO_3$)[2,3,4] and potassium niobate ($KNbO_3$), [5,6,7] currently used for fiber optic systems yield high performance in the critical areas of data transmission speed and minimal optical loss, but these materials are inferior in the areas of cost, availability and lengthy processing times for crystal growth.[8-9] Consequently, research relating to such devices has been driven towards developing alternative methods and materials for fabricating such devices. Organic polymers have long been recognized as having the potential for surpassing the performance of current inorganic materials such as lithium niobate and potassium niobate in integrated optical devices due to their high electro-optic coefficients, fast response time, low dielectric constants and flexibility of fabrication methods.[10]

NLO Fabrication Methods

Several experimental techniques have been developed for creating nonlinear optically (NLO) active thin films suitable for optical communication and photonic devices.[11,12,13] Electricfield poled polymer films,[14,15] Langmuir-Blodgett films[16,17] and self-assembled organosilane[18] films have all produced NLO-active films with high nonlinear responses. However, poled polymer films face challenges for practical device application due to the instability of the acentric alignment of the NLO chromophores, which degrades the electro-optic activity over time. Langmuir-Blodgett films are desirable due to their cheap fabrication and fine control on film thickness and refractive index. However, problems typically arise in the form of poor mechanical stability and high propagation losses due to scattering and insufficient thickness. Ionic self-assembled multilayer (ISAM) films are a recently developed class of materials that allows detailed structural and thickness control at the molecular level, combined with ease of manufacturing and low cost.

The ISAM technique for the deposition of polyelectrolytes has been recently demonstrated through a number of research efforts.[19] The method involves the alternate dipping of a charged substrate into an aqueous solution of a polyanion and polycation at room temperature. The advantages of this technique include simple, rapid, inexpensive production and long-term stability of the acentric $\chi^{(2)}$ without the need for additional processing such as electric-field poling or chemical reactions. Polymer-polymer ISAM films fabricated by Heflin et al.[20] exhibited linear scaling of $I_{2\omega}^{1/2}$ vs film thickness (up to 120 nm), demonstrating the uniform maintenance of orientation with layer-by-layer growth.

ISAM deposition schemes that involve a reactive deposition step alternated with an electrostatic deposition step are evolving into a prevalent class of NLO film fabrication techniques.[21,22,23] Leermakers et al. have extensively studied the adsorption of charged polycations to charged surfaces.[24,25] Their findings state that electrostatics alone provide a sufficient adsorption driving force to overcome the surface charge provided the ionic strength is below a threshold value. Prior studies of the kinetics of polyelectrolyte adsorption onto a charged substrate show that most of the deposition of a self-assembled polymer film could take place in less than a minute given appropriate deposition conditions (i.e. concentration, ionic strength, flow conditions and pH).[26,27] These studies have focused on the relevant parameters driving the adsorption process, leading to a relationship that describes the height of the electrostatic barrier that builds up as a charged polyelectrolyte adsorbs onto a charged substrate. A novel layer-by-layer methodology for fabricating NLO thin films has been developed[28,29] with the aim of increasing the stability of chromophore-dipole orientation, reducing steric constraints from polymer-backbone attachment (often encountered in traditional ISAM films) and producing a large nonlinear optical response. This method builds films layer-by-layer by alternately immersing a substrate into aqueous solutions of an NLO-active polyelectrolyte "glue" and a reactive chromophoric dye. The adsorption of the layers alternates between electrostatic interaction and covalent reaction. The chromophore is attached covalently which yields anisotropic ordering and high second-order NLO activity in these films. The reactive deposition method has been tested with a number of commercially-available monomeric dyes, including Procion Red, Procion Orange and most recently, Procion Brown. The adsorption kinetics of the NLO chromophore Procion Red and poly(alyllamine hydrochloride) {PAH} films measured

using *in-situ* second harmonic generation (SHG) measurements[30,31] and modeled using a Langmuir-type growth model.[32] In this model the adsorbed molecules are assumed to be non-interacting, but inhibiting to other molecules landing on the adsorption site. Laschewsky et al. recently attempted reactive films growth with Procion Red dye and a synthetically-produced amine. The films experienced no regular layer-by-layer growth and exhibited no significant nonlinear optical activity due to inaccurate deposition conditions.

Rinsing Studies

The rinsing process in device and film fabrication has received considerable attention in recent years.[33,34,35,36] With growing wafer sizes in semiconductor manufacturing and the development of the field of thin films for device applications, optimization of the rinse process is critical to time-efficient device manufacturing. As thin polymeric films near large-scale device fabrication, research efforts are being made to automate the manufacturing of such films. The automation of film manufacturing is a requisite for the development of layer-by-layer films as a viable option for electro-optic devices. The rinsing process is essential for layer-by-layer film deposition with good optical film quality.[37,38] Rinsing removes any loosely bound molecules from the surface of the substrate, producing a "clean" surface for the next deposition step.

Rinsing of a substrate can be limited by a number of factors, including (1) surface reaction kinetics, (2) thermodynamics, (3) diffusion of contaminants and (4) convective transport of contaminants. The significance of these factors is determined by the chemistries involved, fluid dynamics and rinse tank geometry.[39] A number of studies aimed at determining the rate limiting factors in rinsing have addressed the process from a theoretical view.[33-36]

Substrates entering a rinse vessel are coated with a thin, liquid carryover layer from the previous fabrication step. Earlier studies have treated this layer as having uniform thickness and a relatively stagnant boundary layer.[40] The removal of such a carryover layer requires diffusion through the boundary layer and then convective transport in the bulk fluid. Later-developed models refute the treatment of the carryover layer as a uniform, stagnant layer. In contrast, these models define the carryover layer as nonuniform collections of liquid droplets that are dependent on the balance between surface tension, viscous and gravitational forces. Rosato et al. note that

previous studies neglected both surface tension and carryover fluid drainage following deposition. The treatment of the carryover thickness T which accounts for all applicable forces is defined as

$$T = \left(\frac{\mu V}{\rho g} \right)^{1/2} Ca^{1/6} \tag{4.1}$$

where μ is the fluid viscosity, ρ is the density, V is the extraction velocity and Ca is the capillary number. The capillary number Ca is a ratio of viscous forces to surface tension forces as given by

$$Ca = \frac{\mu V}{g \sigma} \tag{4.2}$$

where σ is the surface tension.

Prior Studies

A prior study of the fabrication of NLO active films with the polycation poly(alyllyamine hydrochloride) and the NLO active chromophore Procion Brown yielded exceptional results in nonlinear optical response.[41] The studies showed that the optimal deposition conditions for PAH occurred at a neutral pH where the amine groups are highly protonated, which promotes electrostatic film deposition. Optimal deposition of the chromophore occurred at a pH >9 where the amine groups were largely unprotonated so that covalent reaction of the dichlorotrizine and amine groups occur. The studies found that an increase in ionic strength reduced the electrostatic repulsion between incoming adsorbing species and those already absorbed onto the surface for the dye species. The optimal deposition condition was found to take place in the presence of added salt (NaCl) and at pH conditions mentioned above. For Procion Brown films made without added NaCl, the films yielded a $\chi^{(2)}_{zzz} = 30 \text{ x } 10^{-9}$ esu. As the ionic strength of the deposition solution increased to 0.5M NaCl, the $\chi^{(2)}_{zzz}$ increased to 56 x 10^{-9} esu. This value is 28% the $\chi^{(2)}$ value of the organic crystal lithium niobate ($LiNbO_3$), the leading material currently being used for nonlinear optical applications.[42]

Current Studies

This study addresses the aim of automating and optimizing the fabrication of thick, organic nonlinear optical (NLO) films. An automatic slide stainer was utilized in lieu of the manual dipping procedure employed in prior studies. The optimal conditions for this study were determined in the bench-scale experiments discussed in Chapter 3. Bench-scale experiments were also used to determine kinetic parameters associated with contaminant removal from the active-rinse bath in the slide stainer. A base case study (Phase I) was first conducted to determine (1) if any equipment modifications were necessary to fabricate optically homogeneous films and (2) obtain further contaminant build-up data for the active rinse bath for kinetic modeling. Several equipment modifications were employed to aid in the optimization of dipper operation and film fabrication, including the addition of forced convection in the deposition baths and increased agitation in the active rinse bath and modified slide holders. A second study (Phase II) was conducted utilizing the optimized conditions determined in Chapter 3 and equipment modifications deemed necessary from Phase I. A final study (Phase III) was conducted where the fabrication of a 500 bilayer film (total on both sides) was attempted.

The overall experimental aims of this study were to:

- Optimize the operating parameters of automated dipper operation (i.e. rinse time, etc.) to produce optically homogeneous films utilizing a minimal cycle time with minimal consumption of dye.
- Demonstrate the feasibility of using the automated dipper to fabricate a thick film with suitable optical characteristics needed for electro-optic modulator devices.

Experimental

Materials. All aqueous solutions were made with deionized water (Barnstead, resistivity > 17 MΩ/cm). The polycation poly{allylamine hydrochloride}, (Aldrich, lot 06305DI, MW ~ 70,000) was used as received to prepare a solution with a concentration of 0.01M repeat unit basis (r.u.). The dichlorotriazine chromophore used for this study was Procion Brown MX-GRN (Pro Burnt Orange 515, Pro Chemical and Dye, Somorset, MA, CAS 68892-31-9). The films were deposited onto glass microscope slides (Fisher Scientific) prepared using the RCA cleaning procedure[43] in which the substrates were immersed in a 6:2:1 solution of H_2O, H_2O_2 (Hydrogen Peroxide 30%,

Fluka, lot 1018886) and NH_4OH (Aldrich, lot 016816) at 70 ± 5 °C for 20 minutes. The slides were then rinsed and placed in a 6:2:1 acid bath consisting of H_2O, H_2O_2 and HCl (EM Science, lot 42326) for 20 minutes and were then rinsed and baked at 130°C for one hour.

Dye Purification. While the manufacture of optical materials traditionally requires highly pure reagents, commercially available azo dyes originally manufactured for textile industry use are usually impure. The purity of the commercially available chromophore used in this study, Procion Brown, was determined by HPLC to be highly variable. [44] Reactive impurities can interfere with the molecular ordering of the primary chromophore and further decrease NLO performance. Procion Brown was purified to remove ionic salts and buffers that are in the as-received powder.

Earlier studies conducted within this research group[41] developed a manual dye purification procedure that was utilized in this study for all 0.0M NaCl and 0.5M NaCl cases at a dye concentration of 5 mg/ml (Series 4009). Solid phase extraction (SPE) with octadecyl functionalized silica was used to desalt the dye (Alltech High Capacity 75 ml C18 column, lot 173801). The dye was dissolved in 50 mM ammonium acetate (Baker, lot 016816) at ~10 mg/ml. This solution was vacuum filtered with a Buchner funnel to remove any particulate impurities. The column was first washed with ~50 ml of methanol (Budrick & Jackson, lot 42326) followed by at least 100 ml (~5 bed volumes) of 50 mM ammonium acetate solution and then the dye solution. The column was again flushed with >100 ml of the ammonium acetate solution, allowing the column to run dry. The dye molecules were eluted from the C_{18} packing by passing ~20 ml of methanol through the column. This solution was collected and the methanol was removed by a centrifuge vacuum. Inductively coupled plasma (ICP) emission spectroscopy analysis (Virginia Tech Soil Analysis Lab, SpectroFlame Modula ICP) showed a ~90% reduction in the Na^+ concentration (Table 1) of purified Procion Brown dye.

Table 1. Results of ICP analysis for purified and unpurified Procion Brown dye. Procion Brown was purified using the manual purification method. Data reported as part per million.

Dye/Concentration	Na	Fe	K	Ca	Si	S
Procion Brown/ 5 mg/ml (Unpurified)	1180	0.21	159.5	0.87	0.45	231
Procion Brown/ 5 mg/ml (Purified)	135.2	0.04	35.7	1.64	0.45	596

Due to lengthy processing times, the manual procedure was converted to an automated flash chromatography-based procedure. This procedure was utilized to purify dye for all experiments conducted with a reduced dye concentration (1 mg/ml) with 0.5M added NaCl. A flash chromatography system (CombiFlash Retrieve) equipped with a solid phase extraction column (RediSep Reverse Phase C_{18}, 43 g, 35-60 μm particle size) was used to desalt the as-received dye. The chromatography system was operated at the optimal flowrate of the column (45 ml/min). The dye was dissolved in 50 mM ammonium acetate (Baker, lot 016816) at ~20 mg/ml. This solution was then vacuum filtered with a Buchner funnel to remove any particulate impurities. The column was first washed with ~525 ml (~ 7 bed volumes) of methanol followed by ~225ml of 50 mM ammonium acetate solution and then 50 ml of dye solution. The column was again flushed with ~150 ml of the ammonium acetate solution. With the column remaining wet, the dye molecules were eluted from the C_{18} packing by passing ~50 ml of methanol through the column. This solution was collected and the methanol was first reduced by rotary evaporation (Büchi Rotovapor RE-111, T< 40°C) and finally removed by a centrifuge vacuum. Inductively coupled plasma (ICP) emission spectroscopy analysis (Virginia Tech Soil Analysis Lab, SpectroFlame Modula ICP) showed a ~99% reduction in the Na^+ concentration of chromatography-purified Procion Brown dye.

Table 2. Results of ICP analysis for purified and unpurified Procion Brown dye. Procion Brown was purified using the flash chromatography method. Data reported as part per million.

Dye/Concentration	Na	Fe	K	Ca	Si	S
Procion Brown/ 5 mg/ml (Unpurified)	1180	0.17	152.0	1.03	0.45	199.0
Procion Brown/ 5 mg/ml (Purified)	3.26	0.01	0.53	1.65	0.28	628.0

Film Preparation and Characterization

Film Fabrication/Deposition. All aqueous PAH solutions (0.01M repeat unit basis) were stirred overnight and adjusted to a pH of 7.0 prior to film deposition. The aqueous solutions of Procion Brown (5 mg dye/ml [Phase I], 1 mg dye/ml [Phase II, III], 0.5M added NaCl) were stirred for

<5 minutes and adjusted to a pH of 10.5 for film deposition. All Procion Brown solutions were discarded after approximately 5 hours of use. The pH of all aqueous solutions was adjusted using NaOH (0.1N NaOH, Fisher Scientific, lot 024521-24) or HCl (diluted 1N HCl, Fisher Scientific, lot 024735-24). The pH typically drifted less than 0.6 pH units during deposition. All pH measurements were made with an Orion Model 407 specific ion meter.

Films were prepared by the sequential immersion of an RCA-cleaned glass slide into the polycation solution (PAH) for 10 minutes for the initial layer and 5 minutes for each subsequent layer (Phase I) for the 5 minute deposition time experiment. For the optimized conditions experiments, the initial PAH layer was 10 minutes in duration and each subsequent deposition step was 2 minutes in duration (Phase II, Phase III). After the polycation deposition, all slides were then rinsed in an active rinse flow-thru tank utilizing a Hagen 201 water displacement pump to aid in slide rinsing and active tank circulation. Preliminary studies on the flow-through rinse tank set-up determined that the dye concentration in the rinse tank was reduced to 30% of the original concentration within 2 minutes of submersion. Based on these findings, the slides leaving the PAH deposition bath were immersed in the flow-through rinse tank for 2 minutes and then submerged into the Procion Brown solution for the designated deposition time. The same rinsing procedure was utilized following each Procion Brown deposition. Sodium chloride (NaCl) (Fisher Scientific, lot 028794) was used as the salt for adjusting the ionic strength of the dye solutions. The polycation and dye solutions were circulated through a powerhead pump (3.4 L/min, max. flowrate) during film deposition to generate forced convection. In order to model the forced convection in the deposition baths as continuously stirred tanks, the Reynolds number for the flow in the dye and polycation baths is defined as

$$\mathrm{Re} = \frac{DV\rho}{\mu} \tag{4.3}$$

where D is the affected distance (width of the deposition bath), V is the velocity of the fluid, ρ is the density of the fluid and μ is the viscosity. Assuming that the fluid properties of both the dye and polycation solutions are similar to those of water, the Reynolds number for the flow in the deposition baths is ~1200, placing the flow in the turbulent flow regime.

UV-Vis Spectroscopy. The films were deposited at room temperature and characterized using UV-Vis spectroscopy (Jasco V-530). Slides were dried with N_2 gas every 10 bilayers (Phase I). Slides fabricated in Phase II and Phase III experiments were air dried. UV absorbance measurements were taken at the Procion Brown absorbance maximum of 407 nm. Linear regression was used to determine the slope in absorbance vs. bilayer number graphs.

Ellipsometry. Film thickness measurements were made using a variable angle spectroscopic ellipsometer (J.A. Woolam Ellipsometer VB-200, with WVASE32 software, Ver. 3.361). Initially a rough scan of each film was taken for wavelengths 250 to 1000 nm at 10 nm intervals. This wavelength range was repeated over angles ranging from 50˚ to 70˚ in 4˚ intervals. The Brewster angle was determined to ±5º from a graph of the phase factor Δ vs. scan angle. Following the determination of the Brewster angle, spectroscopic scan measurements were taken for wavelengths 350 to 800 nm at 40 nm intervals. The wavelength range was repeated over angles within a 10˚ range of the Brewster angle, specifically from 55˚ to 60˚ in 1˚ intervals. The accuracy of each fit was determined by the fit of the experimental amplitude factor ψ and phase factor Δ to the Lorentz oscillator model. Ellipsometric measurements were taken at three points on each slide and averaged. The standard deviations for the thickness measurements were calculated using propagation of error (Appendix A).

Second Harmonic Generation. SHG measurements were made by Professor Heflin's group using a standard setup using a 10-nanosecond pulse width, Q-switched Nd:YAG laser with a fundamental wavelength of 1064 nm.[45,46] The SHG data were averaged over 100 shots per data point. Typical spot radius and pulse energy values were 30 μm and 70 mJ/pulse, respectively. The sample was rotated with respect to the incident beam, accounting for the film deposited on both sides of the substrate, leading to interference fringes of the SHG intensity. The sample was rotated from 30° to 60° away from a normal incidence using a stepper motor controlled rotation stage. The $I^{2\omega}$ value is determined from the peak of the interference fringe in the vicinity of 45°. By comparison to Maker fringes in a 68-bilayer PS-119/PAH ionically self-assembled monolayer (ISAM) film, $\chi^{(2)}$ of a film is obtained from

$$\chi_s^{(2)} = \chi_{ref}^{(2)}\left(\frac{l_{ref}}{l_s}\right)\left(\sqrt{\frac{I_s^{2\omega}}{I_{ref}^{2\omega}}}\right) = \chi_{ref}^{(2)}\left(\frac{l_{ref}}{l_s}\right)\left(\frac{m\, n_b}{\sqrt{I_{ref}^{2\omega}}}\right) = \chi_{ref}^{(2)}\left(\frac{l_{ref}}{l_{s,bilayer}}\right)\left(\frac{m}{\sqrt{I_{ref}^{2\omega}}}\right) \quad (4.4)$$

where l_{ref} is the total path length (film thickness) through the 68-bilayer standard (measured with the films for which $\chi^{(2)}_s$ is being calculated), l_s is the path length through the sample film (film thickness), n_b is the number of bilayers of the sample film, $I^{2\omega}_{\text{ref}}$ is the second harmonic intensity for the 68-bilayer standard, $I^{2\omega}_{\text{s}}$ is the intensity of the second harmonic for the sample film, m is the slope of the plot of the square root of the second harmonic intensity vs. number of bilayers deposited and $l_{s,bilayer}$ is the sample film thickness per bilayer. For the PS-119/PAH standard film l_{ref} = 217.6 nm and $\chi^{(2)}$ = 1.5 x 10^{-9} esu. An optical parametric oscillator (OPO) was incorporated into the SHG set-up (April 2004), altering the prior method for determining the second harmonic intensity. All calculations from measurements performed with the OPO in tact, must adjust the second harmonic intensity to reflect the upward shift of the Maker fringe minima from zero. The $I^{2\omega}_{\text{s}}$ in this case is calculated by

$$I_s^{2\varpi} = I_s^{2\varpi}{}_{peak} + I_s^{2\varpi}{}_{\min imum} \quad (4.5)$$

Tilt Angle. The tilt angle of the films was determined by SHG measurements at varying polarizations (*s*- or *p*-) of incident light. The measurements were taken using a standard setup of 10-nanosecond pulse width, Q-switched Nd:YAG laser with a fundamental wavelength of 1064 nm.[47] The SHG data were averaged over 100 shots per data point. Typical spot radius and pulse energy values were 30 μm and 70 mJ/pulse, respectively. The SHG data were taken at both *s*- and *p*- polarizations of light. The maximum of the second harmonic intensity generated from the *p*-polarized light is represented as $I_{2\omega}^{p\to p}$ while, $I_{2\omega}^{s\to p}$ represents the *s*-polarization maximum second harmonic intensity.

The average tilt angle $\overline{\psi}$ from the film normal was calculated by:

$$\overline{\psi} = arc\cot\sqrt{\frac{1}{2}\left[\sqrt{\frac{I_{2\omega}^{p\to p}}{I_{2\omega}^{s\to p}}}\csc^2\theta - 3\cot^2\theta\right]} \quad (4.6)$$

where θ is the angle of incidence (50˚). From the tilt angle calculation the ratio of s-polarization to p-polarization is determined. The $\chi^{(2)}_{zzz}$ is then calculated using equation 4.7

$$\chi^{(2)}_{zzz} = \frac{\chi^{(2)}_{eff}}{\left(\frac{3}{2\cot^2\overline{\Psi}}\right)^{-1}\sin\theta\cos^2\theta + \sin^3\theta} \tag{4.7}$$

where

$$\frac{\chi^{(2)}_{zzz}}{\chi^{(2)}_{zxx}} = \sqrt{\frac{I^{p\to p}_{2\omega}}{I^{s\to p}_{2\omega}}}\csc^2\theta\, 3\cot^2\theta \tag{4.8}$$

Equipment Layout

All experiments were performed with a Richard-Allen Scientific DS/50 automated slide stainer (Figure 1).

Figure 1. Richard-Allen DS/50 Slide Stainer. (www.rallansci.com)

The slide stainer (35”L x 24”W x 22”H) is equipped with 20 polyphenyline sulfide (PPS) ryton static deposition chambers, one active rinse bath (also constructed of PSS) and a drying chamber. Table 3 and Table 4 provide details of the deposition and rinse baths.

Table 3. Static deposition bath dimensions and specifications.

Dye/Polymer Bath Specifications	
Total liquid volume (to fill line)	600 ml
Total liquid volume w/ powerhead	500 ml
Vessel height	4.25 in
Vessel length	6 in
Vessel width	2 in

Table 4. Active rinse bath dimensions and flow specifications.

Active Rinse Bath Specifications	
Total volume (capacity)	2000 ml
Active liquid volume	1650 ml
Vessel height	4.5 in
Active height (to top of standpipe)	3.5 in
Vessel length	8 in
Vessel width	3.5 in
Flow-thru flowrate (w/powerhead)	1.4 L/min

Equipment Modifications

Slide Holder

The DS/50 is factory-equipped with a 50-slide capacity metal slide basket (Figure 2). The design of this slide holder was determined to be unsuitable for use in these experiments due to a number of design issues: (1) A slide holder composed of metal may produce corrosion due to the high-salt conditions used for dye deposition (0.5M NaCl). (2) The original slide holder is designed with a number of crevices that entrap additional polymer/dye for carryover to the rinse bath. The reduction of carryover volume of polymer/dye is critical for effective rinsing. (3) The original slide holder is designed so that the slides face the flow of the powerhead face-on as opposed to edge-on. With this configuration, only the front-most slide would receive adequate flow for effective rinsing, while the slides towards the back of the holder would mainly rely on diffusion-driven dilution for removal of the carryover layer. (4) The original slide holder grips the slides on the sides, which negatively affects the optical film quality in the lateral regions. While the optical film quality may not likely have a negative effect on the film performance, a major aim of the study focuses on fabricating films with optimal film quality.

With these factors considered, modified slide holders were designed (Figure 3, Figure 4) and constructed. The modified holders were designed to meet the following criteria:

- Non-metal, benign to high salt conditions.
- Minimal surface area for carryover transfer to rinse bath.
- Configured with slides edge-on to water flow.
- Configured to produce films with “clean” edges.

- Seats slides securely in the stream of powerhead pump flow.
- Accomodates all baths with sufficient clearance of the powerhead nozzle.

The modified slide holders were constructed (Virginia Tech Physics Machine Shop) of Delrin® into a monolithic L-bracket configuration (Figure 4). The holder accommodates 4 slides edge-on to water flow. The slides are held vertically from the elevated base of the holder by a series of 4 slots tightened by set screws.

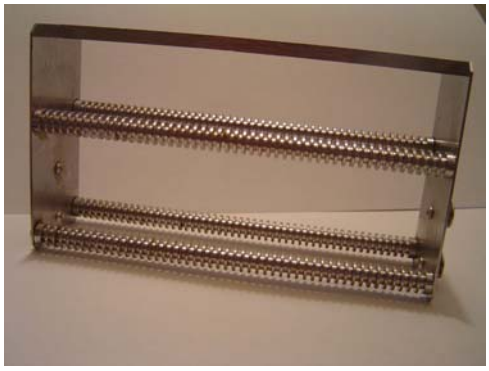

Figure 2. First generation metal slide holder. Contact surface area ~312 cm^2.

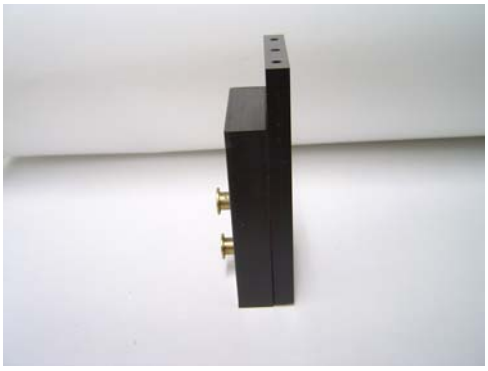

Figure 3. Second generation 2-piece slide holder. Contact surface area ~77 cm^2.

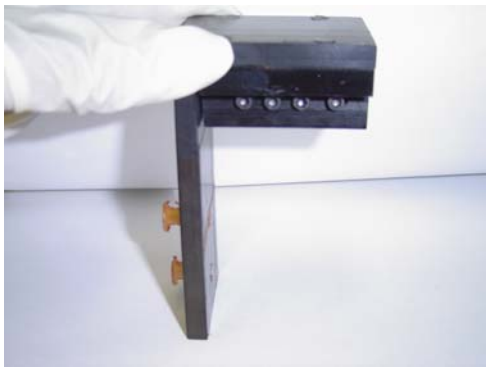

Figure 4. Third generation L-bracket monolithic slide holder. Contact surface area ~60 cm^2.

The modified holders, seat the slides with sufficient clearance from the powerhead nozzle to ensure no detriment to film quality arising from high flow rates and also allow a well-mixed environment in the dipper baths. For the third generation slide holder, approximately 60 cm^2 of the crevice-free slide holder surface contacts the depositing solutions, whereas approximately 312 cm^2 of surface area contacts the solutions with the original slide holder. Therefore, the

modifications to the original slide holder reduced the contact surface area by 80% and the carryover volume by ~83% from the original metal slide holder.

PowerHead Pump

An aquarium powerhead pump was added to the active-rinse bath and deposition baths (Phase II, Phase III) to increase fluid circulation. The increased circulation was intended to increase rinsing efficiencies and overcome any potential diffusive limitations encountered in the deposition process. The Reynolds number was estimated for all baths containing a powerhead pump. The Reynolds number for flow in a rectangular vessel is defined as

$$\mathrm{Re} = \frac{DV\rho}{\mu} \tag{4.9}$$

where D is the affected distance, V is the velocity of the fluid, ρ is the density of the fluid and μ is the viscosity of the fluid. The physical properties of water were used for these calculations (ρ= 1 g/cm^3; μ=0.001Pa-s). The velocity V was calculated using the characteristic area for a rectangular vessel with height H and width W. The effective area was defined as A_{eff}= ($H*W/2$), which was substituted into the expression for velocity

$$V = \frac{Q}{Aeff} = \frac{2Q}{HW} \tag{4.10}$$

where Q is the volumetric flowrate of the pump (3.4 L/min). For the static deposition baths, the Re~1170 and for the active-rinse the Reynolds number ~3200.

Blotting Step

A blotting step was added to the film fabrication process to remove excess deposition solution accumulated at the ends of the slides (Figure 5) and the solution forced between the slides by capillary action.

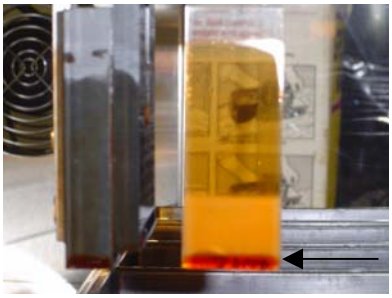

Figure 5. Typical dye bead to be removed by blotting step.

This step is performed in a staining vessel lined with Kimwipes. The height of the blotting surface was carefully adjusted as to not activate the fail-safe obstruction mechanism in the dipper's robotic arm.

Design of Experiments

This study aims to optimize the operating parameters of automated dipper operation (i.e. rinse time, etc.) to produce optically homogeneous films utilizing a minimal cycle time with minimal consumption of materials. Fabrication of ionically self-assembled Procion Brown/PAH films was automated to produce device-applicable films utilizing the optimal conditions (determined in Chapter 3) of the following variables:

- Dye/Polymer deposition time
- Dye concentration
- Rinse Time

The automated operation parameters were closely monitored to determine optimal deposition conditions. The active flow-through bath was modeled as a continuously-stirred tank reactor to determine the optimal rinse time and overall effectiveness of the rinse step, the most critical step to proper film formation. Automatically fabricated films were characterized by absorbance, film thickness, tilt angle and second harmonic generation $\chi^{(2)}$.

The study was conducted in three phases:

- Phase I: Base Case Operation
- Phase II: Optimized Condition Operation
- Phase III: Thick Film Fabrication

Phase I: Base Case

This series of experiments was conducted to examine the feasibility of utilizing an automated dipping procedure to fabricate films. This experiment utilized the optimal conditions (deposition pH, polymer/chromophore combination, ionic strength) from previously conducted studies (Table 5). The experiment was conducted with the following objectives:

- Determine if any equipment modifications are necessary to successfully fabricate films.
- Obtain contaminant build-up data for the active rinse bath in an effort to determine the bath's effectiveness in contaminant removal and model its kinetic behavior for the planning of future experiments.
- Fabricate optically homogeneous films that exhibit linear layer-by-layer growth and suitable SHG ($\chi^{(2)}_{zzz} > 25 \pm 5 \times 10^{-9}$ esu).

Table 5. Experimental conditions for base case (Phase I) study.

Experimental Conditions	
Deposition Time	5 min.
Dye Concentration	5 mg/ml
Polymer Concentration	10 mM
Rinse Time	2 min.

Phase I Equipment Set-up

The experiment was conducted in the absence of forced convection in both deposition baths and without blotting steps. A powerhead water pump (Hagen Powerhead 201) was added to the active rinse bath to generate an increase in water circulation and therefore, more effective rinsing behavior.

Table 6. Equipment set-up for base case (Phase I) study.

Equipment Modifications	
Active-Rinse Bath Pump	Y
Forced Convection in Deposition Baths	N
Blotting Steps	N

Phase I Results

Homogeneity. The films conducted in Phase I of experiments exhibited poor optical homogeneity. The films exhibited good optical homogeneity the first 20 bilayers (both sides) of dipper operation. Deposition of subsequent bilayers, marked heterogeneities in the form of dye aggregates. The film quality was mainly attributed to the observed cross-contamination between the dye and polymer baths for this set of experiments. The slide holder utilized for this experiment was constructed of two connected pieces of Delrin (Figure 3). The joint between the pieces provided a space for capillary-drawn fluid to reside. With the fluid inaccessible to turbulent flow of the active rinse bath, dye/polymer solution was transferred between deposition baths, introducing contamination in both the dye and polymer baths.

Plots of second harmonic intensity, as a function of incidence angle (measured at three separate positions) for films made in this study (Figure 6), lacked the superposition often seen in manually-fabricated films (Figure 7).

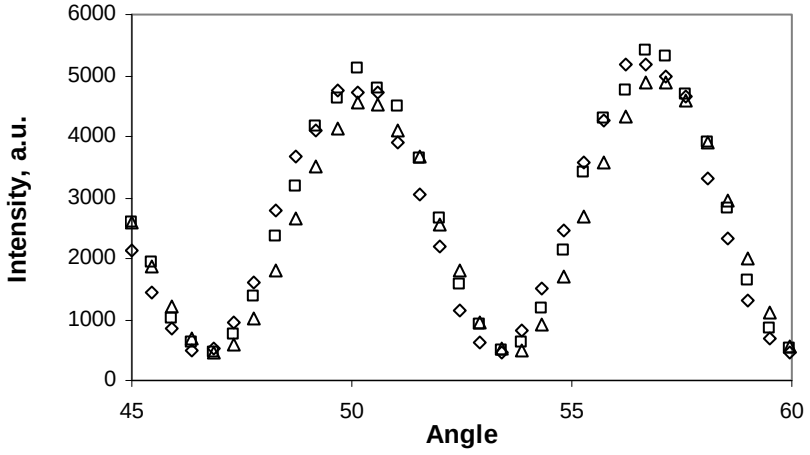

Figure 6. Plot of second harmonic intensity vs. incidence angle at three different positions. ◊=Position 0; □=Position 10; Δ=Position 20; Slides made with automatic slide stainer (Series 4009). Graphical alignment of the three measurements signifies film homogeneity. Peak minima landing at zero signifies homogeneity in the form of equivalent films on both sides of the substrates. *Measurements taken before installation of OPO*

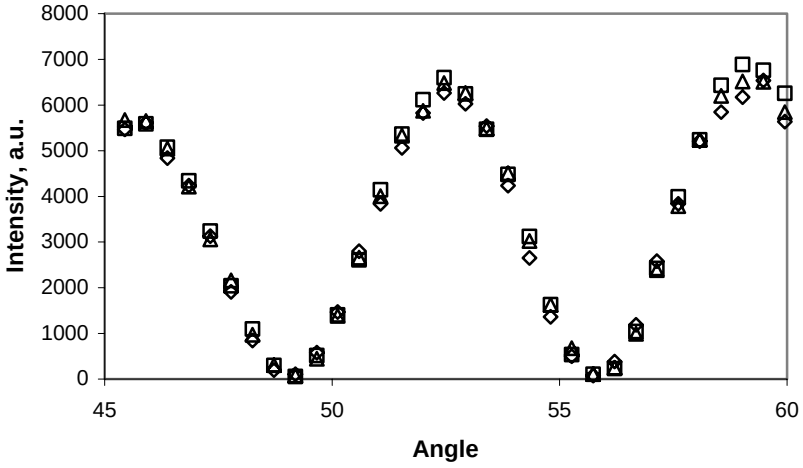

Figure 7. Plot of second harmonic intensity vs. incidence angle at three different positions. ◊=Position 0; □=Position 10; Δ=Position 20; Slides made with manual dipping procedure. Graphical alignment of the three measurements signifies film homogeneity. Peak minima landing at zero signifies homogeneity in the form of equivalent films on both sides of the substrates. *Measurements taken before installation of OPO*

Absorbance per bilayer. The UV absorbance of the films displayed a linear increase with the number of bilayers deposited (Figure 8) for all films in this study. This linear increase is characteristic of layer-by-layer deposition for self-assembled films. The slope of this linear relationship between the absorbance and number of bilayers (total on both sides) is proportional to the amount of dye deposited per layer.

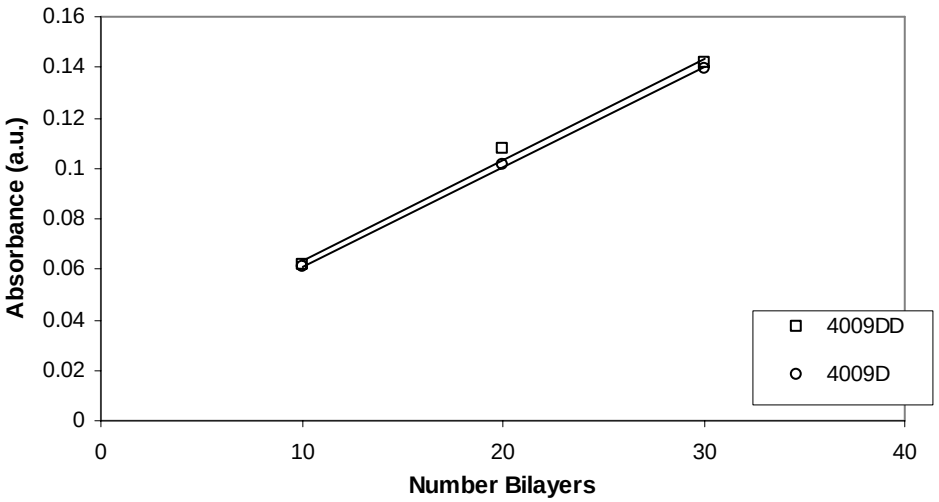

Figure 8. Plot of UV-Vis absorbance (λ=407 nm) vs number of bilayers (total on both sides) for Procion Brown (PB)/PAH films fabricated utilizing an automated slide stainer (Series 4009). PAH 10mM RU (pH 7.0); PB 5mg dye/ml, 0.5M added NaCl (pH 10.5). Linear plot denotes layer-by-layer growth.

The absorbance per bilayer of the films in this study correlate well with films deposited utilizing a manual dipping procedure. Both slide sets used identical deposition conditions (Table 7).

Table 7. Absorbance per bilayer for automatically-fabricated films (4009) compared to those fabricated manually (4001).

Series ID	Deposition Time (minutes)	Absorbance per bilayer
4009	5	0.00396 ± 0.0004
4001	5	0.00203 ± 0.0001

Ellipsometry

Film thicknesses were obtained from a fit to a two-layer model. The first layer represented the glass substrate used for deposition whereas the second layer represented the self-assembled film (Lorentz oscillator model). The film thickness data and optical constants (*n* and *k*) obtained from the two-layer model correlate well (Figure 9, Figure 10) with prior ellipsometric data for similar deposition conditions, indicating a reliable fit to the two-layer model developed for this study.

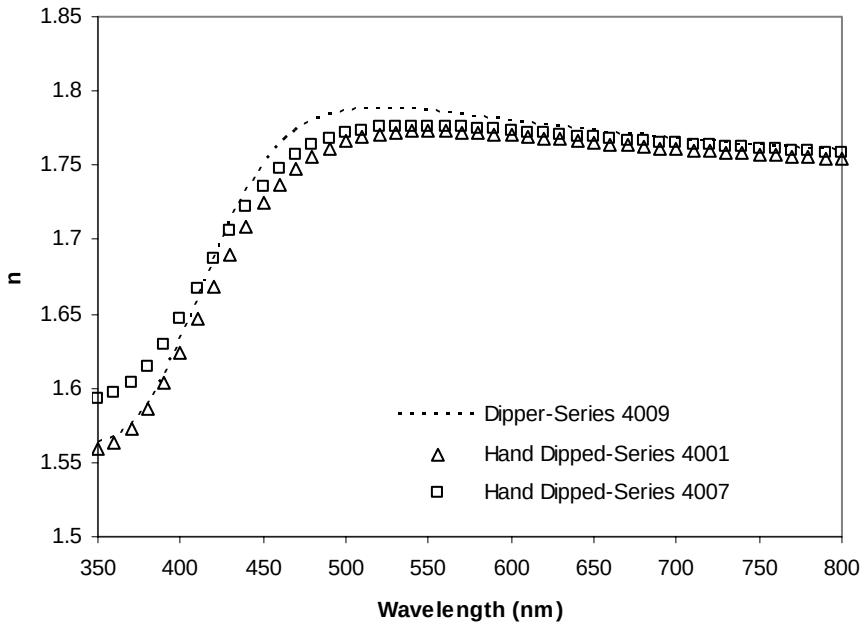

Figure 9. Plot of refractive index n vs. wavelength of PAH/PB films fabricated with an automated slide stainer (Series 4009) compared to those fabricated manually (Series 4001, 4007).

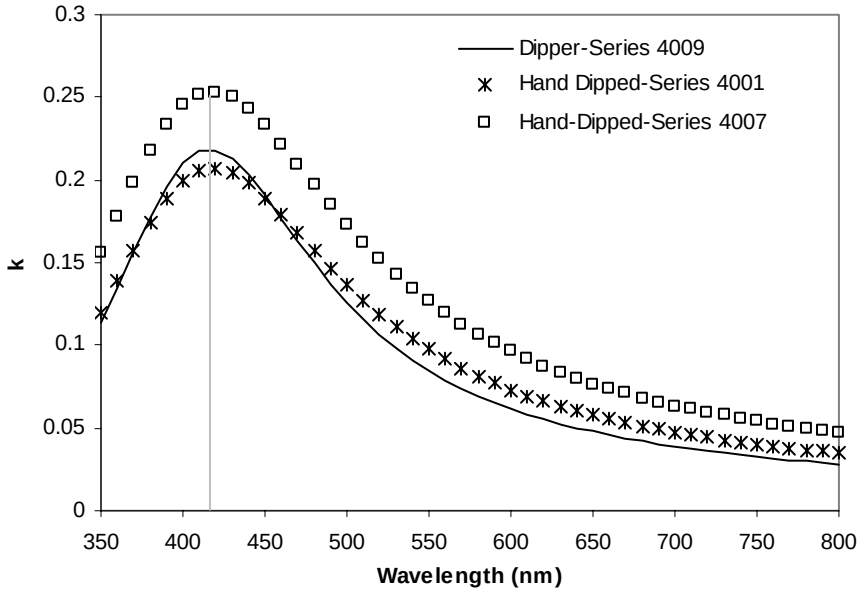

Figure 10. Plot of extinction coefficient *k* vs. wavelength of PAH/PB films fabricated with an automated slide stainer (Series 4009) compared to those fabricated manually (Series 4001, 4007). The maximum of the extinction coefficient corresponds with the Procion Brown absorbance maximum of λ=407 nm.

Bilayer thickness (Table 8) and refractive index results were averaged over three measurements for each slide containing the highest number of bilayers deposited.

Phase I Conclusions

A base-case automated film fabrication experiment was conducted as a feasibility study. The films compared well with manually-fabricated films for values of thickness and optical constants. However, the films exhibited relatively poor optical homogeneity and modest $\chi^{(2)}$ values. A number of areas for potential improvement, particularly in film quality and processing time lead to opportunities for further optimization. Moreover, processing times were on the order of 14 minutes per bilayer deposited so that the current process used in Phase I is not adequate for fabricating thick, device-suitable films. This issue was addressed in Phase II of experiments with the reduction of deposition and rinsing times. Improvement of the optical quality of the automatically-fabricated films and optical performance $\chi^{(2)}$ was also investigated in Phase II with additional equipment modifications implemented.

Table 8. Summary of results (Phase I Experiments) base case automated film fabrication compared to hand dipped films(*) with identical deposition conditions. PAH 10mM, pH 7.0; Procion Brown 5 mg dye/ml, 0.5M added NaCl, pH 10.5.

Tilt Angle	$\chi^{(2)}_{zzz}$	$\chi^{(2)}_{eff}$	Abs/bilayer	Thick./bilayer	Dep. Time (min)	Convection	Dye Conc.	# Bilayers
40.5, 38.9	**35.9**	17.3 ± 3.0	0.00396	1.09 ± 0.19	5	N	5 mg/ml	30
39.3, 38.8	**48.1**	21.9 ± 4.6	0.00203	0.88 ± 0.11	5	N	5 mg/ml	40

Phase II: Optimized Conditions

This series of experiments was conducted to examine the consistency of results from manually executed experiments versus those experiments fabricated with an automated dipping procedure. The optimal conditions determined in the series of experiments conducted in *Chapter 3: The Effect of Forced Convection, Deposition Time and Concentration on Properties of NLO Films* were used in Phase II experiments. The experiment was conducted with the following objectives:

- Examine the consistency of results from manually executed experiments with those experiments fabricated with an automated dipping procedure.
- Utilize optimized conditions on the dipper in an effort to reduce dye consumption and overall processing time.

- Determine the feasibility of introducing forced convection into the deposition baths for prolonged dipping experiments.
- Determine the necessity of additional equipment modifications for film fabrication.
- Obtain contaminant build-up data for the active rinse bath in an effort to determine the bath's effectiveness in contaminant removal and model its kinetic behavior for the planning of future experiments.
- Fabricate optically homogeneous films that exhibit linear layer-by-layer growth and suitable SHG ($\chi^{(2)}_{zzz} > 25 \pm 5 \times 10^{-9}$ esu).

Determination of Optimal Deposition Time

The deposition time for the dipper experiments was determined from the series of experiments conducted in *Chapter 3: The Effect of Forced Convection, Deposition Time and Concentration on Properties of NLO Films*. In that series of experiments, the deposition time of the dye and polymer adsorption steps were varied while the dye concentration, polymer concentration and rinse time were all held constant (Table 9).

Table 9. Design of experiments matrix for deposition time study. "X" denotes fixed variable.

Variable		
Deposition Time		0.5 – 5 min.
Dye Concentration	X	5 mg/ml
Rinse Time	X	2 min.

The deposition time for the dye and polymer baths were fixed to equal values for all experiments. The effectiveness of the varying deposition times was characterized by the SHG of the sample films, specifically the second-order susceptibility $\chi^{(2)}_{zzz}$ (Figure 11).

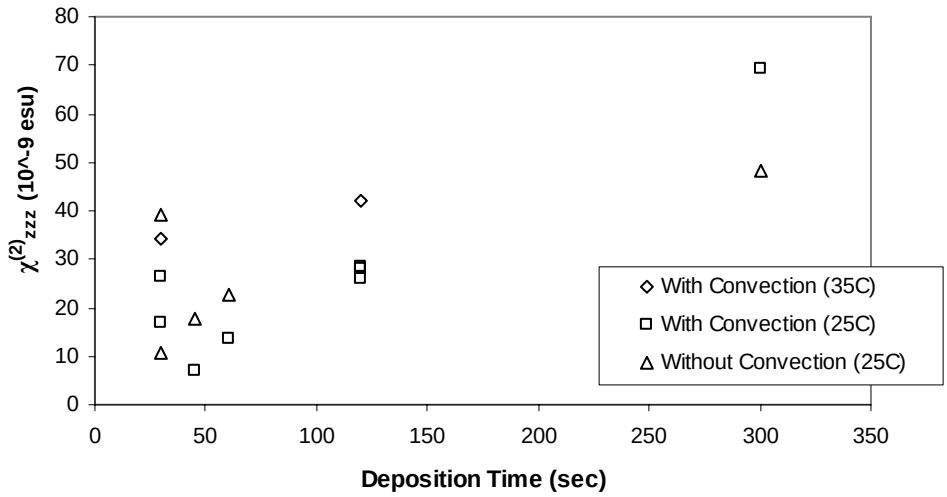

Figure 11. Plot of $\chi^{(2)}_{zzz}$ as a function of deposition time (Chapter 3 experiments). All slides deposited in the presence of convection and at room temperature. PAH, 10mM, pH 7.0; PB, 5 mg/ml, pH 10.5.

For deposition times less than 2 minutes, the $\chi^{(2)}_{zzz}$ decreased sharply. *Based on the requirement of $\chi^{(2)}_{zzz} > 25 \pm 5 \times 10^{-9}$ esu, a 2 minute deposition time was selected for Phase II of dipper experiments.*

Determination of Optimal Rinse Time

Rinsing of the glass substrate can be limited by a number of factors, including (1) surface reaction kinetics, (2) thermodynamics, (3) diffusion of contaminants and (4) convective transport of contaminants. The significance of these factors is determined by the chemistries involved and fluid dynamics. Optimization of the flow in the rinse tank is essential to effective rinsing. For the purposes of this work, an optimized active rinse tank must meet the following criteria:

- Achieve 99% reduction of original dye concentration utilizing minimal volumes of water in a minimal processing time.
- Uniform rinsing of each slide surface for homogeneous film formation.

The initial rinse time for the dipper experiments was determined from a series of bench-scale dilution experiments. Further optimization of the rinse time was achieved from data taken during dipper experiments that utilized the initial rinsing time.

Bench-Scale Simulated Overflow Experiments

The bench-scale experiments utilized a replicated overflow bath set-up to simulate the operation of the active rinse chamber found in the dipper. The experiments utilized a powerhead pump and continuously flowing water supply to examine the removal rate of dye contamination in the simulated rinse bath. The set-up consisted of a steady water flow, inducing fluid overflow over the vessel edges, and a horizontally-directed flow from the powerhead pump (Figure 12).

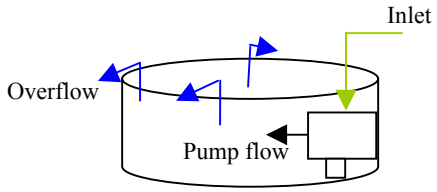

Figure 12. Schematic of bench-scale flow-thru set-up.

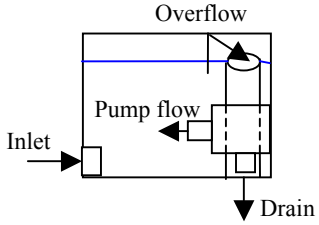

Figure 13. Schematic of DS/50 active rinse tank set-up.

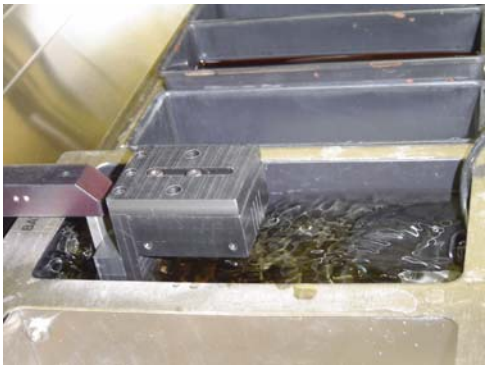

Figure 14. DS/50 active rinse bath in operation.

A fixed volume of dye (concentration= 5 mg/ml) was injected into the overflow bath (~1 ml). This volume was taken as an estimated upper bound for the carryover volume from the dye deposition bath. Samples were then drawn from the rinse bath at fixed-time increments. The samples were drawn at one-minute increments over the duration of 5 minutes, the standard deposition time for previously conducted experiments. Absorbance measurements of each solution sample were taken at the absorbance maximum of Procion Brown, λ=407 nm.

The concentration of dye in the overflow bath was calculated from absorbance measurements related by the Beer-Lambert Law, the linear relationship between absorbance and concentration of an absorbed species. For experimental measurements made in terms of transmittance (*T*)

$$T = \frac{I}{I_o} \tag{4.11}$$

where I is the intensity of light after it passes through the sample and I_0 is the initial light intensity.[48] The relationship between absorbance A and transmittance T is written as

$$A = \log\left(\frac{1}{T}\right) = \log_{10}\left(\frac{I_0}{I}\right) \tag{4.12}$$

where A can be related to the wavelength-dependent extinction coefficient, the path length and the species concentration c.

$$A = \varepsilon l c \tag{4.13}$$

where A is the measured absorbance, ε is The extinction coefficient ε of Procion Brown is 2.6 x 10^{-3} nm^2/molecule and the path length of a standard cuvet is 1 cm.

Figure 15 illustrates the exponential decay in dye concentration in the overflow bath as a function of time. The dotted line across the bottom of the graph represents the baseline value of pure water with respect to the original dye concentration C_0 at time t=0.

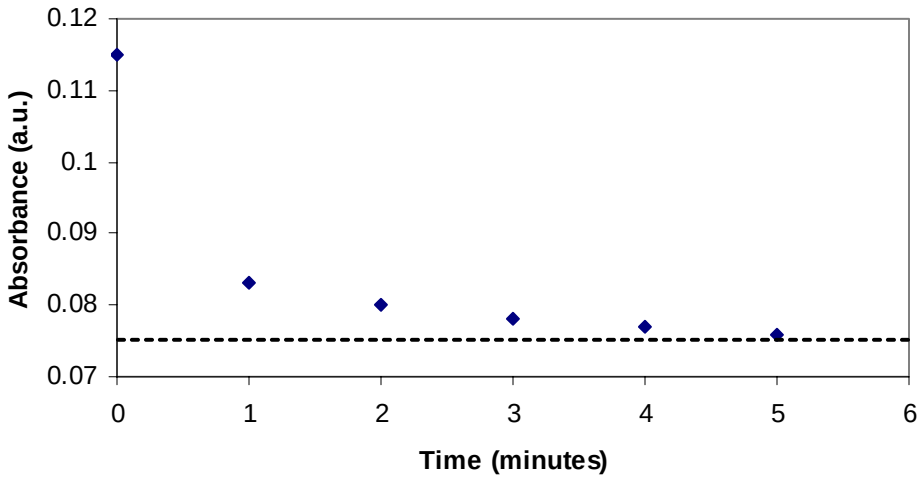

(a)

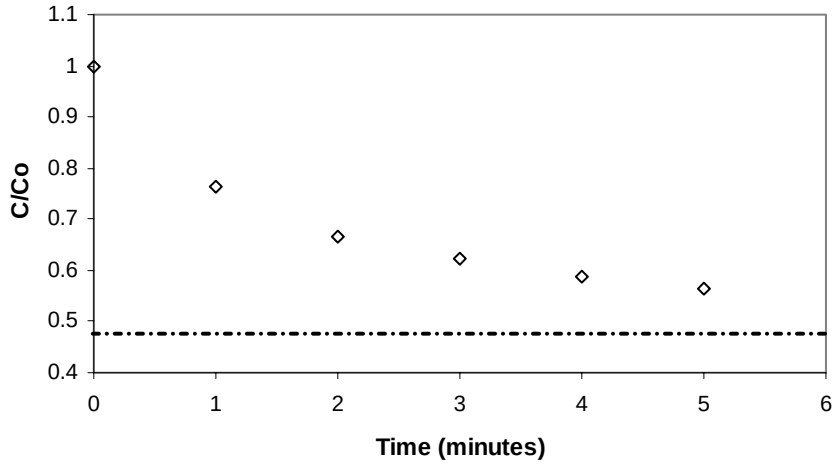

(b)

Figure 15 a-b. Plot of absorbance (a) dye concentration (C_{dep}= 5mg/ml) (b) in an overflow bath as a function of time. Overflow rate~1.4 L/min.

The overflow set-up achieves a 99% reduction in dye concentration (C_{dep}) upon instantaneous contact with the bulk rinse fluid. The concentration decay stabilized after approximately 2 minutes of fluid overflow. *Based on this data, a rinse time of 2 minutes was selected for subsequent experiments (Phase II) using the slide stainer.*

Slide Stainer Active-Rinse Bath

All rinse data from the DS/50 active rinse bath were taken during normal operation of the slide stainer while fabricating films. The bench-scale experiments provided a preliminary estimate of the system kinetics. The dye concentration in the active rinse bath at a given time *t* was calculated from absorbance measurements of samples drawn from the bath at set time increments of 15 or 30 seconds for approximately 2 minutes following a dye deposition step. The exponential decay of concentration (Figure 17) is indicative of contaminant removal from a perfectly stirred tank vessel (CST). A continuous-stirred tank (CST) is well-mixed and as a result, the reactor is modeled as having no spatial variations in temperature and most importantly, concentration.[49]

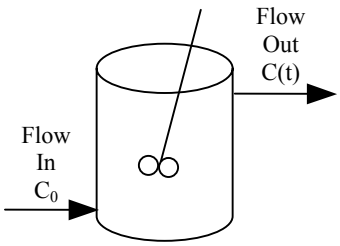

Figure 16. Continuous-stirred tank reactor.

Convection characteristically dominates the dilution and removal of a species from the system and the carryover volume is assumed to dissolve immediately upon contact with the bulk fluid in the vessel. The concentration of the carryover species decreases exponentially with time and fits the following expression

$$C(t) = C_0 e^{-t/\tau} \qquad (4.14)$$

where C is the concentration of contaminant (dye) at time t, C_0 is the initial concentration of the contaminant and τ is the residence time.

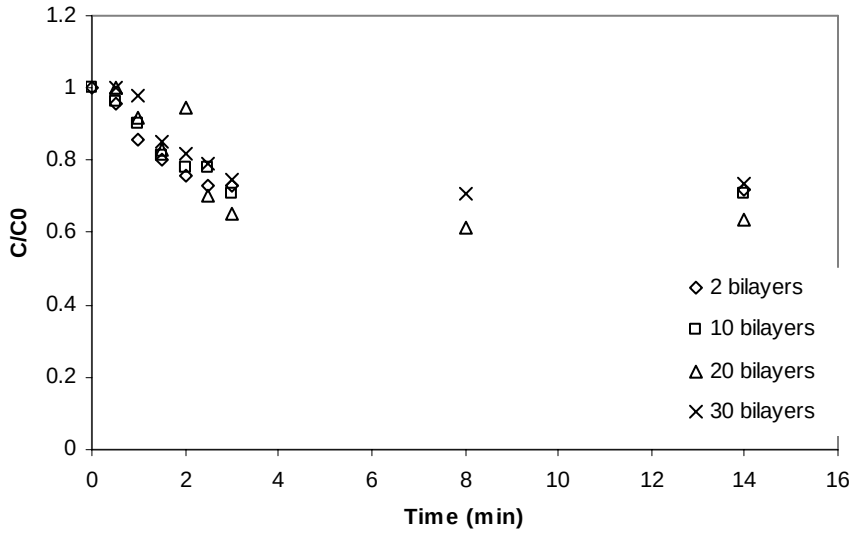

Figure 17. Plot of dye concentration vs. time for active-flow rinse bath; (C_{dep})= 5 mg/ml; C_0~$6E^{-3}$ mg dye/ml. Exponential decay in concentration indicative of well-stirred tank (CST). (Series 4009)

For C_0=6 E^{-3} mg dye/ml, C_{dep}=5 mg dye/ml, an estimated carryover layer thickness of 50 μm and a rinse vessel with V=1.65 L, concentration calculations correspond with a carryover volume approximately 2 ml (in absences of a blotting step). The slide holder is estimated to account for approximately 0.4 ml of carryover volume and the slides (4) are estimated to carry over approximately 1.6 ml of deposition fluid (~0.4 ml/slide). For the Phase II experiments, a blotting step was introduced into the procedure. For this set of experiments C_0=$4E^{-3}$ mg dye/ml and C_{dep}= 1 mg dye/ml. Figure 17 shows no increase in rinse bath dye concentration from the first 2 bilayers deposited to the last 30 layers deposited. This data proves that there is no significant dye build-up over the course of complete film fabrication.

The residence time was calculated to estimate the turnover efficiency of the active flow rinse tank. The theoretical residence time is related to the tank geometry by the following relation[50]

$$\tau = V_t / Q \qquad (4.15)$$

where V_t is the volume of the tank and Q is the volumetric flowrate of the water in the tank. The theoretical residence time for the active rinse tank is τ=1.2 minutes. A τ approximately equal to the volumetric flowrate Q indicates convection limited transport by way of perfectly-stirred conditions. However, an exponential fit of the experimental data approximates an average residence time τ= 6.4 minutes, 5 times greater than the theoretical residence time value. The

longer residence time may indicate a two-step process that involves both diffusive and convective transport. The removal of such a carryover layer is characterized by diffusion through the boundary layer followed by convective transport into the bulk fluid. The result supports the hypothesis that there could be a relatively uniform, stagnant carryover layer with relatively small surface tension forces (and significant viscous forces) which could require an extended time to remove.

The dye concentration in the active rinse bath was plotted as a function of time for two dipper experiments (Figure 18) with 2 minute rinse times programmed. Each data set was fit to an exponential model (C_{theor} Fit). The samples were drawn in 15 second intervals for two minutes, to determine the feasibility of reducing the rinse time additionally from 2 minutes to 1 minute. Concentration plotted as a function of time indicates a high initial concentration as the dye leaves the carryover layer and enters the bulk solution. The concentration proceeds to experience a long, steady decay with time.

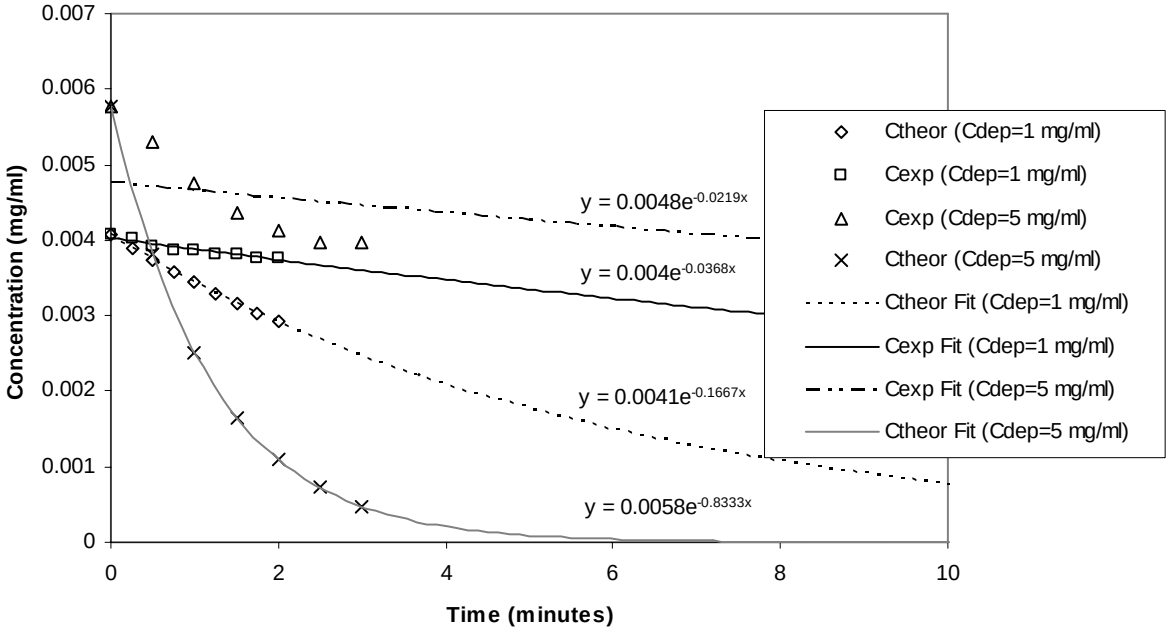

Figure 18. Plot of experimental C_{exp} and theoretical C_{theor} concentration vs time for dipper experiments conducted with a dye concentration of 5 mg/ml and 1 mg/ml.

The two cases of deposition concentration of 5 mg/ml and 1 mg/ml were selected to examine how the effect of a 5 fold reduction in deposition dye concentration on the kinetics of rinsing in the active flow bath. The reduction of dye in the active rinse bath is stabilized at approximately 2 minutes for the 5 mg/ml case. The 5 fold reduction in dye concentration to 1 mg/ml resulted in the stabilization of dye removal in less than a minute. However*, a 1 minute rinse time was selected to ensure dye turnover and proper removal of any loosely bound molecules from the slide surfaces.*

Determination of dye concentration

The dye concentration for the dipper experiments was determined from the series of experiments conducted in *Chapter 3: The Effect of Forced Convection, Deposition Time and Concentration on Properties of NLO Films*. In that series of experiments, the dye concentration time of the dye deposition step was varied while the deposition time, polymer concentration and rinse time were all remained constant (Table 9).

Table 10. Design of experiments matrix for dye concentration study. "X" denotes fixed variable.

Variable		
Deposition Time	X	2 min.
Dye Concentration		1 - 5 mg/ml
Rinse Time	X	2 min.

The deposition time for the dye and polymer bath were kept equal for each experiment (i.e. t_{dye}= $t_{polymer}$). The effect of varying dye concentration was mainly characterized by the second-order susceptibility $\chi^{(2)}_{zzz}$ (Figure 19).

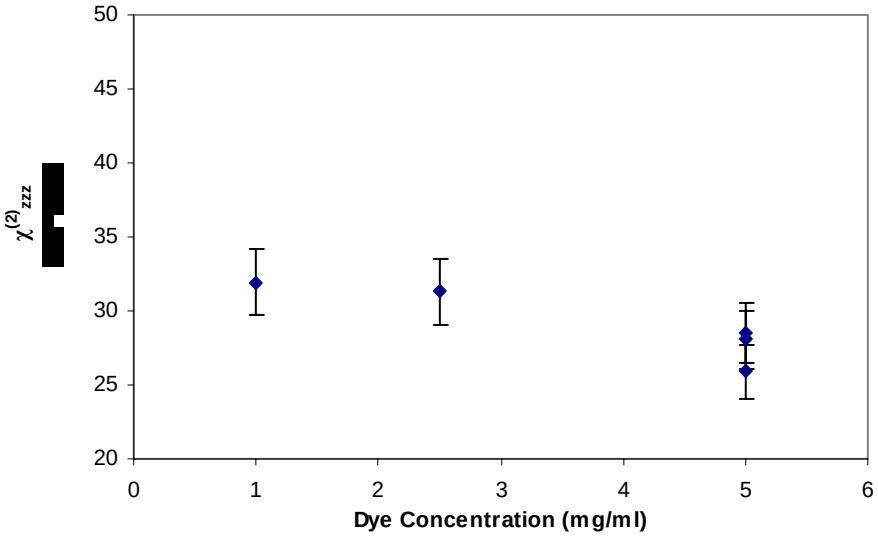

Figure 19. Plot of $\chi^{(2)}_{zzz}$ as a function of dye concentration (Chapter 3 experiments). All slides deposited in the presence of convection, at room temperature and with a deposition time of 2 minutes. PAH, 10mM, pH 7.0; PB, pH 10.5.

Conditions that exhibited a $\chi^{(2)}_{zzz} > 25 \pm 5 \times 10^{-9}$ esu were deemed suitable for automated fabrication. Figure 19 shows less than a 5% difference in $\chi^{(2)}_{zzz}$ for a 5-fold reduction in dye solution concentration, well-within the typical error reported for $\chi^{(2)}$ values (~10-20%). *A dye concentration of 1 mg/ml was selected for the Phase III experiments based on these findings.*

Phase II Experimental

Equipment Set-up

The experiment was conducted in the presence of forced convection in both deposition baths and with blotting steps. A powerhead water pump (Hagen Powerhead 201) was added to the active rinse bath to generate an increase in water circulation and therefore, more effective rinsing.

Table 11. Equipment set-up for Phase II study.

Equipment Modifications	
Active-Rinse Bath Pump	Y
Forced Convection in Deposition Baths	Y
Blotting Steps	Y

Table 12. Experimental conditions for Phase II study.

Experimental Conditions	
Deposition Time	2 min.
Dye Concentration	1 mg/ml
Polymer Concentration	10 mM
Rinse Time	2 min.
Number Bilayers (both sides)	80

Phase II Results

Homogeneity. The films conducted in Phase II of experiments exhibited improved optical homogeneity in comparison to slides fabricated in Phase I. The addition of the modified slide holder (Figure 4) and blotting steps can be attributed to a significant reduction in carryover volume, which is critical for effective rinsing and fabricating optically homogeneous films.

Plots of second harmonic intensity, as a function of incidence angle (measured at three different positions) for films made in this study (Figure 20), lacked the superposition often seen in manually-fabricated films (Figure 7). However, the films exhibited less than a 15% difference in SHG intensity over a distance of 8 mm on the film.

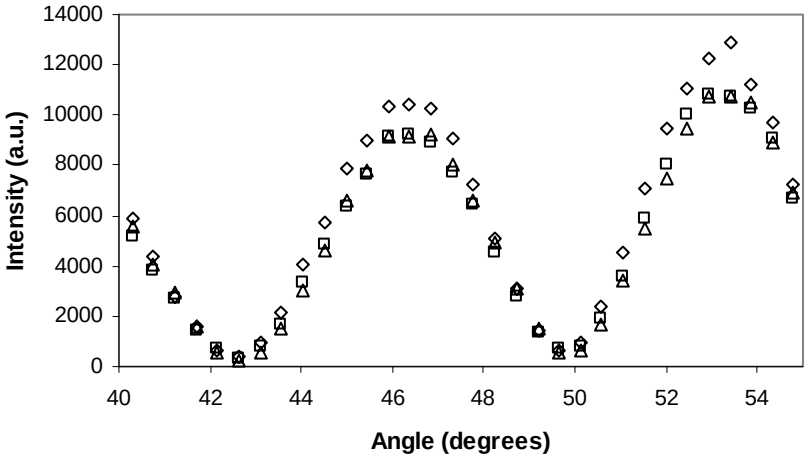

Figure 20. Plot of second harmonic intensity vs. incidence angle at three different positions. ◊=Position 0; □=Position 4; Δ=Position 8; Slides made with automatic slide stainer (Series 4249). Graphical alignment of the three measurements signifies film homogeneity. Peak minima landing at zero signifies homogeneity in the form of equivalent films on both sides of the substrates. *Measurements taken after installation of OPO*

Absorbance per bilayer. The UV absorbance of the films increased linearly with the number of bilayers deposited (Figure 21) for all films in this study. This linear increase is characteristic of layer-by-layer deposition for self-assembled films. The slope of this linear relationship between the absorbance and number of bilayers is proportional to the amount of dye deposited per layer. There was a slight deviation from linearity as the slides approached the 80 bilayer mark.

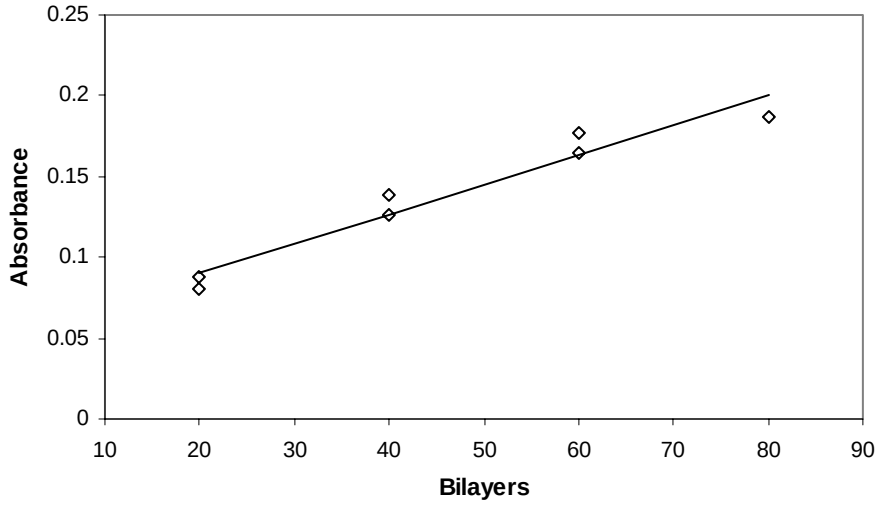

Figure 21. Plot of UV-Vis absorbance (λ=407 nm) vs number of bilayers (both sides) for Procion Brown (PB)/PAH films fabricated utilizing an automated slide stainer (Series 4249). PAH 10 mM RU (pH 7.0); PB 1mg dye/ml, 0.5M added NaCl (pH 10.5), 2 minute deposition time. Linear plot denotes regular layer-by-layer growth.

This deviation is attributed to the expired pot life of the dye solution, characterized by marked increase in dye hydrolysis. Dye solution is typically used 5-6 hours before disposal. The 6 hour mark was approached at 60 deposited bilayers (total on both sides). This experiment was conducted with a secondary goal of probing the time-dependence of dye hydrolysis and the corresponding effect on film quality. The dye solution was in use for approximately 8 hours (for 80 bilayers, both sides), which is the primary factor attributing to marginal optical quality.

The kinetics of hydrolysis are first order with respect to the dichlorotriazine dye. The first order rate constant k for Procion Brown dye was extracted from a plot of $-\ln(1-X_A)$ versus time, where X_A is the fractional conversion of the dye. The fractional conversion of the first order kinetics of dichlorotrizine dye is described by

$$-\ln(1-X_A) = kt \tag{4.16}$$

$$X_A = 1 - e^{-kt} \tag{4.17}$$

For a pH of 10.5, Procion Brown has a first order rate constant k=3 x 10^{-3} min^{-1}, with a half-life of 4 hours. With the fractional conversion defined as the ratio of the concentration of unhydrolyzed dye at time t, $c(t)$ to the initial mass of dye c_0, the unhydrolyzed concentration of dichlorotriazine dye as a function of time is given by

$$c(t) = c_0\left(1 - e^{-kt}\right) \tag{4.18}$$

For a Procion Brown dye solution with an initial concentration of 1 mg dye/ml, the concentration of unhydrolyzed dye at time t is given by

$$c(t) = \left(1 - e^{-3x10^{-4}t}\right) \tag{4.19}$$

For example, after an elapsed time of 8 hours, the mass of hydrolyzed dye is increased to 67 mg (0.13 mg/ml), an 87% decrease in reactive Procion Brown molecules. At these conditions, a significant amount of dye molecules can be hydrolyzed in solution in a time span of 2 hours.

Ellipsometry

Film thicknesses were obtained from an ellipsomteric fit to a two-layer model. The first layer represented the glass substrate used for deposition whereas the second layer represented the self-assembled film (Lorentz oscillator model). The film thickness data and optical constants (n and k) obtained from the two-layer model correlate well (Figure 22) with prior ellipsometric data for identical deposition conditions, indicating a reliable fit to the two-layer model developed for this study.

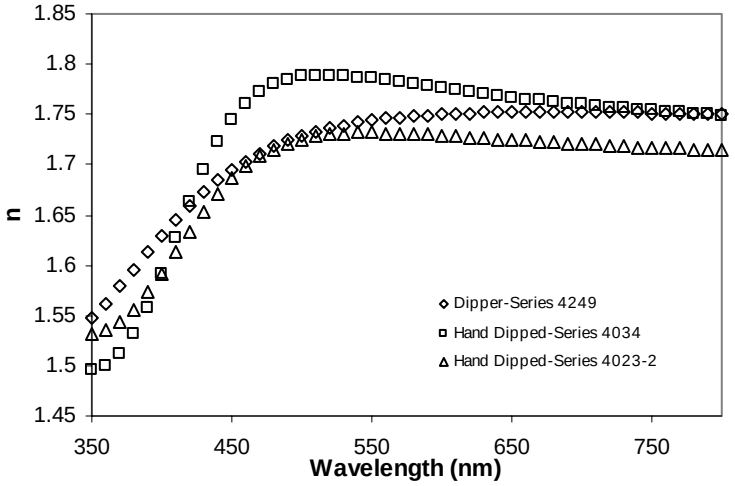

Figure 22. Plot of refractive index n vs. wavelength of PAH/PB films fabricated with an automated slide stainer (Series 4249) compared to those fabricated manually (Series 4034, 4023-2).

Bilayer thickness (Table 14) and refractive index results were averaged over three measurements for each slide with the highest number of bilayers.

SHG Results. The second harmonic intensity generated by the films exhibit the expected quadratic scaling as a function of bilayer number (for films up to 80 bilayers (both sides). This demonstrates uniform maintenance of orientation as successive layers are deposited.

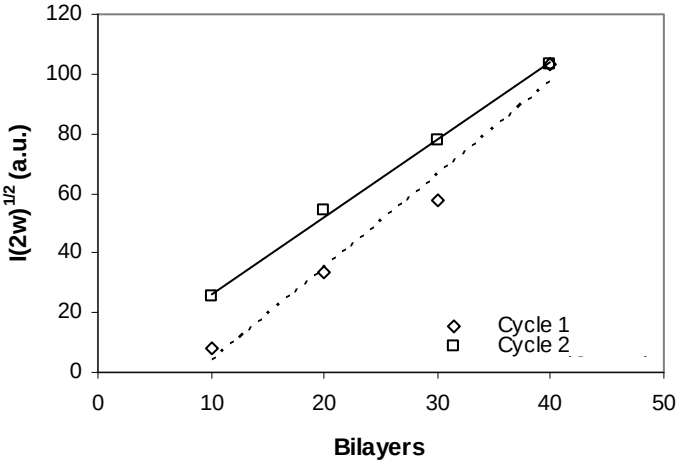

Figure 23. Square root of second harmonic intensity as a function of the number of PAH/Procion Brown bilayers. Films were fabricated utilizing an automatic slide stainer (Series 4249).

Slides were deposited in rotations throughout the four positions on the slide holder (Table 13).

Table 13. Slide rotation assignments for Phase II experiments. The number in parenthesis is the number of bilayers to be deposited on both sides of each film.

Slot #1	Slot #2	Slot #3	Slot #4
Slide D (80)	Slide C (60)	Slide B (40)	Slide AA (20)
	Slide A (20)	Slide BB (40)	Slide CC (60)

The number in parenthesis is the number of bilayers to be deposited on each film. Slides labeled C, B and AA were all grouped as Cycle 1 in Figure 23. These slides were deposited during the first 6 hours of the experiment, prior to significant dye hydrolysis. Slides CC, BB and A were all plotted as Cycle 2 on Figure 23. These slides were deposited at the latter end of the deposition cycles, where the dye is known to undergo significant hydrolysis. The $\chi^{(2)}$ value for Cycle 1 ($\chi^{(2)}_{zzz}$= 40.1 x 10^{-9} esu) was approximately 9% greater than the value for slides deposited during Cycle 2 ($\chi^{(2)}_{zzz}$ = 50.0 x 10^{-9} esu). The slide rotation and dye pot life utilized for Cycle 1 is representative of prior and all future intended experiments, therefore the $\chi^{(2)}_{zzz}$ value reported for Phase II experiments is that of Cycle I.

Table 14. Summary of results (Phase II Experiments) automated film fabrication. PAH 10mM, pH 7.0; Procion Brown 1 mg dye/ml, 0.5M added NaCl, pH 10.5, 2 minute rinse, Series 4249 compared to hand-dipped films (Series 4244).

Cycle	Tilt Angle	$\chi^{(2)}_{zzz}$	$\chi^{(2)}_{eff}$	Abs/bilayer	Thick./bilayer	Dep. Time (min)	Convection	Dye Conc.	# Bilayers
1	37.4°	**30.0**	12.1 ± 2.9	0.00184	0.97 ± 0.12	2	Y	1 mg/ml	80
2		**25.1**	10.1 ± 3.6						
Series 4244	40.8°,41.2°	**31.9**	16.4 ± 2.1	0.00173	0.79 ± 0.10	2	Y	1 mg/ml	60

Phase II Conclusions

An automated film fabrication experiment was conducted utilizing conditions optimized in hand-dipping experiments and a base-case dipper experiment. The films compared well with manually-fabricated films in the values of thickness and optical constants. The films exhibited improved optical homogeneity from base-case studies, with less than a 7% difference in SHG

values over a 8mm-distance on the slide. Absorbance per bilayer trends displayed linear growth with bilayer number, indicating regular layer-by-layer growth. The films experienced slight deviation from linearity in the latter stages of the experiment, where the dye solution is known to posses a significant degree of dye hydrolysis. The second harmonic intensity generated by the films exhibited the expected quadratic scaling as a function of bilayer number for films up to 80 bilayers (total on both sides), corresponding to a film thickness of 40 nm. The study demonstrated the feasibility of a 5 –fold reduction in dye concentration and a 60% reduction in processing time. Kinetic modeling of the slide stainer active-rinse bath resulted in the proposal of a further reduction in rinse time by 50%. The significant reduction in processing time, quadratic scaling of second harmonic intensity with film thickness, and improved optical homogeneity all lend support to the possibility that the automated dipper might be capable of fabricating films with quality and thickness sufficient for an EO modulator device. Phase III of this study will address the automated fabrication of a thicker film.

Phase III: Thick Film Fabrication

Phase III Experimental

Equipment Set-up

The experiment was conducted in the presence of forced convection in both deposition baths and with blotting steps, as was done in Phase II.

Table 15. Equipment set-up for Phase III study.

Equipment Modifications	
Active-Rinse Bath Pump	Y
Forced Convection in Deposition Baths	Y
Blotting Steps	Y

Table 16. Experimental conditions for Phase III study.

Experimental Conditions	
Deposition Time	2 min.
Dye Concentration	1 mg/ml
Polymer Concentration (r.u. basis)	10 mM
Rinse Time	1 min.
Number Bilayers (total on both sides)	500

Phase III Results

Homogeneity. The films fabricated in Phase III of experiments exhibited improved optical homogeneity in comparison to slides fabricated in Phase I and Phase II. These films exhibited less than a 5% variation in SHG intensity over a 8 mm distance on the film.

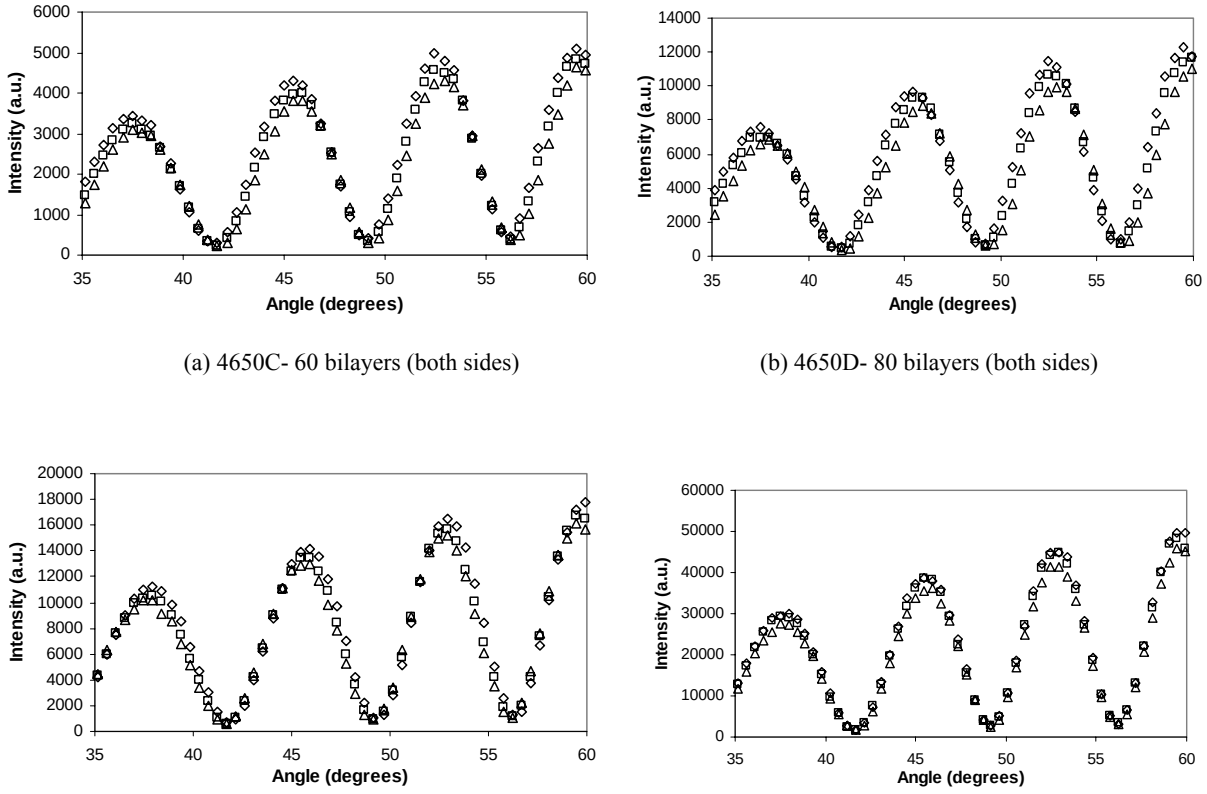

(a) 4650C- 60 bilayers (both sides)

(b) 4650D- 80 bilayers (both sides)

(c) 4650E- 100 bilayers (both sides)

(d) 4650F- 200 bilayers (both sides)

Figure 24. Plot of second harmonic intensity vs. incidence angle at three different positions. ◊=Position 0; □=Position 4; Δ=Position 8; Slides made with automatic slide stainer (Series 4650). Graphical alignment of the three measurements signifies film homogeneity. Peak minima landing at zero signifies homogeneity in the form of equivalent films on both sides of the substrates. *Measurements taken after the installation of the OPO.*

Films with 20-200 deposited bilayers (both sides) exhibited excellent optical homogeneity. Films greater than 200 bilayers displayed poor optical homogeneity. These films delaminated from the glass substrate upon contact with water. The source of the delamination is undetermined, but will be probed in future studies.

Absorbance per bilayer

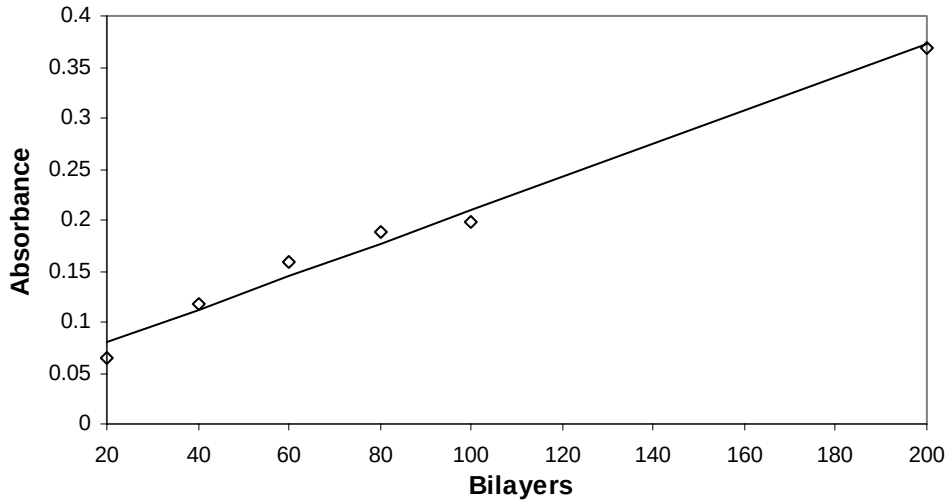

Figure 25. Plot of UV-Vis absorbance (λ=407 nm) vs number of bilayers for Procion Brown (PB)/PAH films fabricated utilizing an automated slide stainer (Series 4650). PAH 10 mM RU (pH 7.0); PB 1mg dye/ml, 0.5 M added NaCl (pH 10.5), 2 minute deposition time. Linear plot denotes regular layer-by-layer growth.

Ellipsometry

Film thicknesses were obtained from an ellipsomteric fit to a two-layer model. The first layer represented the glass substrate used for deposition whereas the second layer represented the self-assembled film (Lorentz oscillator model). The film thickness data and optical constants obtained from the two-layer model correlate well with prior ellipsometric data for similar deposition conditions, indicating a reliable fit to the two-layer model developed for this study. Bilayer thickness (Table 18) and refractive index results were averaged over three measurements for each slide with the highest number of bilayers.

SHG Results. The square root of the second harmonic intensity generated by the films exhibited relatively significant quadratic scaling (Figure 26) as a function of bilayer number (for films up to 200 bilayers (total on both sides), demonstrating uniform maintenance of orientation as successive layers are deposited.

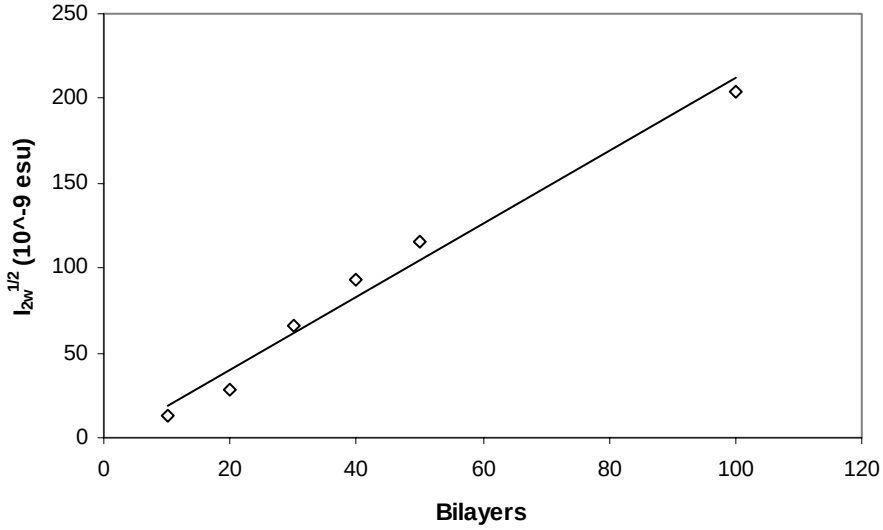

Figure 26. Square root of second harmonic intensity as a function of the number of PAH/Procion Brown bilayers. Films were fabricated utilizing an automatic slide stainer (200 bilayers, total both sides).

The slides were deposited in rotations throughout the four positions on the slide holder (Table 17).

Table 17. Slide rotation assignments for Phase III experiments. The number in parenthesis is the number of bilayers to be deposited on both sides of each film.

Slot #1	Slot #2	Slot #3	Slot #4
Slide I (500)	Slide H (400)	Slide F (200)	Slide A (20)
	Slide E (100)	Slide GG (300)	Slide B (40)
			Slide C (60)
			Slide D (80)
			Slide G (300)

Table 18. Summary of results (Phase III Experiments) automated film fabrication. PAH 10mM, pH 7.0; Procion Brown 1 mg dye/ml, 0.5M added NaCl, pH 10.5, 1 minute rinse, Series 4560.

Tilt Angle	$\chi^{(2)}_{zzz}$	$\chi^{(2)}_{eff}$	Abs/bilayer	Thick./bilayer	Dep. Time (min)	Convection	Dye Conc.	# Bilayers
36.1°	22.9	9.5 ± 2.2	0.00162	0.99 ± 0.08	2	N	1 mg/ml	200

Phase III Conclusions

A series of experiments was conducted to fabricate a 500 nm-thick hybrid covalent self-assembled film. Deposition conditions determined from a series of manually fabricated films (Chapter 3) were employed in this study to fabricate the thick film with a minimal cycle time and

utilizing minimum materials (i.e. dye, DI water, etc.). The major aim of fabricating a 500 nm-thick film for potential EO device applications was not achieved for this study. However, a 100 nm-thick film was fabricated with quadratic scaling of the square root of the second harmonic intensity with film thickness. Films 150 nm and greater in thickness experienced significant heterogeneities and delamination from the glass substrate at various film locations. Thicker films deposited in the study lacked the physical robustness often characteristic of films with covalently bonded entities. The root of the film delamination potentially stems from a number of sources. Cross-contamination between the cationic and anionic deposition solutions is an unlikely possibility due to the excellent optical quality of films deposited simultaneously with the slides experiencing delamination. However, insufficient rinsing or inappropriate pH conditions for extended dipping experiments are also likely possibilities. The rinsing step for PAH is known to be relatively longer than that of Procion Brown because unattached entangled polymer chains, encountered in semi-dilute solutions ($C>C^*$), must detangle from adsorbed chains to be removed from the surface. If these loosely bound chains were to remain at the film surface, successive built-up layers could eventually delaminate from the glass substrate. Procion Brown is deposited under high pH conditions (pH=10.5) for the covalent reactive deposition step of hybrid film formation. High pH conditions are known to dissolve silica groups on glass, potentially providing another delamanation mechanism over a prolonged period of exposure.

Overall Conclusions

A series of automated hybrid covalent film fabrication experiments were conducted with the aim of optimizing the deposition process and replicating current manual deposition methods. Kinetic modeling parameters of the rinsing process were determined from monitoring the absorbance of dye build-up in the active rinse bath. The rinse bath was found to adhere to the kinetic trends of a continuously-stirred tank vessel (CST) with immediate dilution of the dye upon contact with the bulk rinse fluid. The theoretical residence time varied significantly from the experimentally-obtained theoretical time, potentially implying a rinsing process with two-step diffusive and convective transport barriers. Stagnant flow fields in the rinse tank also could manifest in the form of an elevated residence time. Contaminant species residing in these stagnant flow regimes could definitely have a detrimental effect on the efficiency of contaminant removal from the bulk fluid. Equipment modifications employed in dipper operation (i.e.

powerhead, blotting step, etc.) proved essential for good optical film quality. Films fabricated in the presence of convection with a blotting step following each deposition step exhibited a marked increase in optical homogeneity in comparison to base case studies in which these equipment modifications were neglected. Films fabricated with the automated process correlated very well with manually-fabricated films in terms of thickness, optical constants, absorbance per bilayer and second harmonic generation. The $\chi^{(2)}$ values obtained for films in this study were comparable to those previously obtained for identical chemistries. Optically homogeneous films up to 100 nm were fabricated for the first time utilizing the hybrid covalent deposition method in this study. These films exhibited the expected quadratic scaling of the second harmonic intensity with bilayer number, indicating stabilization of acentric ordering with increasing layers deposited. In future work, the kinetics of PAH rinsing and adsorption should be studied using a quartz crystal microbalance and biological amine assays. Furthermore, the effect of high pH conditions on glass substrates should be studied utilizing any number of surface characterization techniques, such as AFM or prolifometry. Process and equipment modifications are necessary to fabricate films thicker than 100 nm. The automated process stands for improvement particularly in the area of slide holder design. Increasing the gap between slides will greatly improve the rinsing efficiency which is critical for optically homogeneous films. These modifications will attest this automated process as a feasible means for fabricating thick, EO device-capable films.

References

[1] Wise, D. L.; Wnek, G. E.; Trantolo, D. J.; Cooper, T. M.; Gresser, J. D. Photonic Polymer Dekker, New York (1998) Ch. 14 Polymeric Optical Guided-Wave Devices, 517.

[2] L.-H. Peng, L.-H.; Hsu, C.,-C, Shih, Y.-C 'Second-Harmonic Green Generation from Two-Dimensional Chi[sup (2)] Nonlinear Photonic Crystal with Orthorhombic Lattice Structure' *Appl. Phys. Lett.* **83** (2003) 3447-3455.

[3] Ni, P.; Ma, B.; Wang, X.; Cheng, B.; Zhang, D. 'Second-Harmonic Generation in Two-Dimensional Periodically Poled Lithium Niobate Using Second-Order Quasiphase Matching' *Appl. Phys. Lett.* **82** (2003) 4230-4238.

[4] Zeng, X.; Chen, X.; Chen, Y.; Xia, Y.; Chen, Y. 'Observation of all-optical wavelength conversion based on cascaded effect in periodically poled lithium niobate waveguide' *Optics & Laser Technology* ***35*** (2003) 187-190.

[5] Kim, J. H.; Yoon, C.S. 'Domain switching characteristics and fabrication of periodically poled potassium niobate for second-harmonic generation' *Appl. Phys. Lett.* **81** (2002) 3332-3338.

[6] Beckers, L.; Buchal, C.; Fluck, D.; Pliska, T.; Günter, P. 'Potassium niobate waveguides: He^+ implantation in bulk single crystals and pulsed laser deposition of thin films' *Materials Science and Engineering A* **253** (1998) 292-295.

[7] Fluck, D.; Pliska, T.; Günter, P.; Beckers, L.; Buchal, C. 'Blue-light second-harmonic generation in ion-implanted KNbO[sub 3] channel waveguides of new design' *Appl. Phys. Lett.* **69** (1996) 4133-4139.

[8] Kitamura, K.; Yamamoto, J. K.; Iyi, N.; Kimura, S. 'Stoichiometric $LiNbO_3$ single crystal growth by double crucible Czochralski method using automatic powder supply system' *J. Crystal Growth* **116** (1992) 327-343.

[9] Takagi, T.; Fujii, T.; Sakabe, Y. 'Growth and characterization of $KNbO_3$ by vertical Bridgman method' *Journal of Crystal Growth* **259 (**2003) 296-301.

[10] Williams, D. J., ed. 'Nonlinear optical properties of organic and polymeric materials' ACS Symposium Series 233, American Chemical Society: Washington, DC, 1983.

[11] Thakur, M.; Titus, J.; Mishra, A. 'Single-crystal thin films of organic molecular salt may lead to a new generation of electro-optic devices' *Opt. Eng.* **42** (2003) 456-458.

[12] Koeste, M.; Laschewsky, A.; Jonas, A. M.; Verbiest, T. 'Orientation of functional groups in polyelectrolyte multilayers studied by second-harmonic generation (SHG)' *Colloids and Surface A* **198-200** (2002) 275-280.

[13] Kaino, T. 'Waveguide fabrication using organic nonlinear optical marerials' *J. Opt. A: Pure Appl. Opt.* **2** (2002) R1-R7.

[14] Yu, H.H.; Hwang, S.-J. 'E-O functional waveguide using the electric-field-poled polymeric material for integrated-optic devices' *Optics Communications* **219** (2003) 183-192.

[15] Ma, H.; Liu, S.; Luo, J.; Suresh, S.; Liu, L.; Kang, S. H.; Haller, M.; Sassa, T.; Jen, A. K. Y.; Dalton, L. R. 'Highly efficient and thermally stable electro-optical dendrimers for photonics' - *Adv. Funct. Mater* **12** (2002) 565-574.

[16] Sottini, S.; Grando, D.; Palchetti, L.; Giorgetti, E.; Ricceri, R.; Gabrielli, G. 'Organic films for guided nonlinear optics' *Materials Science and Engineering* **C5** (1998) 167-172.

[17] Ashwell, G. J.; Jackson, P. D.; Crossland, W. A. 'Noncentrosymmetry and second harmonic generation in Z-type Langmuir-Blodgett Films' *Nature* **368** (1994) 438-440.

[18] Wang, W.; Zhu, P.; Marks, T. J.; Ketterson, J. B. 'Ultrafast frequency-selective optical switching based on thin self-assembled organic chromophoric films with a large second-order nonlinear response' *Appl. Phys. Lett.* **81** (2002) 2169-2171.

[19] Decher, G.; Hong, J. D.; Schmitt, J. 'Buildup of ultrathin multilayer films by a self-assembly process: consecutively alternating adsorption of anionic and cationic polyelectrolytes on charged surfaces' *Thin Solid Films* **210/211** (1992) 831-835.

[20] Heflin, J. R.; Figura, C.; Marciu, D.; Liu, Y.; Claus, R. O. 'Thickness dependence of second harmonic generation in thin films fabricated from ionically self-assembled monolayers' *Appl. Phys. Lett.* **74** (1999) 495-497.

[21] Koeste, M.; Laschewsky, A.; Verbiest, T. 'Films grown from polyamines and reactive dyes by alternating adsorption/surface activation' *Mater. Sci. Eng. C* **10** (1999) 107-113.

[22] Wang, X.; Balasubramanian, S.; Li, L.; Jiang, X.; Sandman, D. J.; Rubner, M. F.; Kumar, J.; Tripathy, S. 'Self-assembled second order nonlinear optical multilayer azo polymer' *Macromol. Rapid Commun.* **18** (1997) 451-459.

[23] Lvov, Y.; Yamada, S.; Kunitake, T. 'Nonlinear optical effects in layer-by-layer alternate films of polycations and an azobenzene-containing polyanion' *Thin Solid Films* **300** (1997) 107-110.

[24] Leermakers, F. A. M.; Oever, J. M. P.; Zhulina, E. B. 'On the charge overcompensation of quenched polyelectrolyte stars electrostatically adsorbed onto a quenched oppositely charged planar surface' *J. Chem. Phys.* **118** (2003) 969-980.

[25] Klushin, L.I.; Skvortsov, A.M.; Leermakers, F.A.M 'Exactly solvable model with stable and metalstable states for a polymer chain near an adsorbing surface' *Physical Review E* **66** (2003) 036114/1-036114/16.

[26] Geffroy, C.; Labeau, M. P.; Wong, K.; Cabane, B.; Stuart, M. A. 'Kinetics of adsorption of polyvinylamine onto cellulose' *Colloids and Surfaces A* **172** (2000) 47-56.

[27] Dijt, J. C.; Stuart, M. A.; Fleer, G. J. 'Kinetics of polymer adsoprtion and desorption in capillary flow' *Macromolecules* **25** (1992) 5416-5423.

[28] Van Cott, K. E.; Guzy, M.; Neyman, P.; Brands, C.; Heflin, J. R.; Gibson, H. W.; Davis, R. M. 'Layer-by-layer deposition and ordering of low-molecular weight dye molecules for second-order nonlinear optics' *Angew. Chem. Int. Ed.* **41** (2002) 3236-3328.

[29] Heflin, J. R.; Neyman, P. J.; Guzy, M.; Shah, S. M.; Davis, R. M.; Van Cott, K. E.; Wang, H.; Gibson, H. W.; Brands, C. 'Hybrid covalent/ionic self-assembly of organic second order nonlinear optical films, in Organic Thin Films for Photonic Applications, OSA Trends in Optics and Photonics Series **64** (2002) 3-8.

[30] Brands, C.; Neyman, P. J.; Guzy, M. T.; Shah, S.; Davis, R. M.; Van Cott, K. E.; Wang, H.; Gibson, H. W.; Heflin, J. R. 'In situ measurements of the formation of ionically self-assembled monolayers by second harmonic generation' *MRS Symp. Proc.* **707** (2002) DD12.5.1-6.

[31] Brands, C. 'Interface effects and deposition process of ionally self-assembled monolayer films: in situ and ex situ second harmonic generation measurements' Ph.D. Thesis, Virginia Tech 2003.

[32] Langmuir, I. 'The adsoprtion of gases on plane surfaces of glass, mica and platinum' *Am. Chem. Soc.* **40** (1918) 1361-1403.

[33] Parker, R.; Chiarello, R. P. 'Extreme rinse optimization' 17th Annual Semiconductor Pure Water and Chemicals Conference, Santa Clara, CA (1998) 323-341.

[34] Kempka, S.N.; Torczynski, J. R.; Geller, A. S.; Rosato, J. J.; Walters, R. N.; Sibbett, S. S. 'Evaluating the efficiency of overflow wet rinsing' *Micro* (1995) 41-46.

[35] Lindquist, P. G.; Walters, R. N.; Throngard, J. O.; Rosato, J. J. 'Determination of rinsing parameters using a wafer gap conductivity cell in wet cleaning tools' Proceedings of the Materials Research Society, San Francisco, CA (1995).

[37] Hoogeveen, N.; Cohen Stuart, M. A.; Fleer, G. 'Formation and stability of multilayers of polyelectrolytes' *Langmuir* **12** (1996) 3675-3681.

[38] Lvov, Y.; Ariga, K.; Onda, M.; Ichinose, I.; Kunitake, T. 'A careful examination of the adsorption step in the alternate layer-by-layer assembly of linear polyanion and polycation' *Colloids and Surf. A* **146** (1999) 337-346.

[39] Rosato, J. J.; Walters, R. N.; Hall, R. M.; Lindquist, P. G.; Spearow, R. G.; Helms, C. R. 'Studies of rinse efficiencies in wet cleaning tools' Proceedings of Electrochemical Society 184th Meeting, New Orleans, LA 1993.

[40] Tonti, A. Proceedings of the Second International Symposium on Cleaning Technology in Semiconductor Device Manufacturing, Ruzyllo, J.; Novak, R. E. ed. **PV92-12** (1992) 41.45.

[41] Guzy, M. Organic self-assembled layer-by-layer thin films for second-order nonlinear optics, Ph.D. Thesis, Virginia Tech, 2003.

[42] Ni, P.; Ma, B.; Wang, X.; Cheng, B.; Zhang, D. 'Second-Harmonic Generation in Two-Dimensional Periodically Poled Lithium Niobate Using Second-Order Quasiphase Matching' *Appl. Phys. Lett.* **82** (2003) 4230-4239.

[43] Itano, M.; Kern, F.; Miyashita, M.; Ohmi, T. 'Particle removal from silicon wafer surface in wet cleaning processes' *IEEE Trans. on Semicond. Manu.* **6** (1993) 258-267.

[44] Van Cott, K.; Amos, T.; Gibson, H.; Davis, R.; Heflin, J. 'Characterization of the purity and stability of commercially available dichlorotriazine chromophores used in nonlinear optical materials' *Dyes and Pigments* **58** (2003) 144-145.

[45] Neyman, P.; Guzy, M.; Shah, S; Davis, R.; Van Cott, K.; Wang, H.; Gibson, H.; Brands, C.; Heflin, J. 'Second-Order Nonlinear Optical Responses of Ionically Self-Assembled Films: Polycation Variations and Dianionic Chromophores', *SPIE Proceedings* **4461** (2001) 214-226.

[46] Neyman, P. Nonlinear Optical Properties and Structural Characteristics of Ionically Self-Assembled Nanoscale Polymer Films Influenced by Ionic Concentration and Incorporation of Monomer Chromophores, MS Thesis, Virginia Tech 2004.

[48] Dean, J. A. "Lange's Handbook of Chemistry" McGraw-Hill, New York 1999.

[49] Fogler, H. S. "Elements of chemical reaction engineering" Prentice Hall, New Jersey 1999.

[50] Hill, C. G. "An introduction to chemical engineering kinetics and reactor design" Wiley and Sons, New York, 1977, 273.

Chapter 5

Fabrication and Optical Testing of Polymeric /NLO Chromophore Films for Optical Waveguides

Introduction

Over the last decade great attention has been paid to the study of various polymer systems for use in optical communication devices. This technology can be applied to several devices, such as frequency modulators, tunable filters, broadband optical modulators and waveguides. The use of waveguides has been studied with the aim of obtaining smaller and cheaper functionality for optical circuits. Waveguides utilize less power for switches and modulators than traditional integrated optic devices due to the fact that the electro-optic (EO) effect reduces the distance that the electric-field must be applied. Therefore, a smaller voltage is required to operate such devices.[1] Traditionally, inorganic materials, such as lithium niobate ($LiNbO_3$)[2,3,4] and potassium niobate ($KNbO_3$)[5,6,7] have been used for electro-optic devices. These materials yield high performance in the critical areas of data transmission speed and minimal optical loss, but in comparison to organic materials, they are relatively expensive and require lengthy processing times for crystal growth.[8,9] Organic/polymeric molecules have attracted an increasing amount of interest due to their potential application to nonlinear optic (NLO) devices. This interest is not only motivated by the potentially large NLO response, but also by the versatility, ease of processing and ready availability of such materials. Organic molecules can be tailored to possess high hyperpolarizabilities and may be processed into good optical quality thin films. Consequently, research relating to electro-optic devices has been driven towards developing alternative methods and materials for fabricating such devices. The overall objective for polymer-based EO devices is to fabricate a device with:

- a high electro-optic coefficient r_{33} ($r_{33,\ LiNbO3}$= 30 pm/V)
- a low half wave voltage V_π (< 1V) and
- stable optical activity under (1) mechanical stress, (2) electric field poling, and (3) elevated thermal conditions.

Furthermore, the device must be fabricated in a time efficient and cost-effective manner.

Electro-optic (EO) Device Fabrication

Several techniques have been developed for fabricating polymeric electro-optic devices. Guest-host systems,[10,11,12] poled polymer systems,[13,14,15,16] and recently self assembled systems[17] have all produced polymeric electro-optic devices with comparable electro-optic coefficients (in comparison to lithium niobate). Guest-host systems are favorable due to the fact that the guest-host system does not require chemical attachment of a chromophore to a host polymer. Therefore, these systems can be fabricated at a lower cost than side-chain and cross-linked systems, both of which are synthesized with more complicated reactions. Guest-host systems also achieve more efficient electric field poling than other systems in comparison. However, guest-host systems experience rapid decay in NLO properties and the chromophore concentration in the polymer system is low, which further limits NLO activity.[18] Poled polymer systems possess good mechanical properties, high EO efficiency and moderately high thermal stability (with cross-linking). But problems arise with the long-term relaxation of the dipole orientation, typically induced by an externally applied electric field. Incorporating high T_g polymers into the backbone of the chromophore can reduce these problems. However, the incorporation of these polymers into the backbone limits the solubility and viscosity control of the solutions, which is problematic for the spin-casting technique that is typically utilized to fabricate such films.

A recent class of novel self-assembled systems based on Procion dye chemistry has been developed with the aim of increasing the stability of the dipole orientation, reducing steric-constraints from backbone attachment, and producing a large nonlinear optical response. These systems have good mechanical stability, fine control on thickness and refractive index and may be fabricated at a relatively low cost compared to inorganic materials. Prior analysis of self-assembled systems for electro-optic applications has pointed to processing time and thermal stability as primary areas of weakness for these systems. However, recent studies (Chapter 4) have made two key advancements in these areas: (1) Findings show that a 60% reduction in deposition time (5 minutes reduced to 2 minutes) can be achieved with negligible effect to nonlinear optical activity. (2) Films fabricated from this novel class of films are able to withstand a temperature of 150°C for 24 hours with only a 9% decrease in second-order NLO susceptibility $\chi^{(2)}$ that completely recovered upon cooling (P. Neyman, PhD Thesis).

Electro-optic Effect (Theory/Measurement)

The electro-optic (EO) effect is described as the modification of optical parameters produced by the application of low-frequency electric fields. Specifically, the EO effect refers to changes in the optical dielectric tensor of a medium when a low frequency electric field is applied to the medium.[19] This effect is achieved by placing the medium between two electrodes and applying a voltage to the electrodes. The EO effect can alter the absorption as well as refraction properties of the medium. A change in the refractive properties with an applied electric field is an effect called electro-refraction. This phenomenon is most commonly referred to as the linear electro-optic effect. For a nonlinear optical medium in the presence of both an optical field (oscillating at optical frequency ω) and an applied electric field, the nonlinear polarization of the medium can be written as

$$P_i^{\omega} = 2\varepsilon_0 \chi_{ijk}^{(2)} \left(E_j^{\omega}\right)\left(E_k^{\omega}\right) \tag{5.1}$$

where ε_0 is the dielectric constant, $\chi^{(2)}$ is the second order susceptibility, E_j and E_k are the electric fields and the subscripts refer to the directions of polarization of the fields. Using symmetry relations and the refractive index tensor n_{ijk}, the electro-optic (or Pockels) tensor r_{ijk} is derived

$$r_{ijk} = -\frac{2\chi_{ijk}^{(2)}}{n_i^2 n_j^2} \tag{5.2}$$

The symmetry of the electro-optic tensor and tensor algebra is used to reduce the first two subscripts and write $r_{ijk} = r_{jik} \rightarrow r_{lk}$. The subscripts are then transformed to numbers, which gives the familiar convention of the linear electro-optic coefficient r_{33}. The refractive index is related to the electro-optic coefficient by

$$n = n_0\left(1 - \frac{1}{2} n_0^2 r_{33} E\right) \tag{5.3}$$

where n_o is the original refractive index and E is the applied electric field. The linear electro-optic coefficient r_{33} of polymeric electro-optic materials is often measured using optical interferometry. The most commonly used methods for measuring the EO effect include the

waveguide method,[20] the Michelson[21,22] interferometer, the Fabry–Perot interferometer,[23,24,25] Mach–Zehnder interferometer [26,27,28,29] and the reflection method.[30,31] An EO measurement can be performed using a number of configurations including two-beam wavefront interferometry and single-beam polarization interferometry. The single-beam reflection interferometry method was introduced by Teng and Man and later modified by others.[32,33] This method is based on the polarization rotation of a laser beam due to the electro-optic effect. The EO effect is measured while a polymeric film undergoes low-voltage electrical poling. For this technique, the electro-optic coefficient is defined as

$$r_{33} = \frac{3\lambda I_m}{4\pi V_m I_c} \frac{\left(n^2 - \sin^2\theta\right)^{1/2}}{n^2 \sin^2\theta} \tag{5.4}$$

where λ is the wavelength of light, I_m is the modulation amplitude, I_c is the half-max laser intensity, V_m is the applied modulation voltage, θ is the incident angle of the laser beam and n is the refractive index of the film. This method is relatively complicated, but has proven to be (1) more time efficient and (2) more tolerant of light absorption, often encountered in polymer systems, than the more conventional waveguiding method. This, the reflection method has proven to be an accurate and widely-used technique to measure the electro-optic coefficient for polymeric electro-optic devices.

Current Studies

Polymeric electro-optic devices have been successfully fabricated utilizing a number of alternate methods. This study employed a novel hybrid covalent-electrostatic deposition scheme to fabricate a polymeric electro-optic waveguide device with an electro-optic coefficient comparable to that of lithium niobate. This method builds films layer-by-layer by alternately immersing a substrate into aqueous solutions of polyelectrolyte "glue" and a reactive chromophore dye.[34,35,36] The adsorption of the layers alternates between electrostatic interaction and covalent reaction. The polyelectrolyte is electrostatically attached to the charged surface of the substrate, while the chromophore is covalently attached, which yields anisotropic ordering and high second-order nonlinear optical (NLO) activity in these films. In this study, the commercially-available NLO chromophore Procion Brown-MX GRN and the optically inactive polymer poly(allylamine hydrochloride) (PAH) were used to assemble device-capable films.

Procion Brown/PAH films were deposited onto an indium tin oxide (ITO)-coated substrate to fabricate a three-layer coplanar electrode waveguide device. This work specifically aims to demonstrate the feasibility of utilizing a hybrid deposition scheme to fabricate electro-optic devices. This work also aims to determine the effect of solution ionic strength on waveguide device performance and finally to demonstrate the performance of such devices in terms of the linear electro-optic coefficient.

Experimental

Materials. All aqueous solutions were made with deionized water (Barnstead, resistivity > 17 MΩ/cm). The polycation poly{allylamine hydrochloride}, (Aldrich, lot 06305DI, MW ~ 70,000) was used as received to prepare a solution with a concentration of 0.01M repeat unit basis (R.U.). The dichlorotriazine chromophore used for this study was Procion Brown MX-GRN (Pro Burnt Orange 515, Pro Chemical and Dye, Somorset, MA, CAS 68892-31-9). The films were deposited onto a glass substrate pre-coated with a 1200 ± 100Å-thick indium tin oxide (ITO) layer (Delta Technologies, Stillwater, MN). Eight aluminum (Al) electrode plates approximately 2000 Å thick were then formed on top of the ISAM film layer (Figure 1) by thermal evaporation (~ 4 x 10^{-6} Torr) (done by Prof. Heflin's group, A. Gopal). The transparent conducting ITO layer acted as the bottom poling electrode and the aluminum layer acted as the top poling electrode. The ITO-coated slides were cleaned using a base cleaning method where the slides are first immersed in a 9:1:2 solution of H_2O, H_2O_2 and NH_4OH in an ultrasonic bath for 30 minutes and were then rinsed with DI water and dried under nitrogen. The structure of the two-electrode ISAM device is shown schematically in Figure 2.

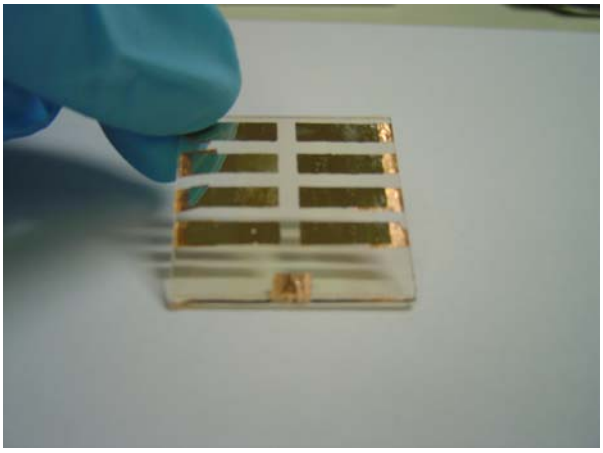

Figure 1. Dual-poling electrode (ITO/Al) electro-optic device, ~50 nm-thick. PAH, pH 7.0, 10mM r.u.; Procion Brown, pH 10.5, 5 mg dye/ml; 0.5M added NaCl.

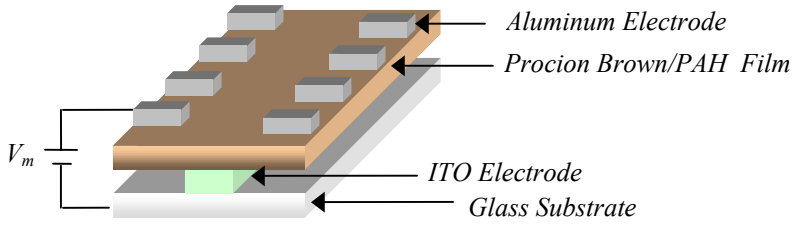

Figure 2. Schematic of dual-poling electrode electro-optic device.

Dye Purification. While the manufacture of optical materials traditionally requires highly pure reagents, commercially available azo dyes originally manufactured for textile industry use are usually impure. The purity of the commercially available chromophore used in this study, Procion Brown, was determined by HPLC to be highly variable. [37] Reactive impurities can interfere with the molecular ordering of the primary chromophore and further decrease NLO performance. Procion Brown was purified to remove ionic salts and buffers that were in the as-received powder.

Earlier studies conducted within this research group employed a manual dye purification procedure that was utilized in this study for all 0.0M NaCl and 0.5M NaCl cases at a dye concentration of 5 mg/ml. Solid phase extraction (SPE) with octadecyl functionalized silica was used to desalt the dye (Alltech High Capacity 75 ml C18 column, lot 173801). The dye was dissolved in 50 mM ammonium acetate (Baker, lot 016816) at ~10 mg/ml. This solution was

vacuum filtered with a Buchner funnel to remove any particulate impurities. The column was first washed with ~50 ml of methanol (Budrick & Jackson, lot 42326) followed by at least 100 ml (~5 bed volumes) of 50 mM ammonium acetate solution and then the dye solution. The column was again flushed with >100 ml of the ammonium acetate solution, allowing the column to run dry. The dye molecules were eluted from the C_{18} packing by passing ~20 ml of methanol through the column. This solution was collected and the methanol was removed by a centrifuge vacuum. Inductively coupled plasma (ICP) emission spectroscopy analysis (Virginia Tech Soil Analysis Lab, SpectroFlame Modula ICP) showed a ~90% reduction in the Na^+ concentration of purified Procion Brown dye.

Table 1. Results of ICP analysis for purified and unpurified Procion Brown dye. Procion Brown was purified using the manual purification method. Data reported as part per million.

Dye/Concentration	Na	Fe	K	Ca	Si	S
Procion Brown/ 5 mg/ml (Unpurified)	1180	0.21	159.5	0.87	0.45	231
Procion Brown/ 5 mg/ml (Purified)	135.2	0.04	35.7	1.64	0.45	596

Film Preparation and Characterization

Film Fabrication/Deposition. Films were prepared by a manual deposition method involving the sequential immersion of an ITO-coated glass slide into the polycation solution (PAH) for 10 minutes for the initial layer and 5 minutes for each subsequent layer. The slide was then rinsed with copious amounts of deionized water and submerged into the Procion Brown solution (5 mg/ml) for 5 minutes, following the same rinsing procedure. All aqueous PAH solutions (10 mM on a repeat unit basis) were stirred overnight and adjusted to a pH of 7.0 for film deposition. Procion Brown solutions were discarded approximately 5-6 hours after use, due to dye hydrolysis. The pH of all aqueous solutions was adjusted using NaOH (Fisher Scientific, lot 024521-24) or HCl (Fisher Scientific, lot 024735-24). All pH measurements were made with an Orion Model 407 specific ion meter. Sodium chloride, NaCl (Fisher Scientific, lot 028794) was used as the salt for adjusting the ionic strength of the dye solutions. For the 0 M NaCl case, four slides were made with a total (both sides) of 100 bilayers on each slide. For the 0.5 M NaCl case, two slides were made with a total (both sides) of 100 bilayers on each slide. All slides were approximately 50 nm thick.

UV-Vis Spectroscopy. The films were deposited at room temperature and characterized using UV-Vis spectroscopy (Milton Roy Spectronic 1201). Slides were dried with N_2 gas every 10 bilayers and the UV-Vis absorbance measurements were performed at the absorbance maximum of Procion Brown (407 nm).

Tilt Angle. The tilt angle of the films was determined by SHG measurements (Prof. Heflin's group, P. Neyman) at varying polarizations (*s*- or *p*-) of incident light. The measurements were taken using a standard setup of 10-nanosecond pulse width, Q-switched Nd:YAG laser with a fundamental wavelength of 1064 nm[38] The SHG data were averaged over 100 shots per data point. Typical spot radius and pulse energy values were 30 μm and 70 mJ/pulse, respectively. The SHG data was taken for both the *s*- and *p*- polarizations of light. The maximum of the second harmonic intensity generated from the *p*-polarized light is represented as $I_{2\omega}^{p\to p}$, while $I_{2\omega}^{s\to p}$ represents the *s*-polarization maximum second harmonic intensity.

The average tilt angle $\overline{\psi}$ from the film normal is calculated by:

$$\overline{\psi} = arc\cot\sqrt{\frac{1}{2}\left[\sqrt{\frac{I_{2\omega}^{p\to p}}{I_{2\omega}^{s\to p}}}\csc^2\theta - 3\cot^2\theta\right]} \tag{5.9}$$

where is the angle of incidence. From the tilt angle calculation the ratio of s-polarization to p-polarization is determined. The $\chi^{(2)}_{zzz}$ is then calculated using equation 5.10

$$\chi_{zzz}^{(2)} = \frac{\chi_{eff}^{(2)}}{\left(\frac{3}{2\cot^2\overline{\Psi}}\right)^{-1}\sin\theta\cos^2\theta + \sin^3\theta} \tag{5.10}$$

Electro-Optic Coefficient. A reflection modulated technique[30,39] was utilized to obtain the linear electro-optic coefficient r_{33} (Measurements performed by Dr. Heflin's group, P. Neyman). The input beam was produced by a He:Ne laser (λ=632.8 nm). The light from the laser first passes through a polarizer. The emerging beam then passes through the glass substrate, the ITO layer,

the ISAM film layer and then reflects back out of the glass substrate by an aluminum electrode at 90°. The polarized light then travels through a Babinet-Soleil compensator (to uniformly vary the phase retardation between the *s* and *p* waves), an analyzer and then into a detector. An AC voltage V_m was applied across the polymeric film with the ITO and aluminum layers acting as electrodes. The modulated intensity I_m (proportional to r_{33}) passing through the analyzer was measured by a lock-in amplifier as a function of the applied AC voltage (0-5 V, 10 Hz–10 kHz).

For this measurement technique, the electro-optic coefficient r_{33} is defined as

$$r_{33} - r_{13} = \frac{\lambda I_m}{2\pi V_m I_c} \frac{\left(n^2 - \sin^2\theta\right)^{1/2}}{n^2 \sin^2\theta} \tag{5.13}$$

where λ is the wavelength of light, I_m is the modulation amplitude, I_c is the half-max laser intensity, V_m is the applied modulation voltage, θ is the incident angle of the laser beam and n is the refractive index of the film.

From symmetry considerations, this model assumes $r_{33} = 3r_{13}$. This assumption is widely used in literature[40,41,42,43,44,45]and is valid when[46] the material does not have liquid crystal ordering, the optical frequencies used are not near chromophore resonance ranges, the material is not under mechanical stress, the molecules are one-dimensional in the sense that only one spatial component of the dipole moment is significant, and when the first order hyperpolarizability β has a significant magnitude. In the case of this study, the conditions are satisfied for the Procion Brown chromophore and the assumption is valid. Under this assumption, r_{33} - r_{13}=2/3 r_{33} and equation 5.13 simplifies to

$$r_{33} = \frac{3\lambda I_m}{4\pi V_m I_c} \frac{\left(n^2 - \sin^2\theta\right)^{1/2}}{n^2 \sin^2\theta} \tag{5.14}$$

Further simplification of the equation leads to

$$r_{33} - r_{13} = \frac{I_m}{V_m I_c}\left(1.007x10^5\ pm\right)A \tag{5.15}$$

where the term A is a collection of constants:

$$A = \frac{\left(n^2 - \sin^2\theta\right)^{1/2}}{n^2 \sin^2\theta} \tag{5.16}$$

Results/Discussion

Absorbance per bilayer. For all films in this study the absorbance of the films increased linearly with the number of bilayers deposited (Figure 1) which is characteristic of uniform layer-by-layer deposition for ISAM films. The slope of this linear relationship between the absorbance and number of bilayers is proportional to the amount of dye deposited per layer.

Table 2. Absorbance per bilayer slopes of films deposited onto ITO-coated slides used in this study compared to films deposited onto uncoated glass slides. PAH 10mM RU, pH 7.0, PB 5mg/ml, pH 10.5. Values of films on glass are cited from Chapter 3.

Slide Substrate	Film Conditions	Absorbance/bilayer
ITO/Glass	0.0 M NaCl	0.0013 ± 0.0001
Glass	0.0 M NaCl	0.0009 ± 0.0001
Glass	0.0 M NaCl	0.0009 ± 0.0001
ITO/Glass	0.5 M NaCl	0.0018 ± 0.0001
Glass	0.5 M NaCl	0.0021 ± 0.0001
Glass	0.5 M NaCl	0.0024 ± 0.0001

The absorbance per bilayer slopes in this study compare well to those obtained in earlier studies (Table 2).

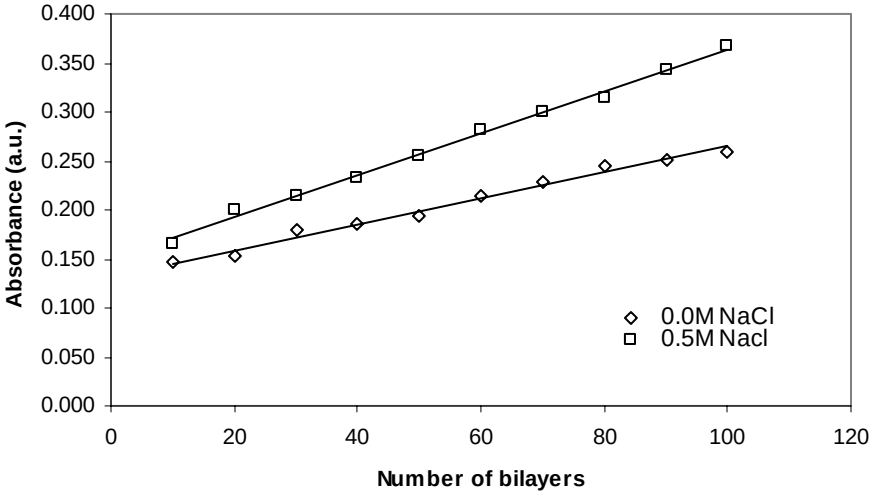

Figure 3. Plot of UV-Vis absorbance (λ=407 nm) as a function of bilayer number (total on both sides) for Procion Brown (PB) films deposited onto an ITO substrate with varying salt concentrations. PAH 10mM RU, pH 7.0, PB 5mg/ml, pH 10.5.

Homogeneity. The films exhibited good homogeneity when inspected visually. Absorbance measurements were taken at three different spots on each slide to assess the homogeneity of the films. The standard deviation between absorbance measurements was approximately 0.003 for the majority of the slides. The standard deviation of absorbance measurements of multiple locations on each slide was less than 10%. These small standard deviations are further indications of film homogeneity and uniform film deposition.

Tilt Angle/Electro-Optic Coefficient. The measurement conditions and EO coefficient results are summarized in Table 3. Prior ellipsometric measurements of Procion Brown films determined refractive index n_0 to be 1.76 and 1.67 for the 0.5 M NaCl and 0.0 M NaCl cases respectively. With an applied voltage of 5.0 V for all devices measured, the electro-optic coefficient was found to be r_{33} = 4.1 ± 0.3 pm/V and r_{33} = 13.6 ± 1.2 pm/V for the 0.0 M NaCl and 0.5 M NaCl cases respectively (The reported values are averages of measurements taken on multiple devices and the errors are standard deviations). An incident angle θ of 45º was used for all electro-optic coefficient calculations. The magnitude of the electro-optic coefficient in this study is compared to other organic/polymeric electro-optic systems and inorganic electro-optic materials in Table 4. The r_{33} value obtained in this study for the 0.5M added NaCl case compares well (~50%) to that of lithium niobate ($LiNbO_3$), the current leading organic material for electro-

optic devices. The three approximate fold increase in r_{33} seen for films with added salt (0.5M NaCl) compared to those with no added salt is attributed to the increase in dye packing associated with an increase in ionic strength. For one case of added salt, one slide was soaked overnight to remove any potential free charge carriers remaining from the high-salt deposition conditions. There was no apparent effect on the r_{33} or film orientation resulting from soaking the slide (Table 3).

Table 3. Summary of electro-optic coefficient measurement conditions. Two devices (electrodes) were tested per slide. $r_{33}(LiNbO_3)$= 30 pm/V.

Film Conditions	Device #	I_m (μV)	I_c (V)	r_{33} (pm/V)	Tilt Angle (°)
0.0 M NaCl	1	13.1	0.150	3.9	45.6
	5	18.5	0.195	4.3	
0.5 M NaCl	1	61.8	0.152	14.3	41.9
	2	52.7	0.157	11.8	
0.5 M NaCl	4	71.4	0.182	14.2	42.5
(soaked overnight)	3	63.2	0.161	14.2	

Table 4. Comparison of electro-optic coefficient of inorganic and organic polymeric materials.

Material	r_{33} (pm/V)	Reference
$LiNbO_3$	30.8	[47]
$KNbO_3$	25.0	
Azo Dye (Disperse Red #1)/PMMA	9.0	[12]
Azo Dye (Procion Brown)/PAH	13.6	*

*Measured in this study

Conclusions

This study probed three major areas: (1) the feasibility of utilizing a hybrid deposition scheme to fabricate electro-optic devices, (2) the suitability of Procion Brown/PAH films for such devices, (3) the measurement of the electro-optic coefficient of Procion Brown/PAH films utilizing a reflection modulation technique, (4) the effect of added salt on waveguide device performance in terms of electro-optic coefficient and (5) the use of a programmable dipper to make EO device-suitable films.

A novel hybrid electrostatic-covalent self-assembly method was used to fabricate a polymeric thin film for an electro-optic device. The films were characterized by UV-Vis absorbance, chromophore tilt angle and electro-optic coefficient. The three-layer coplanar electrode device was fabricated using indium tin oxide (ITO) and aluminum as the bottom and top poling electrodes, respectively. The presence of added salt was found to increase the electro-optic coefficient r_{33} by a factor of 3. Using a single-beam reflection modulated technique, the electro-optic coefficient of devices fabricated using this method was determined to be comparable (~50%) to that of lithium niobate, the current state-of-the-art inorganic material for electro-optic devices.

References

[1] Bechtel, J. H.; Menders, J.; Zang, D. Y. 'Electro-optic polymer integrated optic devices and future applications' *Fiber and Int. Opt.* **22** (2003) 211-224.

[2] L.-H. Peng, L.-H.; Hsu, C.,-C, Shih, Y.-C 'Second-harmonic green generation from two-dimensional chi[sup (2)] nonlinear photonic crystal with orthorhombic lattice structure' *Appl. Phys. Lett.* **83** (2003) 3447-3450.

[3] Ni, P.; Ma, B.; Wang, X.; Cheng, B.; Zhang, D. 'Second-harmonic generation in two-dimensional periodically poled lithium niobate using second-order quasiphase matching' *Appl. Phys. Lett.* **82** (2003) 4230-4232.

[4] Zeng, X.; Chen, X.; Chen, Y.; Xia, Y.; Chen, Y. 'Observation of all-optical wavelength conversion based on cascaded effect in periodically poled lithium niobate waveguide' *Optics & Laser Technology* ***35*** (2003) 187-190.

[5] Kim, J. H.; Yoon, C.S. 'Domain switching characteristics and fabrication of periodically poled potassium niobate for second-harmonic generation' *Appl. Phys. Lett.* **81** (2002) 3332-3334.

[6] Beckers, L.; Buchal, C.; Fluck, D.; Pliska, T.; Günter, P. 'Potassium niobate waveguides: He^+ implantation in bulk single crystals and pulsed laser deposition of thin films' *Materials Science and Engineering A* **253** (1998) 292-295.

[7] Fluck, D.; Pliska, T.; Günter, P.; Beckers, L.; Buchal,C. 'Blue-light second-harmonic generation in ion-implanted KNbO[sub 3] channel waveguides of new design' *Appl. Phys. Lett.* **69** (1996) 4133-4135.

[8] Kitamura, K.; Yamamoto, J. K.; Iyi, N.; Kimura, S. 'Stoichiometric $LiNbO_3$ single crystal growth by double crucible Czochralski method using automatic powder supply system' *J. Crystal Growth* **116** (1992) 327-332.

[9] Takagi, T.; Fujii, T.; Sakabe, Y. 'Growth and characterization of $KNbO_3$ by vertical bridgman method' *Journal of Crystal Growth* **259 (**2003) 296-301.

[10] Anestopoulos, D.; Tsigaridas, G.; Persephonis, P.; Giannetas, V.; Spiliopoulos, I.; Karastatiris, P.; Mikroyannidis, J. 'Electro-optic characterization of two novel organic materials in thin polymeric films' *Chem. Phys. Lett.* **390** (2004) 98-103.

[11] Ono, H.; Misawa, K.; Minoshima, K.; Ueki, A. 'Complex electro-optic constants of dye-doped polymer films determined with a mach-zehnder interferometer' *J. Appl. Phys.* **77** (1995) 4935-4940.

[12] Hayden, L. M.; Sauter, G. F.; Ore, F. R.; Pasillas, P. L. 'Second-order nonlinear optical measurements in guest-host and side-chain polymers' *J. Appl. Phys.* **88** (1990) 456-465.

[13] Lu, J.; Yin, J.; Deng, X.; Shen, Q.; Cao. Z.; 'Device-quality second-order nonlinear optical poly(ester-imide) for electro-optic applications' *Opt. Mat.* **25** (2004) 17-23.

[14] Hwang, S. –J.; Yu, H. H.; Wang, J. 'Electro-optic modulators formed by in-plane electric-field-poled polymer waveguides' *Opt. Comm.* **233** (2004) 341-352.

[15] Yu, H. H.; Hwang, S. –J. 'E-O functional waveguide using the electric-field-poled polymeric material for integrated-optic devices' *Opt. Comm.* **219** (2003) 183-192.

[16] Lee, K. S.; Wu, J. W.; Lee, M. H.; Kim, H. K.; Won, Y. H. 'Measurement of the linear electrooptic effect in poled polymer thin films with coplanar electrodes' *Opt. and Quant. Elect.* **27** (1995) 347-354.

[17] Chang, H. J.; Ha, N. Y.; Kim, A.; Lim, J.; Park, B.; Park, E. –J.; Im, J. –H.; Kim, J. –H.; Lee, S. –H.; Wu, J. W. 'Characterization of electro-optic properties of self-assembled monolayer by attenuated total reflection' *Opt. Mat.* **21** (2002) 413-416.

[18] Wei, S.; Zhenyu, Z.; Qiwei, P.; Qingtian, G.; Lina, Y.; Changshui, F.; Dong, X.; Hongzhen, W.; Jinzhong, Y. 'Nonlinear optical properties and chromophore electrostatic interactions for the poly(ether ketone) guest-host polymer films' *Macromolecules*, **34** (2001) 2002-2007.

[19] Sutherland, R. L. *Handbook of Nonlinear Optics*, Marcel Dekker, (2003).

[20] Horsthius, W. H. G.; Krijnen, G. J. M. 'Simple measuring method for electro-optic coefficients in poled polymer waveguides' *Appl. Phys. Lett.* **55** (1989) 616-618.

[21] Maertens, C.; Detrembleur, C.; Dubois, P.; Jérôme, R.; Blanche, P.-A.; Lemaire, Ph. C. 'Synthesis and electrooptic properties of a new chromophore dispersed or grafted in a carbazolyl methacrylate matrix' *Chem. Mater.* **10** (1998) 1010 -1016.

[22] Ding, Y. J.; Mu, X.; Yin, X. 'Electro-optic and electromechanical properties of poled polymer thin films' Appl. Phys. Lett. **79** (2001) 3749-3751.

[23] Meyrueix, R.; Dickens, M. J.; Lemonnier, O.; Lecomte, J. P.; Tapolsky, G. 'Fabry-Pérot interferometry applied to the study of piezoelectric and electro-optical properties of a poled NLO polyurethane' *Opt. Comm.* **110** (1994) 445-455.

[24] Zhang, D. M.; Yi, M. B.; Tian, X. J.; Sun, W.; Hou, A. L.; Sun, J. Z.; Ma, Y. G.; Tian, W. J.; Shen, J. C. 'External electro-optic measurement utilizing poled polymer-based asymmetric Fabry-Perot reflection film' *J. Appl. Phys.* **86** (1999) 6184-6188.

[25] Chen, K. X.; Yang, H.; Zhang, H. B.; Zhao, Y.; Yi, M.B. 'Sampling high-frequency signals using a poled-polymer asymmetric Fabry-Perot microcavity as an electro-optic probe tip' *Appl. Phys. B* **74** (2002) 363-366.

[26] Cho, H. R.; Shin, M. J.; Han, S. H.; Wu, J. W. 'Mach–Zehnder interferometer measurement of the Pockels effect in a poled polymer film with a coplanar electrode structure' *Appl. Phys. Lett*. **69** (1996) 3788-3790.

[27] Song, H. –C.; Oh, M. –C.; Ahn, S. –W.; Steier, W. H.; Fetterman, H. R.; Zhang, C. 'Flexible low-voltage electro-optic polymer modulators' *Appl. Phys. Lett.* **82** (2003) 4432-4434.

[28] Ribeiro, P. A.; Balogh, D. T.; Fonseca, J. L. C.; Giacometti, J. A.; 'Chromophore Relaxation in a Side-Chain Methacrylate Copolymer Functionalized with 4-[*N*-Ethyl-*N*-(2-hydroxyethyl)]amino-2'-chloro-4'-nitroazobenzene' *Macromolecules* **37** (2004) 2618-262.

[29] Geis, W.; Sinta, R.; Mowers, W.; Deneault, S. J.; Marchant, M. F.; Krohn, K. E.; Spector, S. J.; Calawa, D. R.; Lyszczarz T. M. 'Fabrication of crystalline organic waveguides with an exceptionally large electro-optic coefficient' *Appl. Phys. Lett.* **84** (2004) 3729-3731.

[30] Teng, C. C.; Man, H. T. 'Simple reflection technique for measuring the electro-optic coefficient of poled polymers' *Appl. Phys. Lett*. **56** (1990) 1734-1736.

[31] Shuto, Y.; Amano, M. 'Reflection measurement technique of electro-optic coefficients in lithium niobate crystals and poled polymer films' *J. Appl. Phys.* **77** (1995) 4632-4638.

[32] Mortazavi, M. A.; Knoesen, A.; Kowel, S. T.; Henry, R. A.; Hoover, J. M.; Lindsay, G. A. 'Second-order nonlinear optical properties of poled coumaromethacrylate coplymers' *Appl. Phys. B* **53** (1991) 287-294.

[33] DeMartino, R. N.; Allen, D. E.; Keosian, R.; Khanarian, G.; Haas, D. R.

[34] Van Cott, K. E.; Guzy, M.; Neyman, P.; Brands, C.; Heflin, J. R.; Gibson, H. W.; Davis, R. M. 'Layer-by-layer deposition and ordering of low-molecular weight dye molecules for second-order nonlinear optics' *Angew. Chem. Int. Ed.* **41** (2002) 3236-3328.

[35] Heflin, J. R.; Neyman, P. J.; Guzy, M.; Shah, S. M.; Davis, R. M.; Van Cott, K. E.; Wang, H.; Gibson, H. W.; Brands, C. 'Hybrid covalent/ionic self-assembly of organic second order nonlinear optical films, in Organic Thin Films for Photonic Applications, OSA Trends in Optics and Photonics Series **64** (2002) 3-8.

[36] Guzy, M. 'Organic Self-Assembled Layer-by-Layer Thin Films for Second-Order Nonlinear Optics', Ph. D. Thesis, Virginia Tech, 2003.

[37] Van Cott, K.; Amos, T.; Gibson, H.; Davis, R.; Heflin, J. 'Characterization of the purity and stability of commercially available dichlorotriazine chromophores used in nonlinear optical materials' *Dyes and Pigments* **58** (2003) 144-145.

[40] Mohlmann, G. R.; Horsthuis, W. H.; van der Vorst, C. P.; McDonach, A.; Copeland, M.; Duchet, C.; Fabre, P.; Diemeer, M. B.; Trommel, E. S.; Suyten, F. M.; Van Daele, P.; Van

[41] Kuzyk, C. C.; Dirk, M. W. "Characterization Techniques and Tabulations for Organic Nonlinear Optical Materials" Marcel Dekker, (1998).

[42] Singer, K. D.; Kuzyk, M. G.; Sohn, J. E. 'Second-order nonlinear optical processes in orientatioanlly-ordered marerials: relationship between molecular and macroscopic properties' *J. Opt. Soc. Am. B* **4** (1987) 968-976.

[43] Wu, J. W. 'Birefringent and electro-optic effects in poled polymer films: steady state and transient properties' *J. Opt. Soc. Am. B* **8** (1991) 142-152.

[44] Nahata, A.; Shan, J.; Yardley, J. T.; Wu, C. 'Electro-optic determination of the nonlinear-optical properties of a covalently functionalized disperse red 1 copolymer' *J. Opt. Soc. Am. B* **10** (1993) 1553-1564.

[45] de Ridder, R. M.; Driessen, A.; Rikkers, E.; Lambeck, P. V.; Diemeer, M. B. 'Design and fabrication of electro-optic polymer modulators and switches' *Opt. Mater.* **12** (1999) 205-214.

[46] Anestopoulos, D.; Tsigaridas, G.; Persephonis, P.; Giannetas, V.; Spiliopoulos, I.; Karastatiris, P.; Mikroyannidis, J. 'Electro-optic characterization of two novel organic materials in thin polymeric films' *Chem. Phys. Lett.* **390** (2004) 98-103.

[47] Sutherland, R. L. *Handbook of Nonlinear Optics*, Marcel Dekker, (2003).

Chapter 6
Conclusions

This study focused on investigating the influence of several pertinent processing variables that affect the challenges of fabricating hybrid reactive films for application to electro-optic devices. Specifically, this study investigated (1) the effect of forced convection, varying deposition time and varying dye concentration on the properties of PAH/Procion Brown films fabricated via the hybrid reactive deposition scheme, (2) the automation and optimization of the fabrication of thick NLO active films and (3) the use of the hybrid covalent-electrostatic deposition scheme to fabricate a polymeric waveguide device with an electro-optic coefficient comparable to that of lithium niobate ($LiNbO_3$).

Processing Variables Study

Effect of Convection

At fixed deposition time and concentration conditions, the presence of convection had little demonstrated effect on films with deposition times shorter than 2 minutes. For the 5 minute case, the presence of convection correlated with a ~45% increase in $\chi^{(2)}_{zzz}$ values and 25% increase in absorbance per bilayer. The tilt angle and film thicknesses both seemed relatively unaffected by the presence of convection.

Effect of Deposition Time

At a constant dye concentration of 5 mg/ml, the deposition time had little effect on SHG for deposition times less than two minutes. Deposition times ranging from 30 - 60 seconds, showed no significant difference in SHG for most cases. In the presence of convection, the increase in deposition time from 2 minutes to 5 minutes showed a 2.4 fold increase in $\chi^{(2)}_{zzz}$ and a 30% increase in absorbance per bilayer.

Effect of Dye Concentration

For a deposition time of 2 minutes in the presence of convection, the dye solution concentration was successfully reduced 5-fold (from 5 mg/ml to 1 mg/ml) with less than a 5% difference in $\chi^{(2)}_{zzz}$, less than a 15% decrease in absorbance per bilayer and no detriment to film quality. These results strongly indicate that the deposition conditions

remain well outside of the transport-limited regime at a dye concentration of 1 mg/ml. Rather, the surface reaction rate apparently is controlling.

Effect of Temperature

Depositing slides at an elevated temperature (~35°C), had an undetermined effect on $\chi^{(2)}_{zzz}$, but showed a 15% increase in absorbance per bilayer. There was less than a standard deviation in difference between some $\chi^{(2)}_{zzz}$ values for films with a 30 second deposition time deposited at room temperature and the film deposited at 35°C (30 second deposition time).

Overall, the optical quality of the films made in this study was excellent and consistently exhibited linear layer-by-layer growth. For all conditions studied, the slides consistently showed bilayer thickness values ~0.95 ±0.1 nm/bilayer deposited, corresponding well to previous studies. Most slides exhibited quadratic scaling of the second harmonic intensity with film thickness. In some cases, this relationship deviated from linearity for the first 20 bilayers deposited, suggesting that the films undergo an initial phase where the chromophores gradually gain preferential orientation. Further analysis should be given in the small-bilayer range (2-20 bilayers, both sides) to identify any potential phenomena regarding chromophore orientation in this range.

As previously mentioned, many data points for shorter deposition times (30 sec – 2 minutes) have overlapping $\chi^{(2)}_{zzz}$ values. This suggests that the realm of the experiments conducted in this study may be insufficient to determine specific deposition kinetics of the PAH/dye deposition steps on the order of seconds. Future work should entail more detailed kinetic adsorption analysis of the polymer and dye species utilizing a quartz crystal microbalance (QCM), in-situ SHG measurements and biological amine assays. In-situ SHG studies and QCM measurements will give valuable data relating to the mass transfer coefficient and reaction rate of Procion Brown deposition. Studies of polyelectrolyte adsorption to a charged surface show that a small increase in ionic strength can significantly increase the polymer adsorption rate. Sodium chloride was used in this study as an electrostatic charge barrier in the dye deposition solution (0.5M NaCl). The effect of various halogen salts (i.e. NaBr, NaI) on the adsorption kinetics and NLO

activity should be investigated in future work. A recent study found that solutions containing halogen counterions (50 mM added salt) with a larger ionic radius exhibit a faster adsorption of a species onto an oppositely-charged layer. Larger exchange ions are found to be more loosely bound to the surface and would exchange more rapidly than smaller, more tightly bound ions. Ions with smaller ionic radii (F^-, r=1.33Å; Cl^-, r=1.81 Å) were found to have adsorption rates 53% and 73% (respectively) that of the larger ion I^- (r=2.16 Å).

Dipper Study

A series of automated hybrid covalent film fabrication experiments were conducted with the aim of optimizing the deposition process and replicating current manual deposition methods. Kinetic modeling parameters of the rinsing process were determined from monitoring the absorbance of dye build-up in the active rinse bath. The rinse bath was found to adhere to the kinetic trends of a continuously-stirred tank vessel (CST) with immediate dilution of the dye upon contact with the bulk rinse fluid. The theoretical residence time varied significantly from the experimentally-obtained theoretical time, potentially implying a rinsing process with two-step diffusive and convective transport barriers. Stagnant flow fields in the rinse tank also could manifest in the form of an elevated residence time. Contaminant species residing in these stagnant flow regimes could definitely have a detrimental effect on the efficiency of contaminant removal from the bulk fluid. Equipment modifications employed in dipper operation (i.e. powerhead, blotting step, etc.) proved essential for good optical film quality. Films fabricated in the presence of convection with a blotting step following each deposition step exhibited a marked increase in optical homogeneity in comparison to base case studies in which these equipment modifications were neglected. Films fabricated with the automated process correlated very well with manually-fabricated films in terms of thickness, optical constants, absorbance per bilayer and second harmonic generation. Each compared value encountered less than a standard deviation of difference between each compared value. The $\chi^{(2)}$ values obtained for films in this study were comparable to those previously obtained for identical chemistries and that of lithium niobate. Optically homogeneous films up to 100 nm were fabricated for the first time utilizing the hybrid

covalent deposition method in this study. These films exhibited the expected quadratic scaling of the second harmonic intensity with bilayer number, indicating stabilization of acentric ordering with increasing layers deposited. In future work, the kinetics of PAH rinsing and adsorption should be studied using a quartz crystal microbalance and biological amine assays. Furthermore, the effect of high pH conditions on glass substrates should be studied utilizing any number of surface characterization techniques, such as AFM or prolifometry. Process and equipment modifications are necessary to fabricate films thicker than 100 nm. The automated process stands for improvement particularly in the area of slide holder design. Increasing the gap between slides will greatly improve the rinsing efficiency which is critical for optically homogeneous films. These modifications will attest this automated process as a feasible means for fabricating thick, EO device-capable films.

Electro-Optic Device Fabrication

A novel hybrid electrostatic-covalent self-assembly method was used to fabricate a polymeric thin film for an electro-optic device. The films were characterized by UV-Vis absorbance, chromophore tilt angle and electro-optic coefficient. The three-layer coplanar electrode device was fabricated using indium tin oxide (ITO) and aluminum as the bottom and top poling electrodes, respectively. The presence of added salt was found to increase the electro-optic coefficient r_{33} by a factor of 3. Using a single-beam reflection modulated technique, the electro-optic coefficient of devices fabricated using this method was determined to be comparable (~50%) to that of lithium niobate, the current state-of-the-art inorganic material for electro-optic devices.

Future Work

Recommendations for future work were described for each experimental objective in the sections above. In summary, the following work is recommended for this research effort:

- Further study of films with small numbers of bilayers (1-10 bilayers, one side)
- QCM measurements for more detailed kinetic analysis
- Biological amine assays (HABBA) for potential kinetic analysis
- Study the effect of variation of halogen salts on adsorption kinetics

- Use of resistance meter in rinse bath to characterize contamination
- AFM or other surface techniques to study the stability of glass slides at high pH conditions
- Modification of current slide holder to increase distance between slides
- Synthesis of novel NLO chromophore

Appendix A

Error Analysis Derivation

General Propagation of Error

Given that *x, ... , z* are measured quantities with uncertainties $\sigma_x, \ldots, \sigma_z$ and the measured quantities are used to compute the function $q(x, \ldots, z)$. If the uncertainties in $x, \ldots, z$ are independent, then the uncertainty in q is

$$\sigma_q = \sqrt{\left(\frac{\delta q}{\delta x}\sigma_x\right)^2 + \mathrm{K} + \left(\frac{\delta q}{\delta z}\sigma_z\right)^2} \tag{A.1}$$

Standard Deviation of $\chi^{(2)}_{eff}$

The equation used to calculate $\chi^{(2)}_{eff}$ is as follows

$$\chi^{(2)}_{eff} = \chi^{(2)}_{ref}\left(\frac{l_{ref}}{l_{s,bilayer}}\right)\left(\frac{m}{\sqrt{I^{2\omega}_{ref}}}\right) \tag{A.2}$$

l_{ref} is the total path length (film thickness) through the 68-bilayer standard (measured with the films for which $\chi^{(2)}_s$ is being calculated), $I^{2\omega}_{\mathrm{ref}}$ is the second harmonic intensity for the 68-bilayer standard, m is the slope of the plot of the square root of the second harmonic intensity vs. number of bilayers deposited and $l_{s,bilayer}$ is the sample film thickness per bilayer.

When the equation is simplified by the collection of constants, equation A.2 is reduced to

$$\chi^{(2)}_{eff} = C\left(\frac{m}{l_{s,bilayer}}\right) \tag{A.3}$$

$$C = \chi^{(2)}_{ref}\left(\frac{l_{ref}}{\sqrt{I^{2\omega}_{ref}}}\right) \tag{A.4}$$

For this case, $q = \chi^{(2)}_{eff} = f\left(m, l_{s,bilayer}\right)$

From Equation A.1:

$$\sigma_q = \sqrt{\left(\frac{\delta q}{\delta x}\sigma_x\right)^2 + \mathrm{K} + \left(\frac{\delta q}{\delta z}\sigma_z\right)^2}$$

$$\sigma_{\chi_{eff}^{(2)}} = \sqrt{\left(\frac{A}{l_{s,bilayer}}\sigma_m\right)^2 + \left(\frac{Am}{l_{s,bilayer}^{\ 2}}\sigma_{l_{s,bilayer}}\right)^2} \tag{A.5}$$

Standard Deviation of Bilayer Thickness ($t_{bilayer}$)

The equation used to calculate the film thickness per bilayer is as follows

$$t_{bilayer} = \frac{t_{film}}{n_b} \tag{A.6}$$

where t_{film} is the total thickness of the film and n_b is the number of bilayers in the film (one side of the slide). For this case, $q = t_{bilayer} = f\left(t_{film}, n_b\right)$

From Equation A.1:

$$\sigma_q = \sqrt{\left(\frac{\delta q}{\delta x}\sigma_x\right)^2 + \mathrm{K} + \left(\frac{\delta q}{\delta z}\sigma_z\right)^2}$$

$$\sigma_{t_{bilayer}}^{\ 2} = \sigma_{t_{film}}^2\left(\frac{\delta t_{bilayer}}{\delta t_{film}}\right)^2 + \sigma_{n_b}^{\ 2}\left(\frac{\delta t_{bilayer}}{\delta_{n_b}}\right)^2 \tag{A.7}$$

Since the number of bilayers is an exact number, there is no error and the second term of Equation A.7 cancels.

$$\sigma_{t_{bilayer}} = \sqrt{\sigma_{t_{film}}^2\left(\frac{1}{n_b}\right)^2} \tag{A.8}$$

Standard Deviation of Absorbance per Bilayer and Slope of $I_{2\omega}^{1/2}$ vs. n_b

The standard deviation of the absorbance per bilayer and slope of $I_{2\omega}^{1/2}$ vs. n_b were both determined using linear regression. For two linearly-related variables x and y we expect to fit an expression of the form

$$y = mx + b \tag{A.9}$$

where m is the slope of the line and b is the intersection point of the line at y=0.

The standard deviation of the slope σ_m can be determined from experimentally-obtained data. There is presumably some uncertainty in the measurement of the y values. The uncertainty in the measurements of $y_1 \ldots y_n$ is

$$\sigma_y = \sqrt{\frac{1}{N-2}\sum_{i=1}^{N}\left(y_i - b - mx_i\right)^2} \tag{A.10}$$

where N is the number of data points. For the expression of σ_m an abbreviation for the denominator Δ is used

$$\Delta = N\sum x^2 - \left(\sum x\right)^2 \tag{A.11}$$

The standard deviation of the slope σ_m of a linearly-related set of variables (x, y) is

$$\sigma_m = \sigma_y \sqrt{\frac{N}{\Delta}} \tag{A.12}$$

Appendix B

Ellipsometry

Variable Angle Spectroscopic Ellipsometry (VASE) was used to measure film thickness and optical constants *n* and *k*. Data was acquired at incident angles between 55° and 65° at either 2° or 3° increments. The larger 3° increment was used in some cases to read the model fit to the experimental data more clearly. The Brewster angle was determined to ±5° from the plot of phase factor Δ vs. scan angle. The Brewster's angle for Procion Brown/PAH films was approximately 60°. The measurements were taken in the range of the Brewster's angle, where the optical constants have the maximum sensitivity. Data was typically taken in the range of 350 nm to 1000 nm in 10 nm intervals. In some cases, the measurements were taken from 250 nm to 1000 nm. The initial wavelength was increased from 250 nm to 350 nm to reduce the noise level in measurements and therefore obtain a more accurate fit. The refractive index at 1000 nm and 530 nm obtained from the model fit was used in $\chi^{(2)}_{zzz}$ calculations as n_{1064} and n_{532}, respectively. The smooth side of the frosted end of the slide was used for measurements to eliminate backside reflections.

A two-layer model was used to fit the ellipsometric measurements. The first layer represents the glass substrate used for film deposition. The second layer is a Lorentz oscillator model used to represent the deposited film. A one-term Lorentz oscillator is described as

$$\varepsilon = \varepsilon_1 + i\varepsilon_2 = \varepsilon_\infty + A_m\left[\frac{1}{E + E_n + iB_r} - \frac{1}{E - E_k + iB_r}\right] \qquad \text{(B.1)}$$

The accuracy of each fit was determined by the fit of the exponential amplitude factor Ψ and phase factor Δ to the Lorentz oscillator model. The amplitude of the absorbance A_m, the peak width of the absorbance B_r, film thickness and the infinite relative permittivity $\varepsilon_{1\infty}$ were all fit to one term of the Lorentz model. The photon energy E_n is a function of Planck's constant, the speed of light *c* and wavelength λ.

$$E_n = hc/\lambda = 124\ (eV)/\ \lambda \qquad (B.2)$$

The absorbance maximum of Procion Brown, 407 nm, was used for λ in equation 1. E_n was fixed to 3.0 for Procion Brown films. The model fit parameters were set as follows:

Maximum number of iterations: *100*

Fit default: *Experimental standard deviations*

Thickness: *Min: 1, Max: 1000*

$\varepsilon_{1\infty}$: *Min: 1, Max: 4*

A_m: Max: *100*

B_r: Max: 100

Checks for an acceptable fit:

- $2.0 < n > 1.5$ (refractive index of glass)
- $\varepsilon_{1\infty} < 4$ ($\varepsilon_{1\infty}$ is representative of the film refractive index squared. Polymer films typically have a refractive index no greater than 2.)
- The peak of *k* plotted as a function of wavelength has an absorbance maximum 407 nm ±5 nm. Thicker films (>40 nm) often required the small adjustment of E_n for *k* to align with an absorbance maximum of 407 nm (i.e. for a 40 nm film, E_n= 3.15). This is attributed to some potential minor software errors.
- Thickness~ 1nm/bilayer (one side of film)
- Typical constant values *(*A_m 2.5 – 3.0*,* A_m 3.5 - 5 (for films with absorbance/bilayer>0.002)*,* B_r 1.1 – 2.0)
- Standard deviation of fitted thickness is less than the thickness itself